Philosophiae Doctor (PhD)
Thesis 2021:61

Kinetic investigations of the oxidative cleavage of oligomeric carbohydrates provide novel insights into the catalytic action of fungal lytic polysaccharide monooxygenases

Kinetikkstudier av lytisk polysakkarid monoksygenasers oksidative spalting av karbohydratoligomerer gir ny innsikt i enzymenes katalytiske mekanisme

Lukas Rieder

Kinetic investigations of the oxidative cleavage of oligomeric carbohydrates provide novel insights into the catalytic action of fungal lytic polysaccharide monooxygenases

Kinetikkstudier av lytisk polysakkarid monoksygenasers oksidative spalting av karbohydratoligomerer gir ny innsikt i enzymenes katalytiske mekanisme
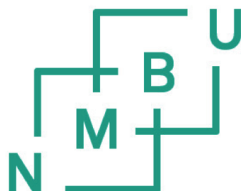
Philosophiae Doctor (PhD) Thesis

Lukas Rieder

Norwegian University of Life Sciences

Faculty of Chemistry, Biotechnology and Food Science

Ås (2021)

This project has received funding from the European Union's Horizon 2020 research and innovation program under the Marie Skłodowska-Curie grant agreement No.722390

Das also war des Pudels Kern!

-Johann Wolfgang von Goethe in Faust

Table of contents

Acknowledgment

The work included into this thesis was performed within the BioOrganic research group and the Protein Engineering and Proteomics group at the Faculty of Chemistry, Biotechnology and Food Science at the Norwegian University of Life Sciences in the period from 2017 to 2021.

First and foremost, I want to express my thankfulness to my main supervisor **Prof. Morten Sørlie** for giving me the chance to perform research in this highly inspiring environment, the outstanding guidance and all trust and freedom I had while working on my thesis. Truly, I could not have wished for a better supervisor.

I would also like to express my gratitude to my co-supervisor **Prof. Vincent Eijsink** for all the support in every possible manner and the very useful, most often very complicated discussions about LPMOs that resulted on many occasions in more questions than answers.

Although only part of my project for a short time, I would like to thank **Dejan Petrović** for giving me the theoretical and practical introduction into the world of LPMO research that set the base for this thesis.

Being part of two such hard working research groups was a great experience and I would really like to thank all the people on the **1st floor** and in the **PEP group** for supporting me**.** Special thanks goes to **Eirik, Simen, Lena, Anton, Ole, Kelsi** and **Ivan** for all the funny moments, great conversations and support in everyday research life.

A thank you goes also to my family and friends back home for their unlimited support whenever needed.

Last but not least my eternal gratitude goes to **Katharina** for being my greatest ally (not only as co-author), for enduring my occasional grumpiness and for being, despite the 1822 km separating us, always at my side. I am so lucky to have you.

Summary

The lytic polysaccharide monooxygenases (LPMOs) are a recently discovered class of redox-active mono-copper enzymes that catalyze the oxidative cleavage of glycosidic bonds in recalcitrant plant or chitin-based biomass, increasing the efficiency of its enzymatic degradation. This makes LPMOs to an attractive target for applications including renewable energy technologies and enzyme engineering projects. Despite recent advances, the catalytic mechanism of these enzymes remains unknown, so there is a clear need for research on the fundamentals of LPMO catalysis. To shed some light on the mysteries of these fascinating enzymes, classical biochemical approaches were used for the functional characterization of selected fungal LPMOs that catalyze the oxidative cleavage of soluble carbohydrates. The research undertaken during the work on this thesis has resulted in highly interesting and novel findings that will contribute to progress in the field.

Paper I: Novel molecular biological tools for the efficient expression of fungal lytic polysaccharide monooxygenases in *Pichia pastoris*, describes a streamlined and effective procedure for the expression and downstream processing of fungal lytic polysaccharide monooxygenases using *Pichia pastoris* as an expression host. The goal of the study was to establish a reliable expression platform that does not suffer from limitations in terms of enzyme availability and to establish a consistent and reproducible production process to support subsequent characterization studies. As proof of concept, we demonstrate the expression of four different LPMOs from three different families, which were purified to homogeneity in a single tag-less size exclusion chromatography step, yielding up to 42 mg of pure enzyme per liter of cultivation broth. We also report the use of a non-native LPMO signal peptide originating from the dolichyl-diphosphooligosaccharide-protein glycosyltransferase subunit 1 (*OST1*) of *Saccharomyces cerevisiae* that generates a correctly processed N-terminus and may thus help avoid obstacles encountered during recombinant LPMO expression.

Paper II: Kinetic characterization of a putatively chitin-active LPMO reveals novel LPMO functionalities and demonstrates the absence of monooxygenase activity, presents a detailed biochemical characterization of an AA11-type LPMO from *Aspergillus fumigatus.* This enzyme, now known as *Af*AA11B, has an atypical LPMO surface topology that is reflected by its preference for soluble chitin oligomers and inability to access the surface of crystalline chitin. In addition to its unique substrate preference, *Af*AA11B has some highly interesting catalytic properties relating to H_2O_2 formation and consumption. We show that its remarkably low redox potential of 114 mV favors the *in situ* formation of H_2O_2 in the presence of an external reductant and O_2. Moreover, in contrast to previous reports, the presence of the H_2O_2-scavenging

horseradish peroxidase (HRP) can inhibit the so-called monooxygenase LPMO reaction by removing H_2O_2 formed *in situ* during cleavage of soluble chito-oligosaccharides. The peroxygenase reaction of *Af*AA11B was studied into more detail by performing classical Michaelis-Menten kinetic analyses with all relevant co-substrates, revealing that *Af*AA11B has a k_{cat} of 4.0 ± 0.6 s^{-1} and K_m values of 8.9 ± 1.0 µM and 200 ± 29 µM for H_2O_2 and $(GlcNAc)_4$, respectively. These kinetic constants together with the clear evidence that the enzyme requires H_2O_2 for $(GlcNAc)_4$ oxidation indicate that *Af*AA11B is indeed a peroxygenase.

Paper III: Fast and specific peroxygenase reactions catalyzed by fungal mono-copper enzymes, follows up on previous observations that the *in situ* production of H_2O_2 is the driving force behind the monooxygenase reaction and that LPMO-catalyzed oxidization of the scissile glycosidic bond is a peroxygenase reaction. In this study, we compared the monooxygenase and peroxygenase reactions by performing comprehensive kinetic studies with *Nc*AA9C and *Ls*AA9A together with three reductants commonly used for LPMO activation. Upon assessing the oxidation of soluble cellulosic substrates under monooxygenase conditions, we observed substantial differences between the AA9 enzymes with respect to enzyme speed as well as effects arising from the choice of reductant. Interestingly, the reductant-specific trends observed in the monooxygenase reaction were also seen for the *in situ* production of H_2O_2, suggesting a strong correlation between H_2O_2 formation and substrate oxidation. This connection was supported by the ability of a H_2O_2-scavanger to inhibit the monooxygenase reaction. To gain deeper insight into the peroxygenase reaction of *Nc*AA9C and *Ls*AA9A, we investigated reductant effects and obtained Michaelis-Menten parameters for Glc_5 conversion. Moreover, we demonstrate that both enzymes are fast and highly specific peroxygenases capable of reaching unprecedent catalytic rates of up to about 100 s^{-1} at 4 °C when soluble cellulosic substrates are present.

Sammendrag

Lytisk polysakkarid monooksygenaser (LPMO) er en nylig oppdaget gruppe med redoksaktive mono-kobberenzymer. LPMOer katalyserer oksidativt brudd av glykosidbindinger i krystallinsk plante- eller kitinbasert biomasse og gjør enzymatisk nedbrytning av biomassen mer effektiv. LPMOenes egenskaper gjør dem til svært interessante kandidater for bruk innen fornybar energi og i utviklingen av ny enzymteknologi. Til tross for økt forståelse av LPMOers virkemåte er den eksakte mekanismen og detaljene i den katalytiske syklusen fremdeles gåtefull, derfor er det nødvendig med mer forskning for å forstå de grunnleggende aspektene ved LPMO-katalyse. De ukjente sidene av disse fascinerende enzymene ble belyst ved hjelp av grunnleggende biokjemiteknikker for en funksjonell karakterisering av LPMOer fra sopp som katalyserer oksidativt brudd av løselige karbohydrater. Forskningen som er gjennomført i denne avhandlingen har resultert i interessante og nyskapende funn, og bidrar til progresjon innenfor forskningsområdet.

Artikkel I: Nye molekylærbiologiske verktøy for effektiv uttrykkelse av fungale lytisk polysakkarid monooksygenaser i *Pichia pastoris*, beskriver en strømlinjeformet og effektiv prosedyre for uttrykkelse og nedstrømsprosessering av lytisk polysakkarid monooksygenaser fra sopp ved bruk av *Pichia pastoris* som vert. Målet med studien var å etablere en enzymuttrykksplattform for å øke tilgjengeligheten av enzymer og sikre sammenlignbare posttranslasjonelle modifikasjoner mellom enzymer for videre enzymkarakterisering. Som proof of concept uttrykte vi fire forskjellige LPMOer fra tre ulike familier og renset disse til homogenitet i ett rensesteg ved bruk av gelfiltrering. Denne prosessen ga et utbytte på 42 mg rent enzym per liter kultiveringsmedie. Videre viser vi at bruken av et ikke-nativt LPMO signalpeptid fra 'dolichyl-diphosphooligosaccharide protein glycotransferase' subenhet 1 (*OST1*) i *Saccharomcyes cerevisiae* resulterer i korrekt prosessering av proteinets N-terminus, som ellers kan være en hindring for å uttrykke rekombinante LPMOer.

Artikkel II: Kinetisk karakterisering av en antatt kitinaktiv LPMO viser ny innsikt i LPMO-funksjonalitet og demonstrerer fraværet av monooksygenaseaktivitet, er en grunnleggende biokjemisk karakterisering av en AA11 type LPMO fra *Aspergillus fumigatus*. Enzymet, nå kjent som *Af*AA11B, har en uvanlig LPMO-overflatetopologi som reflekterer enzymets preferanse for løselige kitinoligomerer og dets manglende evne til å bryte ned krystallinsk kitin. Foruten en unik substratpreferanse, viser *Af*AA11B svært interessante katalytiske egenskaper i form av produksjon og forbruk av H_2O_2. I denne studien viser vi hvordan et uvanlig lavt redokspotensial på 114 mV er fordelaktig for *in situ* produksjon av H_2O_2 når en ekstern reduktant og O_2 er til stede. I motsetning til tidligere studier, viser denne studien

at tilstedeværelsen av en peroxidase (HRP) inhiberer LPMOens monooksygenaseaktivitet ved å fjerne *in situ* generert H_2O_2 når løselige kitinoligomerer brukes som substrat for LPMOen. Peroksygenaseaktiviteten til *Af*AA11B ble studert i detalj ved bruk av Michaelis-Menten kinetikk for alle relevante ko-substrater, og viste en k_{cat} tilsvarende 4.0 ± 0.6 s^{-1} samt K_m -verdier tilsvarende 8.9 ± 1.0 µM og 200 ± 29 µM for henholdsvis H_2O_2 og $(GlcNAc)_4$. Enzymets behov for H_2O_2 for å oksidere kitinoligomersubstratet og kinetikkkonstantene tyder på at *Af*AA11B faktisk er en peroksygenase.

Artikkel III: Raske og spesifikke peroxygenasereaksjoner katalysert av fungale mono-kobber enzymer, følger opp tidligere observasjoner om at *in situ* produksjon av H_2O_2 er drivkraften bak monooksygenasereaksjonen, og at LPMO-katalysert oksidasjon av glykosidbindinger er en peroksygenasereaksjon. I denne studien undersøkte vi monooksygenase- og peroksygenasereaksjonsaktiviteten for *Nc*AA9C og *Ls*AA9A ved å gjennomføre omfattende kinetikkforsøk med tre typiske reduktanter for LPMO-aktivering. Vi sammenliknet LPMOenes evne til å oksidere løselige cellooligosakkarider under monooksygenasebetingelser med tre ulike reduktanter, og observerte en signifikant forskjell i reaksjonshastighet for LPMOene og at valg av reduktant har stor innvirkning på reaksjonshastigheten. Den observerte hastighetstrenden for reduktantene i monooksygenase-reaksjonen reflekterer reduktantenes evne til å produsere H_2O_2 *in situ* og tyder på en sterk korrelasjon mellom mengde H_2O_2 som blir produsert og mengde substrat som blir oksidert. Denne sammenhengen underbygges av resultater som viser at monooksygenaseaktiviteten inhiberes av en 'H₂O₂-scavenger'. For å få en dypere forståelse av peroksygenaseaktiviteten til *Nc*AA9C og *Ls*AA9A analyserte vi reduktanteffekten og Michaelis-Mentenparametere for disse enzymenes oksidasjon av Glc_5. Videre viser vi at begge enzymene har høy spesifikk peroksygenaseaktivitet og er i stand til å oppnå bemerkelsesverdig høye katalytiske hastigheter, opp mot 100 s^{-1} ved 4°C, ved bruk av løselig cellooligosakkarider som substrat.

Abbreviations

AA – auxiliary activities

Af – Aspergillus fumigatus

Ao – Aspergillus oryzea

AscA – Ascorbic acid

CBM – Carbohydrate-binding module

Cys – Cysteine

GA – Gallic acid

GlcNAc – N-acetyl-D-glucosamine

HPAEC-PAD – High-performance anion exchange chromatography with pulsed amperometric detection

HRP – Horseradish peroxidase

k_{cat} – rate constant

K_m – Michaelis constant

k_{obs} – observed rate

LPMO – Lytic polysaccharide monooxygenase

Ls – Lentinus similis

MALDI-ToF MS – Matrix assisted laser desorption ionization - time-of-flight mass spectrometry

Nc – Neurospora crassa

PDB – Protein data bank

SHE – Standard hydrogen electrode

Sm – Serratia marcescens

List of papers

Paper I:

Novel molecular biological tools for the efficient expression of fungal lytic polysaccharide monooxygenases in *Pichia pastoris*

Lukas Rieder, Katharina Ebner, Anton Glieder, Morten Sørlie

Status: Published in Biotechnology for Biofuels

Paper II:

Kinetic characterization of a putatively chitin-active LPMO reveals novel LPMO functionalities and demonstrates the absence of monooxygenase activity

Lukas Rieder, Dejan M. Petrović, Priit Valjamae, Vincent G.H. Eijsink, Morten Sørlie

Status: Submitted to ACS catalysis

Paper III:

Fast and specific peroxygenase reactions catalyzed by fungal mono-copper enzymes

Lukas Rieder, Anton A. Stepnov, Morten Sørlie, Vincent G.H. Eijsink

Status: Submitted to J. Am. Chem. Soc.

Other publications by the author:

Eukaryotic expression systems for industrial enzymes

Lukas Rieder, Nico Teuschler, Katharina Ebner, Anton Glieder

Status: Published in Industrial Enzyme Applications

1 Introduction

1.1 Oxygen

1.1.1 Boon and bane

Molecular oxygen or dioxygen (O_2) is a diradical and accounts for about 21% of the molecules in our atmosphere. Oxygen levels in the atmosphere increased dramatically around 2.4 billion years ago, resulting in the mass extinction of anaerobic life forms in the so-called Great Oxidation Event (GOE). The GOE was caused by the photosynthetic activity of cyanobacteria in the primordial soup, which produced vast amounts of O_2. Although photosynthesis existed before the GOE, most of the produced O_2 was reduced by oxygen sinks and so never reached the atmosphere [1], [2]. After the initial mass extinction, the increased atmospheric oxygen levels led to the emergence of multicellular organisms that use the oxidative breakdown of glucose into H_2O and CO_2 as their main source of energy, enabling the shift from anaerobic to aerobic life.

However, activated oxygen also has a dark side because under certain conditions it can give rise to very potent oxidants. These so-called reactive oxygen species (ROS) are very electrophilic (i.e., strong oxidants) and include the singlet states of molecular oxygen as well as the various oxygen-centered radicals that are formed during the reduction of O_2 to H_2O (**Figure 1**). Molecular oxygen has two singlet states, known as singlet state 1 ($^1\Delta_g$) and singlet state 2 ($^1\sum_g^+$), both of which are energy-rich non-radicals with a total spin state of 0 because one of the antibonding pi orbitals is fully occupied (in the $^1\Delta_g$ state) or two antibonding pi orbitals are filled antiparallel ($^1\sum_g^+$). This allows singlet oxygen to react spontaneously with organic compounds. Fortunately, the singlet states are not very stable and the overwhelming majority of O_2 molecules in our atmosphere are in the inert triplet ground state ($^3\sum_g^-$) in which the antibonding pi orbitals are occupied by two electrons with parallel spins, resulting in a total spin state of +1 [3]. The electronic configuration of the triplet state prevents molecular oxygen from reacting spontaneously (i.e., oxidizing) with most organic compounds because such reactions are spin-forbidden. To overcome this barrier, oxygen can be activated by a one-electron reduction (which may, for example, happen upon interacting with a transition metal ion), which is the first step in the reduction of O_2 to H_2O. However, the reduction of oxygen in the triplet ground state to the superoxide radical anion, $O_2^{\bullet-}$, is an endergonic process (redox potential -0.33 V vs. SHE at pH 7.0, $\Delta G° > 0$), making this essential first step in the combustion of organic matter inaccessible [4]. Once $O_2^{\bullet-}$ has been formed, its reduction to H_2O_2 (+0.89 V vs. SHE, pH 7.0) via the transfer of one electron and two protons is strongly exergonic ($\Delta G° < 0$), as are all subsequent reactions leading to the formation of H_2O. Despite being a potent oxidant (+0.38 V vs. SHE, pH 7.0), H_2O_2 is a rather

stable molecule under physiological conditions and is an important messenger compound in the cell network [5]. However, one additional proton-coupled electron transfer to H_2O_2 results in the formation of one H_2O and the hydroxyl radical ($OH^\bullet$), which is a potent oxidant (+2.33 V vs. SHE, pH 7.0) and can cause substantial oxidative damage to organic compounds. A fourth one-electron reduction of $OH^\bullet$ together with a proton transfer results in the formation of the fully reduced final product, H_2O [6].
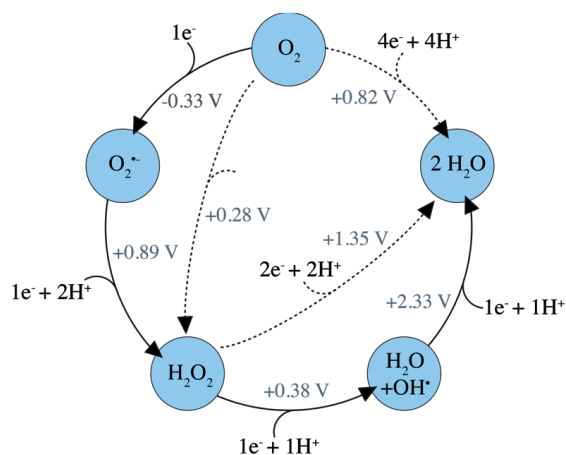

Figure 1. Reduction cycle from molecular oxygen to water showing all intermediate ROS and the reduction potentials at pH 7.0 vs. SHE. Figure adapted from Bissaro *et al.* [7]

1.1.2 Oxidoreductases

In nature, the oxidative power of O_2 is harnessed by enzymes belonging to the oxidoreductase family, which is a highly diverse class that includes all redox-active enzymes that catalyze the transfer of electrons from a donor molecule (the reductant) to an acceptor molecule (the oxidant). The electron transfer process usually involves a cofactor in the enzyme's active site, although this is not always the case [8]. The cofactor is often a metal ion (Cu, Fe, Mn) or a structure incorporating a complex organic moiety such as a heme or flavin group [9]. Its role is to allow electrons to be "stored" in the active site while the protein scaffold directs the stored electrons to the correct position to accomplish stereo and regiospecific oxidation/reduction of the substrate.

Cellular defense mechanisms against ROS involve superoxide dismutases (SODs), which are copper-, zinc-, or manganese-containing enzymes that catalyze the formation of H_2O_2 and O_2 from the reactive $O_2^{\bullet-}$ [10]. Similarly, the heme- or manganese-containing catalases catalyze the

conversion of H_2O_2 into H_2O and O_2 [11]. Enzymes of both classes thus play key roles in preventing oxidative damage to the genome and other critical cell structures.

Although ROS present a risk of damage to cellular components, the controlled activation of O_2 is central to many enzymatic reactions involved in cellular metabolism. Enzymes that activate O_2 for incorporation into a substrate are called oxygenases [12]. A well-known class of monooxygenases are the cytochrome P450 monooxygenases (CYPs), which catalyze the insertion of an oxygen atom into otherwise inert C-H bonds (R-H + O_2 → R-OH + H_2O) in a wide range of organic compounds. This reactivity plays a central role in many processes including drug metabolism in the human body. CYPs are also extremely interesting industrial biocatalysts for the synthesis and valorization of natural products [13]. Key to their catalytic mechanism is the reaction of a reduced Fe(II) ion in the center of a heme group with an O_2 molecule to form a Fe(III)-OO$^•$ complex. The Fe(III) complex is the enzyme's resting state, and the formation of the reactive oxygen species is dependent on an external reduction system that uses NAD(P)H as an electron source. The transfer of an additional electron and double protonation of the Fe(III)-OO$^•$ complex results in the formation of a highly reactive Fe(IV)=O complex known as Compound I, which is the intermediate involved in substrate oxidation. The resting Fe(III) state is regenerated after product release [14].

Similarly, the electrophilic H_2O_2 can be used by peroxygenases to catalyze the oxidation of organic molecules. Like CYPs, fungal unspecific peroxygenases (UPOs) are heme-containing enzymes that insert an oxygen molecule into their substrates (R-H + H_2O_2 → R-OH + H_2O). However, in contrast to the CYPs, the iron center in the active site of the UPOs does not require reduction because the H_2O_2 interacts directly with the resting Fe(III) state to form an Fe(III)-OOH$^-$ complex (Compound 0), which is then heterolytically cleaved under electron re-arrangement to form the Compound I intermediate required for substrate oxidation [15]. It thus appears that the peroxygenase pathway is less complex and more efficient than the monooxygenase pathway.

1.2 Carbohydrates

Carbohydrates make up most of the biomass on our planet and are one of the four main classes of biomolecules along with proteins, nucleic acids, and lipids. Carbohydrates, also known as saccharides or sugars, follow generally but not necessarily the molecular formula of $C_n(H_2O)_n$, whereby n > 3 is required. The hydroxylated aldehyde and ketone compounds with five- or six carbon atoms then usually form five- or six-membered rings of carbon and oxygen atoms known as pentoses (e.g., fructose) and hexoses (e.g., glucose), respectively.

These monosaccharides, can subsequently be covalently linked via condensation reactions that give rise to so-called glycosidic bonds, resulting in the formation of dimers (n = 2), oligomers (n ≤ 12), or larger polymers (n > 12) known as polysaccharides. The glycosidic bond is one of the strongest bonds found in Nature and its formation is catalyzed by glycoside transferases (GTs) that transfer the sugar moiety of an activated sugar donor onto polysaccharides and other molecules such as proteins. Since the glycosidic bonds in sugar polymers can be formed at different positions of the carbon ring and be in either the α or the β configuration relative to the anomeric C1 carbon, the names of carbohydrate dimers, oligomers, and polymers usually specify the orientations and positions of the carbon atoms involved in the glycosidic bonds (e.g., β-1,4).

Due to the enormous diversity of available monomers and possible linkages, the polysaccharides are highly diverse and fulfill a great variety of functions. For example, they are important for structural integrity (e.g., in plant cell walls), energy storage (in the form of starch and glycogen), and complex processes such as cell-cell communication [16].

1.2.1 Cellulose

Cellulose is the most abundant polymer on earth and occurs naturally in the cell walls of plants or as an exopolysaccharide produced by some bacteria. Whatever its origin, cellulose is a linear homopolymer consisting of repeating cellobiose units. Cellobiose is a homodimer of two β-1,4-linked β-D-glucose monomers that are rotated 180° with respect to one-another (**Figure 2**). The linear cellulose chains have lengths ranging from a few hundred to serval thousand repeating units and aggregate into linear crystalline structures and less crystalline more amorphous regions. The microfibrils are held together by strong intramolecular hydrogen bonds and van der Waals forces, making cellulose insoluble and robust.
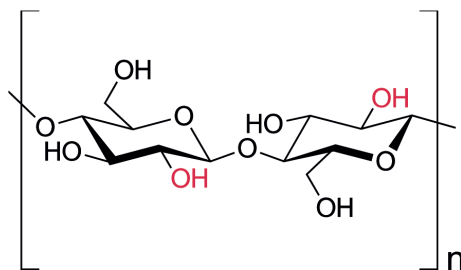

Figure 2. Schematic representation of the repeating cellobiose unit formed by two β-1,4-linked β-D-glucose monomers rotated by 180° with respect to one-another.

The main difference between bacterial and plant-based cellulose is the hydrogen bonding that interconnects the polysaccharides, which causes bacterial cellulose to have a more crystalline appearance than plant-derived cellulose and different chemical properties including greater hydrophilicity [17]. However, most existing cellulose originates from plants and is found in plant cell walls. The plant cell wall consists of three main layers known as the middle lamella and the primary and secondary cell wall (**Figure 3**). In addition to cellulose (35-50%), plant cell walls contain non-cellulosic polysaccharides such as xylan and mannan, which are collectively known as hemicelluloses (10-25%), as well as the polyphenolic material lignin (20-35%), which is mainly formed from paracoumaryl alcohol, coniferyl alcohol, and sinapyl alcohol. All three polymers are found in the primary and secondary cell wall and collectively confer rigidity and resistance to external degradation. The exact structural and chemical composition of the cell wall differs between layers and also between plant species, tissues, and growth phases. On average, it is valid to say that hardwoods have a higher cellulose content than softwoods, and that softwoods are richer in lignin than hardwoods [18].
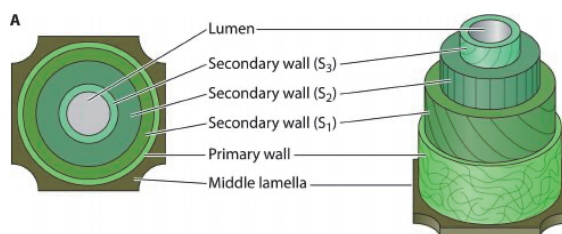
Figure 3. Schematic illustration of the structural composition of the plant cell wall. Figure taken from Rytioja *et al.* [18]

1.2.2 Chitin

Chitin is the second most abundant polymer on earth and exists mainly as a structural component of the fungal cell wall and the exoskeletons of arthropods. It is a homopolymer consisting of repeating β-1,4- linked N-acetyl-D-glucosamine (GlcNAc) monomers. The GlcNAc monomer is a derivate of glucose in which the hydroxyl group (OH) at the C2 carbon atom is substituted with an acetamide group (C_2H_4NO) (**Figure 4A**). As in cellulose, every second monomer in the chitin polymer is rotated 180° relative to its two nearest neighbors. The resulting repeating chitin dimer is called chitobiose.

Three main crystalline forms of chitin exist in nature. The most common is α-chitin, which is isolated from arthropods or shrimp shells. In α-chitin, the chains are aligned in an antiparallel manner with strong inter- and intra-chain hydrogen bonds. β-chitin is mainly found in squid

pens and features chain arranged in a parallel manner with a weaker hydrogen bonding network connecting the sheets, resulting in a more open structure than α-chitin. The last form is γ-chitin, which has both parallel and antiparallel chains and is mainly isolated from fungi and yeasts (**Figure 4B**) [19].
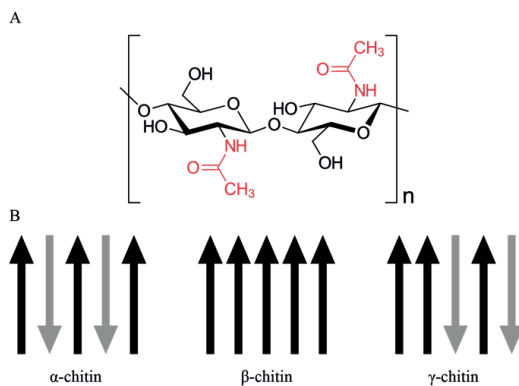

Figure 4. (A) Schematic representation of the repeating chitobiose unit formed from two β- 1,4- linked N-acetyl-D-glucosamine monomers that are rotated 180° with respect to one-another. (B) Chain arrangements found in naturally occurring chitin polymers.

1.3 Enzymatic degradation of recalcitrant biomass

Carbohydrates are omnipresent and available in almost unlimited quantities, making them a potent and sustainable energy source. Unsurprisingly, evolution has adapted organisms from every kingdom of life to use carbohydrates as their prime source of energy. Since most carbohydrates occur in large polymeric structures, Nature has developed different strategies for their extracellular degradation and subsequent transport into cells.

Anaerobic cellulose-degrading bacteria and fungi may degrade and take up extracellular carbohydrates using a multi-enzyme complex known as a cellulosome that is attached to the cell wall [20]. Alternatively, bacteria may express genes within polysaccharide utilization loci (PULs) – clusters of co-regulated and expressed genes whose products are arranged onto the inner and outer membrane of the host and allow to detect, digest, and transport complex carbohydrates. Specialized PULs have been described for the degradation and uptake of cellulose [21], hemicellulose [22] and chitin [23].

In aerobic living organisms, the enzymatic degradation process is based on the secretion of free enzymes into the extracellular space (**Figure 5**). These enzyme cocktails contain a variety of hydrolytic enzymes belonging to several different families, and their secretion is regulated at the transcriptional level [24]. A potential drawback of this approach is that the generated accessible sugars are available to competing organisms. Bacterial secreted enzyme cocktails for

the synergistic degradation of lignocellulose [25] and chitin [26] have been described, along with similar fungal cocktails for lignocellulose degradation [27]. The hydrolytic enzymes in these cocktails are classified as exo- or endo-active depending on their mode of action. As their name suggests, exo-active enzymes attack the polymer from the reducing or non-reducing ends. Notable exo-active enzymes include Cel7A and the Cel6A from *Trichoderma reesei*, which degrade cellulose [28], and ChiA and ChiB from *Serratia marcescens* [26], which act on chitin. Endo-active enzymes attack polymers in amorphous regions; examples include Cel5A from *T. reesei* [29] and ChiC from *S. marcescens* [30]. The degradation of lignocellulose also involves GHs that specifically target hemicellulose, such as xylosidases and mannosidases [31]. The final degradation of the cello/chitiobiose is catalyzed by beta-glucosidase [27] and chitobiase [26], respectively. However, hydrolytic enzymes alone cannot completely degrade complex crystalline biomass, which requires the action of the oxidoreductases as outlined by Bissaro *et al.* [7].
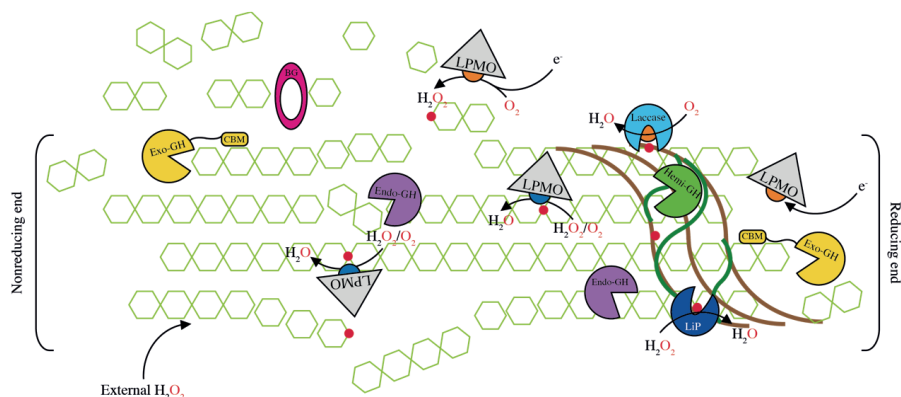
Figure 5. Illustration of the synergistic degradation of lignocellulosic biomass by exo- (yellow) and endo-active (purple) cellulases and hemicellulases (green). The depolymerization process is supported by oxidoreductases such as LPMOs (grey) and lignin modifying (per)oxidases (blue).

As mentioned previously, lignocellulosic biomass contains the polyphenolic material known as lignin as well as sugar-based (hemi)cellulose. Lignin modification is catalyzed by (per)oxidases. Like the previously mentioned per(oxygenases), (per)oxidases are oxidoreductases that depend on co-factors and use either H_2O_2 or O_2 as the final electron acceptor. However, unlike (per)oxygenases, (per)oxidases do not catalyze the insertion of an oxygen atom into the substrate. Lignin-modifying peroxidases that catalyze the reaction 2 R-OH + H_2O_2 → 2 R=O + 2 H_2O were discovered about 30 years ago include manganese (MnPs), lignin (LiPs), and versatile (VPs) peroxidases. Interestingly, the MnPs and the LiPs modify lignin via fundamentally different mechanisms: the heme-containing LiPs interact directly with the

polymer to oxidize its non-phenolic components, whereas the MnPs catalyze the oxidization of the Mn(II) co-factor to Mn(III), which is then released and forms complexes that penetrate into the polymer structure to oxidize the phenolic lignin compounds. The VPs share features of both MnPs and LiPs, and catalyze the oxidation of phenolic and non-phenolic compounds. Another important group of oxidases involved in the depolymerization of lignin are the multicopper-dependent laccases, which catalyze the reaction $4\,R\text{-}H + O_2 \rightarrow 4\,R\cdot + 2\,H_2O$. Laccases interact directly with and oxidize phenolic compounds while simultaneously reducing O_2 to H_2O [32].

More recently, a class of mono-copper enzymes was discovered that interact directly with the surface of crystalline sugar polymers in biomass to create new entry points for hydrolytic degradation, dramatically increasing the efficiency of the enzymatic saccharification process [24], [33]–[35]. These enzymes are known as Lytic Polysaccharide MonoOxygenase (LPMOs) and their powerful oxidation mechanism is the main subject of investigation in this thesis.

1.4 Lytic polysaccharide monooxygenases

1.4.1 History

The idea of a biphasic system for the synergistic degradation of cellulosic biomass was first proposed about 70 years ago by Reese *et al.*, who speculated about the role of non-hydrolytic enzymes in cellulose degradation and the possibility that organisms that can utilize cellulose for growth may do so using a biphasic system. This idea became known as the C_1-C_x theory; put simply, it hypothesizes the existence of a C_1 system that catalyzes the breakdown of crystalline cellulose into a more accessible substrate for the C_x system, which releases oligomers that can be used by the organism as a carbon source [36].

This idea was refined in 1974 by Eriksson *et al.*, who showed that cellulose degradation is more efficient in the presence of oxygen and therefore speculated that oxidoreductases are involved in the depolymerization process [37]. A milestone was achieved in 2005 when it was shown that a 21 kDa protein (CBP21) from *S. marcescens* designated as CBM33 drastically boosted the degradation of chitin in the presence of chitinases [38]. Another breakthrough was made in 2010, when Vaaje-Kolstad *et al.* discovered that the CBM33 protein characterized in the 2005 study did indeed oxidize the glycosidic bonds of a chitin polymer, resulting in the release of oxidized chitin oligomers. This confirmed that CBP21 was truly the first member of a new class of oxidoreductase [39].

These results were quickly followed by the discovery that oxidation of cellulosic substrates is also promoted by another CBM33 protein from *Streptomyces coelicolor (Sc*AA10C/CelS2*)* [40], and members of the GH61 family from *Thermoascus aurantiacus (Ta*AA9A*)* [41] and

Neurospora crassa (*Nc*AA9D, *Nc*AA9E, *Nc*AA9M) [42]. It was thus confirmed that synergistic interactions between oxidoreductases and hydrolytic enzymes are widely exploited in Nature for the efficient degradation of recalcitrant biomass.

Despite their undisputed role in supporting the degradation of complex biomass, it is unlikely that all LPMOs found in nature are primarily involved in the cellulolytic/chitinolytic machineries because some organisms have over 50 genes encoding potential LPMOs [43]. This conclusion is further supported by the observation that bacterial chitin active LPMOs are expressed in ecological niches that do not require chitin degradation [44] and seem to have key roles in the virulence functions of *Pseudomonas aeruginosa* [45]. Similarly, there is evidence that AA9-type LPMOs may be involved in plant pathogenicity [46], and transcriptome studies showed that an AA11-type LPMO is expressed in the fruiting body during the final stage of spore formation in *N. crassa* [47].

1.4.2 Classification

The CAZy database (http://www.cazy.org) includes all currently available information on enzymes that are known (on the basis of biochemical characterization) or suspected (on the basis of bioinformatic analysis) to be involved in the formation, degradation, and modification of glycosidic bonds. The CAZy classifications are based on sequence similarity and distinguish between glycoside hydrolases (GHs), glycosyltransferases (GTs), polysaccharide lyases (PLs), carbohydrate esterases (CEs), and auxiliary activities (AAs).

The largest enzyme family represented in CAZy is the GHs, for which there are over 900 000 entries (April 2021). The LPMOs, which are the focus of this thesis, belong to the most recently introduced AA family [48], which has around 17542 sequence entries (April 2021). Despite having very similar overall structures and activities, LPMOs are subdivided into seven (AA9-AA11 and AA13-AA16) distinct subfamilies that collectively include around 48 % (8359) of the entries in the AA family. Interestingly, only 65 enzymes (<1 %) in this family have been successfully expressed and characterized as of the time of writing (April 2021). An overview of the different families and the enzymes they contain is presented in **Table 1**.

The AA10 family includes cellulose-, hemicellulose-, and chitin-active LPMOs that oxidize 1,4-linked polysaccharides at either the C1 or the C4 position of the scissile glycosidic bond connecting the sugar monomers (see explanation below). The enzymes classified into this subfamily are usually of bacterial origin and were classified as CBM33 proteins before the discovery of LPMOs [39].

The potentially most diverse LPMO family is the AA9s, which emerged from the GH61 family. The members of this family are typically of fungal origin and cleave glycosidic bonds in cellulose by catalyzing oxidation at either the C1 position, the C4 position, or both. Based on the number of characterized enzymes, AA9s appear to be the dominant LPMO family in fungi. However, recent studies have shown that the AA11 family containing chitinolytic C1 oxidizers is the most widespread and probably oldest LPMO family within fungi [49]. Despite their omnipresence in fungal genomes, only a few AA11 enzymes have been biochemically characterized [50]–[52].

Other fungal LPMOs families are the AA13s, AA14s and AA16s, which are described as C1-oxidizing LPMOs active on starch, xylan, and cellulose, respectively [53]–[55]. The AA15 family that includes chitin and cellulose active C1 oxidizing enzymes is probably the most exciting in terms of novel biological functions and substrate specificities because members of this group have been discovered in viral genomes and higher eukaryotes.

Table 1. Overview on the LPMO families found in the CAZy database including the origin, substrate specificity, regioselectivity, number of potential sequences and number of characterized enzymes. Data obtained from: http://www.cazy.org (April 2021).

Family	Origin	Substrate	Regioselectivity	Sequences	Characterized
AA9	Fungal	Cellulose	C1 and/or C4	596	26
AA10	Archean, Bacterial, Eukaryotic, Viral	Cellulose, Chitin, Xylan	C1, C4	6339	30
AA11	Bacterial, fungal	Chitin	C1	159	1
AA13	Fungal	Starch	C1	29	4
AA14	Fungal	Xylan	C1	25	2
AA15	Eucaryotic, Viral	Cellulose, Chitin	C1	267	2
AA16	Fungal	Cellulose	C1	44	1

1.4.3 Structure and other conserved features

1.4.3.1 Domain architecture and surface topology

Based on their domain architectures, LPMOs can, in parallel to their classification into families, be broadly categorized as either single domain or multidomain enzymes. Single domain LPMOs such as *Sm*AA10A [56] or *Ls*AA9A [57] consist, as the name implies, of only the catalytic domain whereas multidomain LPMOs such as *Sc*AA10C [40] or *Nc*AA9C [58] have a carbohydrate binding module (CBM) attached via a linker region.

Regardless of their domain architecture, all LPMOs have very similar catalytic domains with an overall globular shape containing an immunoglobulin-like β-sheet core that stabilizes the

enzyme scaffold [59], [60]. One structural characteristic of LPMOs is the flat surface surrounding the monocopper active site, which is found in most of the discovered enzymes belonging to the AA9 and AA10 families, whose structures are exemplified by *Nc*AA9M (PDB: 4EIS [61]) and *Sm*AA10A (PDB: 2BEM [56]) (see **Figure 6A, B)**. This flat surface is the point of interaction between the protein scaffold and the carbohydrate substrate and is thus highly important for catalysis [62], [63]. Extensive studies of LPMOs and their substrates have shown that several surface exposed amino acids such as Tyr54 and Asp182 in *Sm*AA10A (PDB: 2BEM) or Tyr24 and Tyr210 in *Nc*AA9M (PDB: 4EIS) are essential for the formation of the hydrogen bonding network that causes tight confinement of the enzyme and substrate while also enabling the formation of the reaction cave in which catalysis occurs [61], [62]. Studies of X-ray crystal structures moreover indicate that binding to the sugar substrate changes the position of the copper center because a hydroxyl group of the polymer occupies its available axial position. This suggests that the oxygen-donating co-substrate binds in the available equatorial position of the copper center [57].

However, it appears that some of the newly discovered LPMO families lack the classical flat surface topology. Over evolutionary history, LPMOs that oxidize substrates other than cellulose and chitin have adapted to ensure efficient substrate recognition and oxidation. This is illustrated by the starch-active AA13 family [53]. Based on the X-ray structure of *Ao*AA13 (PDB: 4OPB [64]), it appears that their surface is more grooved and asymmetric (**Figure 6D**), making it better adapted for the oxidation of the helical starch polymer and its α-1,4 glycosidic bonds [64]. Similarly, the AA11 family seem to have an unusual convex and grooved surface that lacks the previously mentioned aromatic amino acids, as exemplified by the structure of *Ao*AA11 (PDB: 4MAI, **Figure 6C).** This is somewhat unexpected since these enzymes are categorized as being active towards crystalline chitin [50]. However, the AA11s appear to be a rather diverse and old family of LPMOs that may have functions beyond carbohydrate depolymerization [49].

The surfaces of the known enzymes of the AA14 family (**Figure 6E**) seem to be even more highly adapted to specific substrates. This specialization is exemplified by *Pc*AA14B (PDB: 5NO7), which was reported to be exclusively active towards the highly crystalline twofold xylan screw that covers the cellulose in plant cell walls [54]. Interestingly, it appears that the substrate binding surface can also be diversified: *Td*AA15A (PDB: 5MSZ), which is currently the only AA15 member with a published structure, has a completely symmetrical surface with aromatic amino acids on each side of the active site, allowing it to oxidize both cellulose and chitin **(Figure 6F**). Based on this observation, it was suggested that the AA15 from the eukaryotic host *Thermobia domestica* evolved over time into a multipurpose enzyme with functions in animal development and food digestion [65].

Despite the different substrate specificities associated with the different LPMO families, several enzymes that are categorized as cellulose active (e.g., *Nc*AA9C, *Nc*AA9M, and *Ls*AA9A) are also active on hemicelluloses. This is probably related to the presence of specific loop structures on the surface close to the active site [66]–[68]

A
Family: AA9

*Nc*AA9M
PDB:4EIS

B
Family: AA10

*Sm*AA10A
PDB: 2BEM

C
Family: AA11

*Ao*AA11
PDB: 4MAI

D
Family: AA13

*Ao*AA13
PDB: 4OPB

E
Family: AA14

*Pc*AA14B
PDB: 5NO7

F
Family: AA15

*Td*AA15A
PDB: 5MSZ
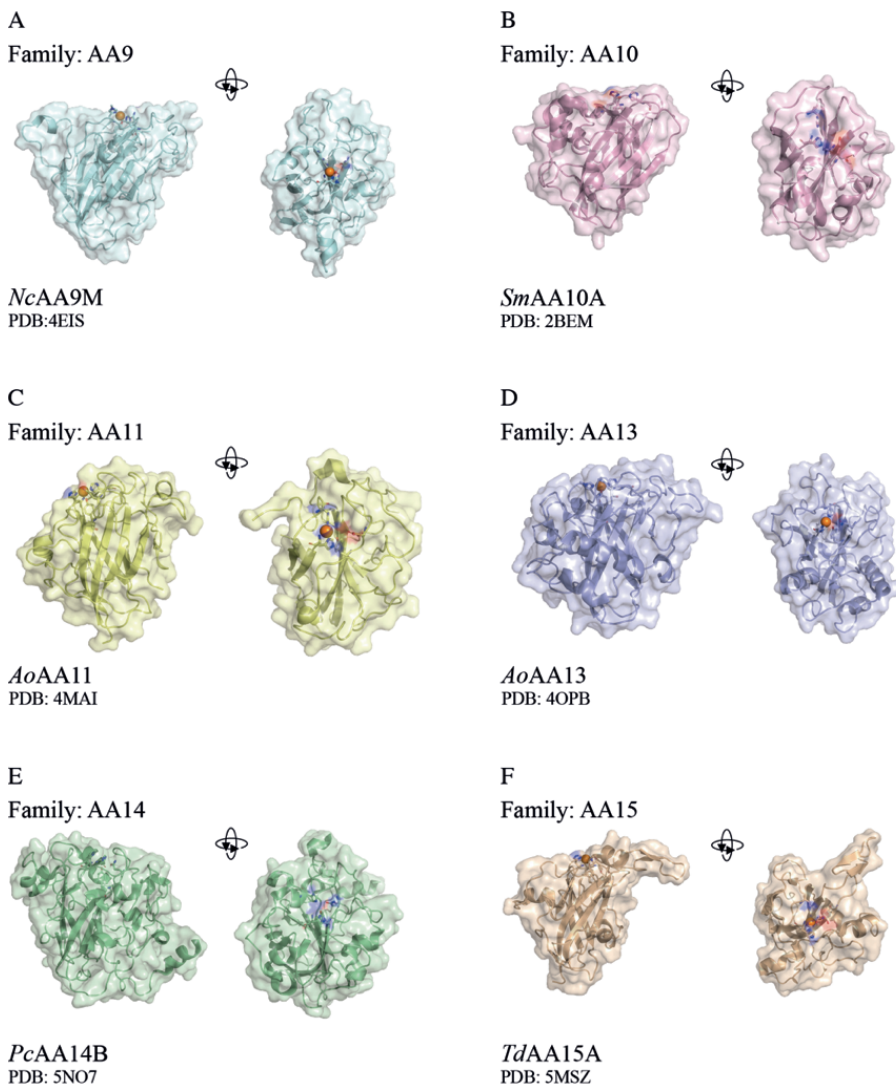
Figure 6. Surface topologies found in the different LPMO families. The enzymes are shown in carton representation with transparent surfaces (60%). The His-brace and aromatic amino acids in the axial position are shown as sticks. The metal centers are displayed as orange (copper) or purple (Zn) spheres. All enzymes were aligned in either a front side view with the N-terminal histidine to the left and the beta-sheet core in a vertical position relative to the page or in a top view showing the substrate binding surface. Enzyme structures were prepared in PyMOL.

1.4.3.2 Oxidation of soluble carbohydrates

In addition to their activity on recalcitrant polysaccharides, it has been reported that some LPMOs catalyze the oxidation of oligomeric carbohydrates. These enzymes are of special interest in this thesis because they are more amenable to detailed kinetical analysis than classical LPMOs active on crystalline polymers. This is because reaction products of soluble oligomeric substrates are easier to quantify.

While it is not completely clear why some LPMOs can oxidize soluble oligomers while others cannot, it seems likely that this ability is related to the properties of the substrate binding surface. Well-studied enzymes of the AA9 family with this ability include *Nc*AA9C (PDB: 4D7U), *Cv*AA9A (PDB: 5NLT) and *Ls*AA9A (PDB: 5ACI) [69], [70]. Interestingly, it was also found that *Sm*AA10A can oxidize chitohexaose but not very efficiently [62].

Crystal structures are available for all of the AA9 enzymes mentioned above. Additionally, *Ls*AA9A has been co-crystalized with a cellohexaose bound close to the active site, enabling study of its enzyme-substrate interactions [57]. By superimposing their structures on one-another and comparing them, it was discovered that all these enzymes have very similar surface topologies with a strikingly convex and rugged substrate binding surface (**Figure 7**). Additionally, their surfaces feature loop structures that protrude from the plane of the active site and appear to flank the bound substrate. Interestingly, sequence alignments indicate that the protruding L3 loop in *Nc*AA9C has an insertion that is absent in other AA9 enzymes lacking activity against oligomeric carbohydrates [68], [71]. The corresponding L3 regions of *Ls*AA9A and *Cv*AA9A have no additional surface loops; instead, their crystal structures feature protrusions in the area of the L8 loop [70]. These loops contrast with the flat surfaces typically found in AA9 and AA10 enzymes (**Figure 6A, B**). A recent study by Frandsen *et al.* concluded that eight amino acids on the surface of *Ls*AA9A (Asn28, His66, Asn67, Ser77, Glu148, Asp150, Arg159, Tyr203) are critical for interactions with soluble cello-oligomers [68]. Interestingly six of these amino acids exist within the L3 and L8 loops, while the other two lie within the L2 (Asn28) and the LC loops (Tyr203). Both the L2 and LC loop regions were previously reported to play critical roles in substrate interaction and regioselectivity [70], [72].
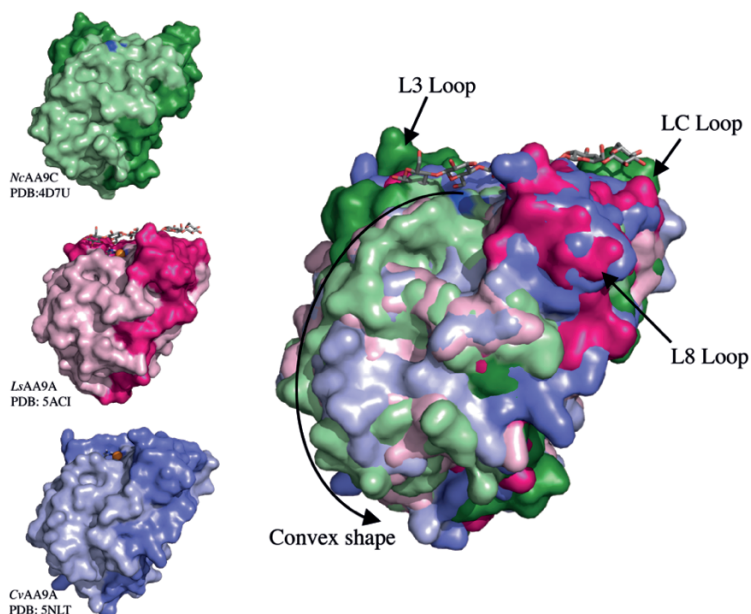
Figure 7. Comparison of the convex and rugged surface topology of *Nc*AA9C (green), *Ls*AA9A (red) and *Cv*AA9A (blue). The arrows and darker shades indicate loop structures potentially important for binding of soluble substrates. All enzymes are identically aligned with the N-terminal histidine to the left. The active site copper center is shown as orange sphere and the cellohexaose polymer which is part of the crystal structure of *Ls*AA9A is shown as brown sticks. Enzyme structures were prepared in PyMOL.

1.4.3.3 Regioselectivity and product detection

It appears that the secret of LPMO catalysis is the correct positioning of the protein scaffold with the copper center in close proximity to the glycosidic bond. The surface thus controls both substrate specificity and the regioselective oxidation of the carbon atoms in the scissile bond. If oxidation occurs at the C1-carbon at the reducing end of the newly formed substrate chain, the LPMO is categorized as a C1 oxidizer. Conversely, if the oxidation occurs at the C4-postion at the nonreducing end of the new polymer, the LPMO is classified as a C4 oxidizer (**Figure 8**). All known LPMOs active on chitin are exclusively C1 oxidizing, but cellulose-active enzymes can oxidize either the C1 or the C4 position or produce mixtures of both products. Independently of the substrate, oxidation of the C1 carbon results in the formation of a 1,5-δ-lactone that undergoes spontaneous hydrolysis to form a more stable aldonic acid [39], [73]. For LPMOs catalyzing C4 oxidation, the first product is a 4-ketoladose that then reacts to form a gem-diol, which is the most stable form of the product in an aqueous environment [42], [69].

Matrix-assisted laser desorption ionization time-of-flight mass spectrometry (MALDI-ToF MS) and high-performance anion exchange chromatography with pulsed amperometric detection

(HPAEC-PAD) are the techniques most commonly used to detect LPMO reaction products. The advantage of MALDI-ToF analysis is that it is fast and substrate oxidation is usually easy to recognize due to the regular pattern of products with different degrees of polymerization (DP): oxidized products in the lactose and ketoaldose forms will have 2 m/z units less than the native polymer whereas the aldonic acid and gem-diol species will have 16 m/z units more than the native polymer. However, regioselectivity cannot not be distinguished by MALDI-ToF analysis because C1- and C4-oxidized reaction products have identical masses [69]. In contrast, HPAEC-PAD analysis can discriminate between these oxidation products and thereby determine regioselectivity because they will elute after different retention times [74]. Additionally, HPLC analysis enables quantification of reaction products, making it the method of choice for assessing LPMO kinetics. However, HPLC analysis is time-consuming and there are innate challenges in detecting C4 oxidized products as they are rather unstable [75].
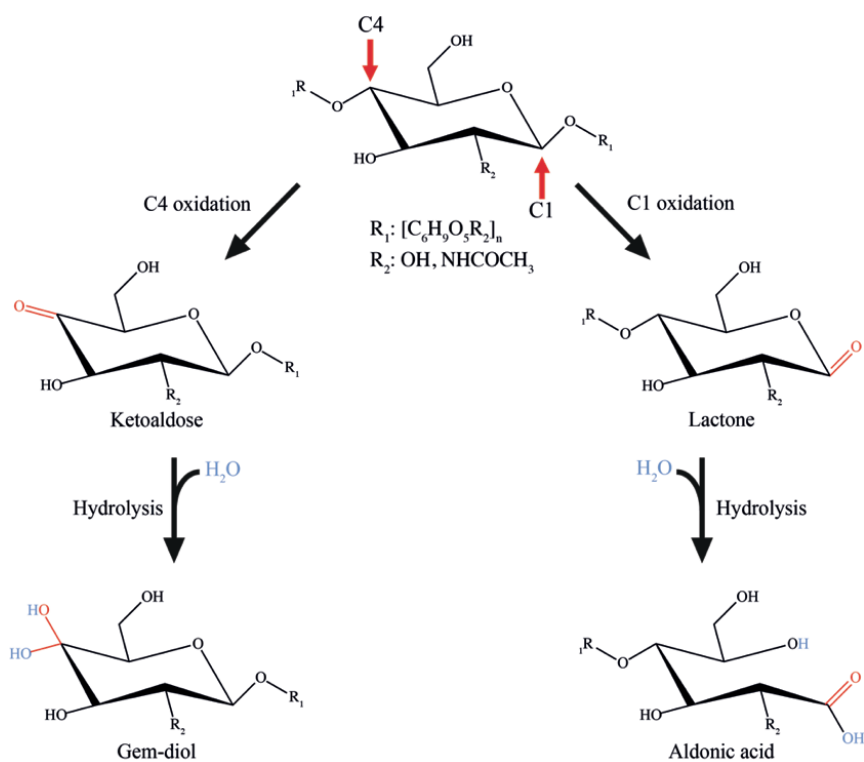

Figure 8. Products obtained from LPMO-catalyzed regioselective oxidation of the C1 or C4 carbons of scissile glycosidic bonds. The formation of the ketoaldose and lactone via C4- and C1-oxidation, respectively, is LPMO catalyzed whereas the formation of the gem-diol and aldonic acid forms results from spontaneous hydrolysis. Figure adapted from Frommhagen *et al.* [76].

1.4.3.4 The mono-copper active site

The most characteristic feature of LPMOs is the surface-exposed active site formed by a pair of highly conserved histidines that coordinate a single copper atom in a T-shaped configuration known as the histidine brace (His-brace). The N-terminal histidine contributes two nitrogen ligands for copper coordination, one from the imidazole in the side chain and one from the N-terminal amino group. The third nitrogen ligand is provided by the imidazole side chain of a second highly conserved histidine [41]. The distances between a coordinating nitrogen and the copper center are typically ~2 Å (**Figure 9**). The His-brace has a strong affinity for reduced Cu(I): its k_d values are typically in the range of ~1 nM. Its affinity for Cu(II) is about 50 times lower (~50 nM) [41], [59], [77].

Due to the critical position of the N-terminal histidine in the His-brace, the correct processing of the N-terminus is indispensable for catalysis. This is particularly important for recombinant expression of LPMOs because all natural LPMO sequences include an N-terminal signal peptide that facilitates secretion to the extracellular environment. Active LPMO expression thus depends on the expression host's ability to recognize and cleave the signal peptide correctly because if any amino acid other than histidine occupies the N-terminal position in the mature LPMO, the enzyme will be inactive [78], [79]. Another interesting observation relating to expression is the posttranslational methylation of the uncoordinated nitrogen atom in the imidazole side chain in the N-terminal histidine, which is observed in fungal but not bacterial LPMOs. It is not yet clear why this posttranslational methylation occurs but it has no detectable influence on catalysis and is therefore probably related to enzyme stability; it may protect the enzyme against autocatalytic damage [80].

LPMOs are not the only enzymes with a His-brace active site architecture: the recently discovered X325 proteins [81] have a remarkably similar overall appearance to LPMOs but seem to be fundamentally different since they do not oxidize polymeric substrates, produce H_2O_2, or even oxidize AscA [82]. It was therefore suggested that they could be involved in cellular copper transportation. This is supported by the resemblance of the potential His-brace of the X325 proteins to that of the CopC protein, which is critical for copper homeostasis [81], [82]. The active sites of the LPMOs differ from the Cu-binding sites of the CopC/X325 proteins in that the latter have an additional asparagine ligand that coordinates the copper. This ligand probably prevents access to the equatorial position of the copper center, which is believed to be the oxygen binding site in the confined LPMO [81], [82].

1.4.3.5 Conserved second sphere amino acids

Besides the His-brace, some highly conserved amino acids can be found in the second coordination sphere surrounding the active site. The axial position of the copper site towards the core of the enzyme is usually occupied by a phenylalanine (Phe) in the bacterial AA10s or a tyrosine (Tyr) in fungal LPMOs (**Figure 9**). However, some exceptions exist - for example, *Sc*AA10B (PDB: 4OY8) has a Tyr instead of a Phe in the axial position [83]. Severe effects on catalysis were observed in mutation studies when the Phe was exchanged for Tyr in an AA10 and *vice versa* in an AA9, indicating the importance of these aromatic amino acids [84], [85]. It was speculated that the aromatic moieties of these amino acids may be the source of the second electron required in the monooxygenase reaction (see below), but recent studies on an AA9 have shown that the tyrosine is catalytically not relevant [86]. It is thus more likely that these amino acids are involved in protecting the enzyme from oxidative damage like the previously discussed methylation of the N-terminal histidine in fungal LPMOs. It might also be that the Phe/Tyr residues are part of an electron path formed by several aromatic amino acids spanning the core of the LPMOs [61], [64]. However, despite discussions in the literature there is currently no biochemical evidence for such a pathway**.**

Also highly conserved in all LPMO families is a position in the equatorial plane close to the copper center that is usually occupied by a glutamate (Glu) or glutamine (Gln) residue. It is typically a Gln in LPMOs of the AA9, AA13 and AA14 families (**Figure 9A, D, E**) and a Glu in AA11 and AA15-type enzymes (**Figure 9C, F**). In AA10s, however, this position does not seem to be strongly conserved; it may be occupied by a Glu or a Gln depending on whether the residue in the axial copper position is Phe or a Tyr [87]. Moreover, the AA9s have a third strongly conserved histidine(His160, **Figure 9A**) that forms a hydrogen bond to the Gln residue [60]. In addition, some exceptions exist; for example, *Sc*AA10B has a third histidine in the second sphere [83].

Although the exact role of the Glu/Gln in the reaction mechanism of the LPMOs is not yet fully understood, mutation studies have revealed significant losses of activity when it is exchanged for other residues in fungal and bacterial LPMOs [56], [63], [85], [88]. One proposed function of the Glu/Gln residues is supporting the formation and stabilization of the reactive oxygen species in the confined LPMO which could explain the significant impact on catalysis [89]–[92]. Additionally it was shown that Glu60 of *Sm*AA10 (**Figure 9B**) can occupy three distinct positions, allowing it to act as a "gate" that may regulate access/diffusion to/from the active site in the confined LPMO [62].
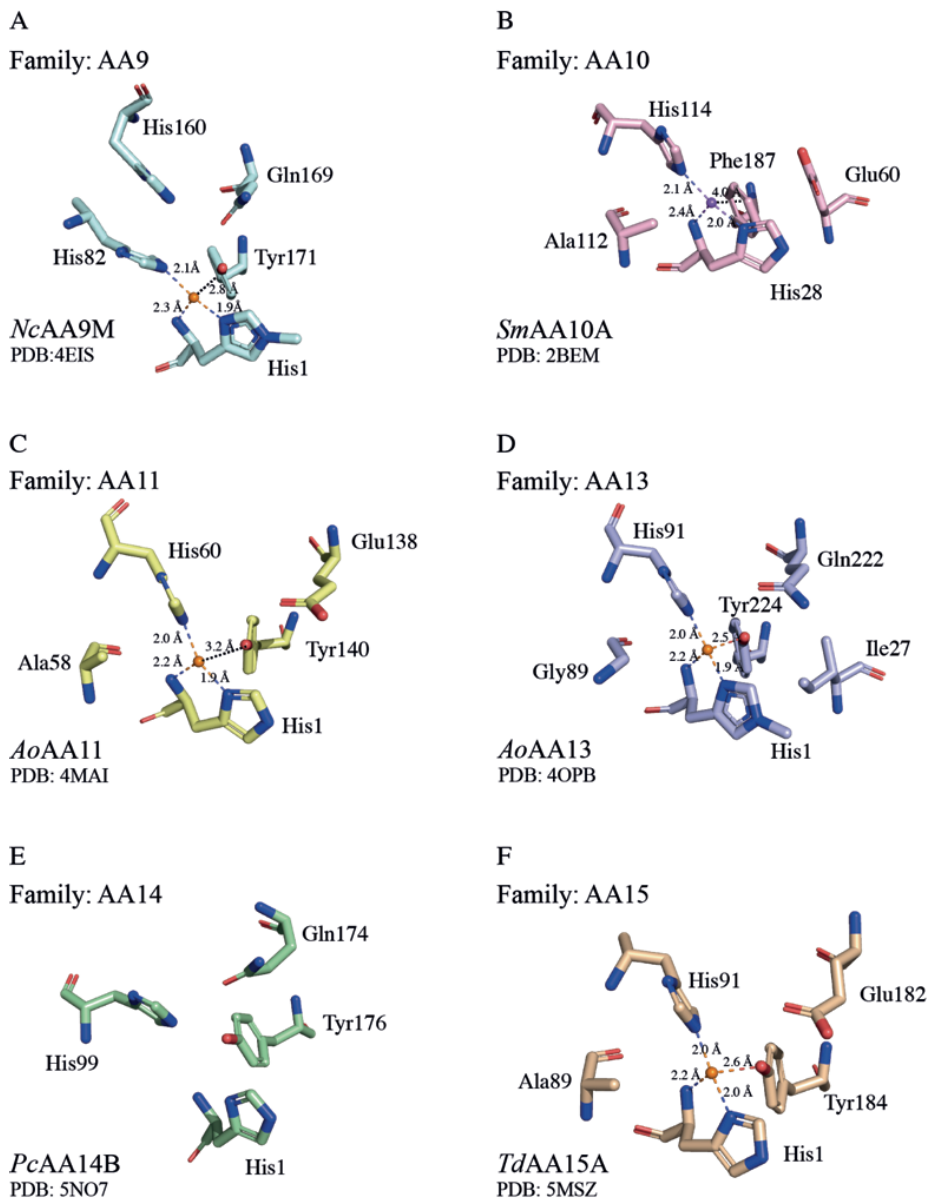
Figure 9. Overview of the active site architectures of the different LPMO families showing all amino acids within 5 Å of the metal center. The individual active sites are aligned identically with the N-terminal histidine in the bottom position and the axial aromatic amino acid pointing to the front. The distances between the copper and the coordinating histidines and between the copper and the non-coordinating phenyl/tyrosine residues are shown using dashed lines. The amino acids are shown in stick representation and metal centers as either orange (copper) or purple (zinc) spheres.

1.4.4 Catalysis

1.4.4.1 Reduction of the copper center

The initial reduction of the copper center by an external electron source is the first step in the catalytic cycle of LPMOs. Electron transfer to the oxidized inactive LPMO-Cu(II) forms the active, reduced LPMO-Cu(I) state that can then interact with the oxygen-containing co-substrate. Interestingly, unlike the cytochrome P450 monooxygenases, LPMOs are not dependent on a highly specific reduction system.

The redox potential of the LPMO-Cu(II)/ LPMO-Cu(I) redox couple ranges from +155 mV to +326 mV but values of ~+240 mV are most common, allowing the LPMOs to accept electrons from compounds with lower redox potentials [93], [94]. In combination with the surface-exposed copper center, this allows LPMOs to interact directly with many different reductants including small organic molecules like AscA [39], [95], cysteine [96], and plant-derived phenolic compounds such as gallic acid [94]. Other potential sources of electrons for LPMO activation include light-driven systems based on photo-catalysts [97], cellobiose dehydrogenase (CDH) [42], [98], and fungal cellooligosaccharide dehydrogenase [99]. However, it should be noted that the choice of reductant may profoundly affect the LPMO reaction [76], [94], [100], [101].

Recent studies have also shown that reduction supports polymer binding in addition to being necessary for LPMO activation [98], [102]. This consistent with that the initial reduction occurs prior substrate binding at the free LPMO because space limitations would prohibit direct reduction of the LPMO-substrate complex by reductants such as CDH [103].

The reduction of the copper center is synonymous with LPMO activation and is central to the formation of the reactive copper-oxygen species that ultimately oxidizes the scissile glycosidic bond. Although this concept is accepted, there is an ongoing debate about whether the incorporated oxygen originates from molecular oxygen or hydrogen peroxide.

1.4.4.2 Productive LPMO catalysis: monooxygenase vs. peroxygenase

Historically, LPMOs have been classified as monooxygenases. This classification was based on the similarity to other copper-containing monooxygenases, the monooxygenatad nature of the reaction products and the circumstance that enzymes required the presence of O_2 and an external reducing agent for substrate oxidation. [41], [42]. Interestingly, the measured rates of the monooxygenase reactions catalyzed by various LPMOs on different substrates are very similar and typically in the range of ~0.05 s^{-1}, suggesting that the reaction rate is bottlenecked by similar factors in all cases [7]. However, the monooxygenase mechanism suffers from the second electron conundrum which describes the problematic scenario than an additional

electron is required to perform substrate oxidation, but the LPMO can only store a single electron at the copper center that originates from its initial reduction [104]. The second electron must thus be delivered, with perfect timing, from another source. Since direct access to the copper site is hindered by the bound carbohydrate, it was suggested that the electron is stored in another part of the enzyme. An alternative hypothesis invoked an electron transport chain through the core of the LPMO [61]. However, no biochemical evidence has been found to support either of these hypotheses and there are no known structural features consistent with either hypothesis that are conserved across LPMO families. It was recently shown that a tunnel connecting the active site complex and solvent is formed in LPMOs upon substrate binding. While this tunnel would provide enough space for O_2 and H_2O_2 to access the active site, space limitations do not allow the access of larger molecules such as reductants [62].

In 2017, the monooxygenase classification was questioned by Bissaro *et al.*, who proposed that LPMO-catalyzed substrate oxidation depends on hydrogen peroxide. Their claim was based on biochemical evidence that supplementing LPMO reactions with H_2O_2 significantly increases the substrate oxidation rate. They also reported experiments using $H_2^{18}O_2$ under aerobic conditions (with unlabeled O_2) in which the reaction products mostly contained ^{18}O. Their results also clearly demonstrated that LPMOs are catalytically active under anaerobic conditions when supplemented with H_2O_2. Moreover, product formation was reduced when aerobic reactions were conducted in the presence of the H_2O_2-scavenging horseradish peroxidase (HRP). Based on these findings it was concluded that LPMOs are a novel class of copper-containing peroxygenases and that a true monooxygenase reaction, if it occurs at all, is probably of negligible catalytic importance [105]. Interestingly, LPMOs are not the first group of oxidoreductases found to depend on a different oxygen source to that originally proposed: the non-heme-iron-dependent epoxidase HppE was classified as an oxidase but later shown to catalyze a peroxidase reaction [106].

The first detailed kinetic study of the peroxygenase reaction catalyzed by *Sm*AA10A showed that the enzyme has a high affinity for a H_2O_2 with a K_m value of ~2 μM [95]. Moreover, the same paper reports a k_{cat} of 6.1 s-1, which is several orders of magnitudes higher than that reported by Vaaje-Kolstad *et al.* in 2010 [39]. Based on these values, the enzyme's k_{cat}/K_m is in the order of ~10^6 M-1s-1, which is similar to the values reported for fungal heme-dependent peroxygenases [107]. Similarly high turnover numbers for the peroxygenase reaction have been confirmed for several enzymes and substrates, leading to the conclusion that the H_2O_2-driven peroxygenase reaction is about three orders of magnitude faster than the monooxygenase reaction [86], [95], [108], [109]. Moreover, LPMOs tend to release products in stochiometric proportion to the amount of added H_2O_2 under peroxygenase conditions, suggesting that one molecule of H_2O_2 is

consumed per molecule of oxidized product. In addition to the higher turnover numbers, studies on the fluorescence of the copper center showed that the re-oxidation of the reduced LPMO is about three orders of magnitude faster with H_2O_2 than with O_2, indicating that reduced LPMO interacts preferentially with H_2O_2 [91].

The use of H_2O_2 as an oxygen donor in the catalytic mechanism does not just increase the rate of reaction; it also solves the second electron conundrum because the required electron and protons would originate directly from the H_2O_2. This is indeed observed in experimental settings: peroxygenase reactions require only small, priming amounts of a reductant (e.g., 20-100 µM) to reduce the copper center whereas monooxygenase reactions are typically performed with 1 mM reductant [39], [105] The peroxygenase reaction thus appears to be less dependent on the reductant, which is also reflected by the finding that under peroxygenase conditions, LPMOs perform 15 to 20 catalytic cycles before returning to the inactive (re-oxidized) LPMO-Cu(II) state [108], [110], [111].

The mechanism by which LPMOs achieve hydrogen atom abstraction in the monooxygenase and peroxygenase mechanisms is not yet fully understood. Several mechanisms for the O_2- and H_2O_2-driven reactions have been proposed since the discovery of LPMOs, as reviewed by authors including Walton & Davies [90] and Chylenski *et al.* [112]. Independent of the oxygen donor, the catalytic cycle starts with the reduction of the copper center to form an LPMO-Cu(I). The oxygen donor and carbohydrate substrate then bind to the enzyme. In the presence of O_2, this may result in the formation of an LPMO-Cu(II)-OO• superoxo intermediate [113]–[115]. A proton-coupled electron transfer is then proposed to occur, resulting in an LPMO-Cu(II)-OOH complex. A second electron transfer would then result in the loss of a water molecule and the formation of an LPMO-Cu(II)-O• complex (**Figure 10, top**) [113], [114]. If H_2O_2 is the oxygen donor, the interaction with the reduced LPMO could result in the formation of an LPMO-Cu(II)-OH species and an •OH radical stabilized by the enzyme-substrate complex. Subsequently, calculations have suggested that the •OH abstracts the proton of the LPMO-Cu(II)-OH, resulting in the release of a water molecule and the formation of an LPMO-Cu(II)-O• species (**Figure 10, bottom**) [92], [105]. Thus, both LPMO reaction mechanisms potentially form the same Cu(II)-oxyl species, which is believed to perform the final hydrogen abstraction from the polysaccharide to form an LPMO-Cu(II)-OH intermediate. In a final rebound mechanism, the LPMO-Cu(II)-OH would hydroxylate the polysaccharide and reform the LPMO-Cu(I) state ready for a new catalytic cycle [113], [114]. The final scission of the glycosidic bond is believed to be spontaneous and results in the release of one native and one oxidized polymer end [42]. It should be noted that several different oxygen-driven mechanisms have been proposed and not all of them result in reconstitution of the reduced LPMO state.

Despite the advantages of H_2O_2 in the catalytic process, it was also reported that LPMOs may be more prone to irreversible inactivation and loss of regioselectivity under peroxygenase conditions [116]. There is evidence that auto-oxidation of the active site amino acids is the main reason for LPMO inactivation, suggesting that the inactivation process is probably due to poor interaction with the carbohydrate substrate, which in turn promotes the unproductive LPMO pathways [63], [105], [108].
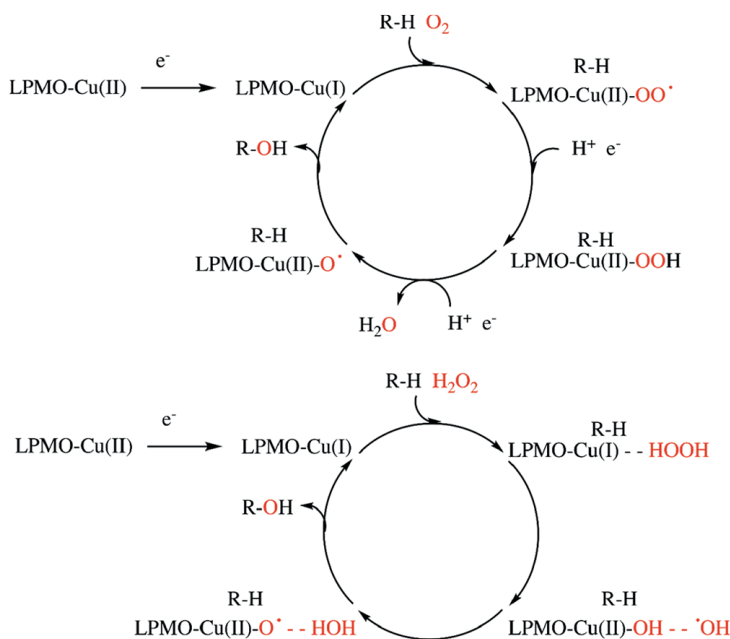
Figure 10. Proposed mechanisms of the monooxygenase (top) and the peroxygenase reactions (bottom) from the initial reduction of the copper center to hydroxylation of the scissile glycosidic bonds. Figure taken from Chylenski *et al.* [112].

1.4.4.3 Unproductive LPMO catalysis

A major challenge in the measurement of LPMO kinetics is that: "everything reacts with everything". This means that the reduced LPMO can catalyze glycosidic bond oxidation in the presence of a carbohydrate via either a monooxygenase or a peroxygenase reaction [39], [105]. In the absence of a carbohydrate, the reduced LPMO reacts with O_2 in an oxidase reaction, resulting in the formation of H_2O_2 [58], [117] but it can also act as a H_2O_2-scavenger in a peroxidase-like reaction [118]. Additionally, the presence of free transition metals such as copper can dramatically affect the rate of reaction, and their effect appears to depend on the choice of reductant [101], [111]. Consequently, the LPMO-catalyzed oxidation of carbohydrates

proceeds in a network of interconnected LPMO-dependent and -independent (side) reactions that may present challenges during data interpretation.

Soon after the discovery of the LPMOs it was shown that the enzymes catalyze an oxidase reaction that forms significant quantities of H_2O_2 when a reductant and O_2 are present but carbohydrates are absent [58], [101]. Although this is well-established, it is not clear how the H_2O_2 is formed. Based on QM/MM studies the best scenario involves a LPMO-Cu(I) that promotes upon interaction with O_2 and the addition of two protons and electrons the dissociation of H_2O_2 from the copper center [117].

When it was discovered that H_2O_2 may be the catalytically relevant co-substrate, it was suggested that the *in situ* accumulation of H_2O_2 is the driving force of the LPMO monooxygenase reaction [105]. This is supported by the finding that product levels are reduced when LPMO reactions with crystalline substrates are performed in the presence of HRP [105], [116]. This observation was found to be invalid for reactions with soluble substrates [116]. However, it is worth noting that peroxygenase reaction on such substrates are extremely efficient (**Paper III**). The hypothesis that the reaction is bottlenecked by the *in situ* production of H_2O_2 would also explain the very similar catalytic rates observed under monooxygenase conditions [7]. Additionally, the finding that HRP can interfere with the LPMO reaction suggests that O_2 reduction via LPMO-Cu(I) is the mechanism of H_2O_2 production; it seems unlikely that H_2O_2 would exit the enzyme-substrate complex to be consumed by HRP rather than being directly consumed in productive LPMO catalysis.

The third reaction LPMOs catalyze is a peroxidase-like reaction in which the LPMO-Cu(I) interacts directly with H_2O_2, resulting in e.g., the oxidation of phenolic compounds [118]. A peroxidase-like reaction may also explain the autocatalytic enzyme inactivation caused by oxidation of active site amino acids. [105]. However, not every interaction between H_2O_2 and LPMO-Cu(I) results in irreversible inactivation [111]. It is also worth noting that irreversible LPMO inactivation occurs under monooxygenase conditions and is not an exclusive problem for H_2O_2 driven reactions [95], [119]. Moreover it was shown that inactivation is strongly connected to carbohydrate binding because a properly confined LPMO is less likely to be inactivated [63], [105], [108], [120].

2 Outline and purpose of this thesis

Lytic polysaccharide monooxygenases are a recently discovered class of redox active enzymes that play a central role in the efficient enzymatic degradation of recalcitrant biomass. Despite their potential importance in saccharification processes, the fundamentals of LPMO catalysis are still not fully understood, leading to difficulties in their practical application due to processes such as rapid enzyme inactivation. The objective of the work presented in this thesis was thus to study the basics of LPMO catalysis, obtain novel insights into the substrate oxidation mechanism, and identify the driving forces behind the enzymatic action.

In **Paper I**, we established a streamlined and universally applicable platform for the recombinant expression of fungal LPMOs in *P. pastoris* to avoid limited availability of the enzymes and enable their consistent production under reproducible conditions. We believe that the availability of this simple, efficient, and high-yielding platform for LPMO production will be of considerable value to researchers working on these enzymes.

With access to a range of LPMOs established, subsequent work focused on biochemical characterization of the LPMO-catalyzed oxidation of soluble substrates. **Paper II** reports the in-depth characterization of a novel AA11 that is preferentially active on chitin oligomers. The presented kinetic studies allowed us to connect the redox potential of *Af*AA11B to the oxidase activity that fuels the subsequent substrate oxidation. We thus concluded that the O_2-driven monooxygenase reaction is of no more than minor catalytic relevance for this enzyme.

To further probe the connection between the LPMO-catalyzed *in situ* production of H_2O_2 and the oxidation of soluble cellulosic substrates, we conducted comprehensive kinetic studies on the monooxygenase, oxidase, and peroxidase reactions of *Nc*AA9C and *Ls*AA9A in combination with three reductants frequently used for LPMO activation. These studies, which are presented in **Paper III,** revealed a significant difference between the enzymes and showed that the choice of reductant strongly affects the catalytic process. Despite this, we found that both enzymes are very fast and highly specific peroxygenases that efficiently use H_2O_2 as a co-substrate for substrate oxidation.

3 Main results and discussion

3.1 Paper I: Novel molecular biological tools for the efficient expression of fungal lytic polysaccharide monooxygenases in *Pichia pastoris*

Despite recent advances, the expression of functional fungal LPMOs in *P. pastoris* remains challenging. Biochemical exploration of LPMOs would be greatly facilitated by the availability of a wide selection of enzymes that can be produced using similar methods and are accessible in large quantities. We therefore developed an efficient *P. pastoris*-based expression platform that uses state-of-the-art recombination cloning and advanced molecular biological tools to make the production of recombination LPMOs as effortless as possible.

As a proof of concept, we report in **Paper I** the fully streamlined manual or BioXP™-mediated cloning of codon-optimized genes encoding *Ls*AA9A, *Nc*AA9C, *Af*AA11B, and *Ao*AA13 into advanced integrative *E. coli*/ *P. pastoris* expression plasmids. The two tested plasmids were the commercially available pBSY3Z plasmid and the pBSYP$_{GCW14}$Z plasmid, which was assembled for this study (**Paper I, Figure 8A**). These plasmids are identical except the regulatory element that controls the transcription of the LPMO gene. In the commercially available plasmid (pBSY3Z), expression is controlled by the P$_{DC}$ promoter, which is a 500 bp promoter fragment of the depressed *CAT1* gene [121], [122]. Conversely, the newly assembled plasmid (pBSYP$_{GCW14}$Z) uses the strong constitutive P$_{GCW14}$ promoter originating from the uncharacterized *CHR1-4_0586* for transcription control. Compared to the conventionally promoters used to express LPMOs in *P. pastoris*, pBSYP$_{GCW14}$Z provides superior transcription strength while pBSY3Z offers exceptionally tight regulation of transcription. Importantly, both regulatory elements are not dependent on induction with toxic methanol**.**

We evaluated the expression system's applicability using the well-described LPMOs *Nc*AA9C and *Ls*AA9A, both of which have previously been expressed in *P. pastoris*, in combination with the native LPMO signal peptide [58], [68]. As expected, both plasmids resulted in LPMO expression, and the initial SDS-PAGE analyses showed that the cultivation supernatant contained almost exclusively recombinant LPMO. We therefore attempted to purify the recombinant enzymes using a single-step size exclusion chromatography process to make downstream processing as effortless as possible. It is worth mentioning that although C-terminal purification tags are commonly used to purify LPMOs, we wanted to avoid their use because they can promote coordination of metal ions potentially causing complications during analysis or even worse inactivation of the enzymes [55]. The performance of the tag-less purification process was evaluated by SDS-PAGE and by assessing the protein concentration during purification (**Paper I, Figure 2, Table 1**). The quantities of enzymes that were obtained

indicated that hardly any protein was lost during the different steps and that about ~25% of the total secreted protein was recovered, yielding up to 42 mg of pure LPMO per liter of culture supernatant. To put the obtained yields into context, we compared our results to previously reported LPMO production yields. Most reported yields for LPMO production using *P. pastoris* come from studies in which fermentation was performed in bioreactors with a methanol feed and longer cultivation times. This will inevitably generate higher protein titers than the simple shake flask cultivation method with undefined YPD media used in our work. To account for this, the comparison was based on enzyme recovery and the total amount of protein obtained after purification. Purification of bioreactor cultivation supernatants using purification strategies similar to those applied in our work typically delivered protein recoveries of <10% and final protein titers ranging from 6 to 90 mg of pure LPMO [58], [123]. We therefore consider our newly developed expression strategy to be a good alternative to existing methods that will be attractive to a wide range of end-users because it requires little time, know-how and, equipment to produce good yields of LPMO. To confirm that the presented approach is applicable to other LPMOs, we expressed *Ao*AA13 [64] with the native signal peptide and the pBSYP$_{GCW14}$Z vector. Expression and downstream processing with the established procedure delivered a homogenous protein stock with protein titers similar to those observed for *Nc*AA9C and *Ls*AA9A. Notably, this is the first report of the expression of an AA13 in a lower eukaryotic expression host.

We assessed the structural integrity of the expressed enzymes by measuring the release of oxidized products by HPAEC-PAD chromatography in the cases of *Ls*AA9A and *Nc*AA9C, and by measuring H$_2$O$_2$ production in the case of *Ao*AA13 (**Paper I, Figure 3, Figure 7A**). In accordance with previous reports, HPLC analyses of the monooxygenase reactions (1µM LPMO, 1mM AscA, 0.1 % phosphoric acid swollen cellulose (PASC)) of *Nc*AA9C and *Ls*AA9A revealed the formation of C4-oxidized reaction products [57], [69]. Similarly, the Amplex Red/HRP assay described by Kittl *et al.* [58] showed that *Ao*AA13 can produce significant amounts of H$_2$O$_2$ yielding a rate of ~0.03 µM*s^{-1} in the presence of 50 µM AscA. These results confirm that our new expression platform is suitable for expressing functional LPMOs, and that a single standard size-exclusion chromatography step is sufficient to obtain pure enzyme while minimizing purification time, equipment use, and the risk of damage to the enzymes.

To further expand the molecular biological toolbox for tailored LPMO expression, **Paper I** demonstrates the successful use of the signal peptide of the dolichyl-diphosphooligosaccharide-protein glycosyltransferase subunit 1 (*OST1*) from *S. cerevisiae* [124] for the secretion of functional LPMOs in *P. pastoris*. We also tested the artificial pre-*OST1*-pro-α-factor signal peptide hybrid, which combines the pre-sequence of *OST1* and the pro-sequence of the α-mating

sequence [125]. These signal peptides were tested in combination with the pBSYP$_{GCW14}$Z promoter (**Paper I, Figure 8B**) and facilitate either posttranslational (pre-*OST1*-pro-α-factor) or co-translational (*OST1*) translocation to the ER as a way for mature proteins to enter the secretion pathway. Our results show that *Nc*AA9C is secreted independently of the chosen signal peptide, indicating that the translocation process has no influence on LPMO expression. However, subsequent HPAEC-PAD chromatography revealed that only *Nc*AA9C secreted using the *OST1* signal peptide could perform substrate oxidation; no oxidation products were observed for the LPMO expressed with the pre-*OST1*-pro-α-factor signal peptide, suggesting that the enzyme was inactive (**Paper I, Figure 5**). To investigate the inactivity of the *Nc*AA9C variant expressed with the pre-*OST1*-pro-α-factor signal peptide, we performed MALDI-ToF MS analysis with the trypsin digested enzymes. This confirmed that the N-terminus of this variant was incorrectly processed as four additional amino acids prior the "N-terminal" histidine, which must occupy the N-terminal position in order for the enzyme to display activity, were discovered. This overhang at the N-terminus corresponded to the Ste13 cleavage site of the pro-sequence of the α-factor, which was previously reported to cause problems with the functional expression of LPMOs and other enzymes [78], [126]. *Nc*AA9C samples expressed with either the *OST1* or the native LPMO signal peptide had identical spectra, confirming the absence of the additional amino acids and thus the correct processing of the N-terminus. (**Paper I, Figure 6**). To determine whether the alternative signal peptide can be used for other LPMOs, we expressed *Af*AA11B in combination with the *OST1* signal peptide. After the usual single-step purification, the analysis of monooxygenase reactions with 1 μM *Af*AA11B, 2 mM (GlcNAc)$_4$ and 1 mM AscA by HPAEC-PAD chromatography showed formation oxidized products, confirming the functional expression of *Af*AA11B with the *OST1* signal peptide (**Paper I, Figure 7B**).

In conclusion, this study demonstrated the successful expression of four LPMOs from three different families with very favorable yields of ~40 mg of pure enzyme per liter of cultivation broth after a simple single-step purification. Additionally, the protocols are standardized, require little equipment, and allow the expression of valuable LPMOs in relatively little time. **Paper I** also reports a yeast-derived signal peptide that enables functional LPMO expression and avoids problems caused by incorrect processing of the native LPMO signal peptides.

3.2 Paper II: Kinetic characterization of a putatively chitin-active LPMO reveals novel LPMO functionalities and demonstrates the absence of monooxygenase activity

Paper II presents the first biochemical characterization of an LPMO belonging to the AA11 family originating from *Aspergillus fumigatus*. The detailed kinetic characterization of *Af*AA11B revealed novel and highly interesting aspects regarding the catalytically relevant oxygen-donating co-substrates of LPMOs.

*Af*AA11B is a two-domain protein consisting of a catalytic domain and an X278 module of unknown function that are connected by a long interdomain linker region. For easy accessibility, the enzyme was recombinantly expressed in *P. pastoris* and purified in three sequential chromatography steps. Based on the X-ray crystal structure of *Ao*AA11 (PDB: 4MAH [50]), which has a sequence similarity of 72.6 % to *Af*AA11B, a homology model of the catalytic domain was built using the online tool SWISS-MODEL. The obtained model features the classical LPMO immunoglobulin-like β-sheet core and surface-exposed histidine brace (**Paper II, Figure 1**) but also has an unusual rugged and convex surface that lacks the aromatic stacking amino acids that normally support polymer binding (**Paper II, Figure S1**).

Initial substrate screenings performed under aerobic conditions with 1 mM AscA as external electron donor revealed that *Af*AA11B oxidizes α- and β- chitin at the C1 carbon atom of the scissile glycosidic bond, in keeping with the substrate specificity reported for all other chitin-active LPMOs. However, time course analyses using α- and β- chitin in "monooxygenase conditions" (1 μm LPMO, 1 mM AscA, 15 g/l chitin) showed that the release of oxidized product is limited because only $\sim$50 μM of products were detected after 60 min incubation. Interestingly, the addition of H_2O_2 resulted in less product formation than when O_2 was used as the oxygen donating co-substrate even though H_2O_2 addition is usually beneficial for LPMO catalysis [105]. Upon changing the substrate in the O_2-driven reactions to $(GlcNAc)_4$ (2 mM), the enzyme released $\sim$200 μM of oxidized products within 60 min, giving a k_{obs} of 0.052 ± 0.004 s^{-1}. Moreover, supplementing the reaction with 100 μM H_2O_2 while lowering the reductant concentration (20 μM) and using 2 mM $(GlcNAc)_4$ as the substrate led to the formation of 100 μM product within 10 min, indicating that H_2O_2 is indeed a better oxygen donor than O_2 (**Paper II, Figure 2A- C**). To investigate the reason for the apparently reduced activity of *Af*AA11B on crystalline chitin, we conducted aerobic experiments with β- chitin in the presence and absence of H_2O_2. After 10 minutes of incubation, we then added fresh $(GlcNAc)_4$, H_2O_2, and AscA to both reactions. Subsequent HPAEC-PAD analysis revealed that reactions with β- chitin and H_2O_2 result in almost immediate inactivation of *Af*AA11B as no additional products were detected after the addition of the fresh co-substrate. However, in reactions performed under

aerobic reaction conditions without added H_2O_2, rapid product formation was observed following the addition of the fresh co-substrates. This indicates that *Af*AA11B has issues accessing the crystalline substrates, which results in rapid inactivation due insufficient protection of the active site when H_2O_2 is present from the beginning (**Paper II, Figure 2D**). The finding that *Af*AA11B cannot efficiently catalyze the oxidation of α- and β-chitin but exhibits significant and rapid activity towards soluble chito-oligosaccharides prompted us to speculate about its biological functions. Because it seemed unlikely that such an enzyme would have evolved as part of the chitinolytic machinery of *A. fumigatus*, we performed additional experiments using substrates such as yeast cell wall components but detected no oxidized products. Nevertheless, we believe that there is more to *Af*AA11B because previous transcriptomic studies of *N. crassa* revealed the upregulation of an AA11 with an X278 module during the final stage of spore formation [47].

The interesting properties of *Af*AA11B prompted us to undertake a detailed kinetic analysis of $(GlcNAc)_4$ oxidation. We first examined the *in situ* production of H_2O_2 because of its known importance for LPMO activity under so-called monooxygenase conditions [101], [105]. To gain deeper insight into this subject, we assessed the ability of *Af*AA11B (1 μM) to produce H_2O_2 in the presence of varying reductant concentrations using the assay outlined by Kittl *et al.* [58]. The measured rates revealed that the oxidase reaction is indeed dependent on the reductant concentration: the rate increased from 0.017 ± 0.01 μM*s^{-1} to 0.183 ± 0.016 μM*s^{-1} when using 50 μM and 1000 μM AscA, respectively. The rate of *in situ* H_2O_2 accumulation is thus significantly higher than that of the apparent monooxygenase reaction (0.052 ± 0.004 s^{-1}) given identical reductant and LPMO concentrations. This suggests that the oxidase activity of *Af*AA11B is high enough to supply the apparent monooxygenase reaction with *in situ* generated H_2O_2, which would make a peroxygenase reaction feasible. However, the measured rates of these reactions cannot be compared directly because the presence of the $(GlcNAc)_4$ substrate will significantly affect the oxidase activity of *Af*AA11B.

Since the first step in H_2O_2 production is endergonic, we investigated the potential correlation between the redox potential of *Af*AA11B and its ability to produce H_2O_2. Interestingly, the redox potential of the *Af*AA11B-Cu(II)/ *Af*AA11B-Cu(I) redox couple is only $+114 \pm 1$ mV, which is the lowest redox potential observed for an LPMO. In contrast, the redox potential for the Cu(II)/ Cu(I) couple is +160 mV and the *Sm*AA10A-Cu(II)/ *Sm*AA10A-Cu(I) redox couple has a potential of +275 mV. To support our hypothesis, we measured the rates of H_2O_2 accumulation catalyzed by $CuSO_4$ and *Sm*AA10A under conditions identical to those used for *Af*AA11B; the resulting H_2O_2 production rates were 0.080 ± 0.002 and 0.001 ± 0.001 μM*s^{-1}, respectively in the presence of

1 mM AscA. We therefore concluded that a low redox potential is beneficial for the *in situ* production of H_2O_2 in the LPMO-catalyzed oxidase reaction. (**Paper II, Figure 3, Table 2**).

To further investigate the connection between *in situ* H_2O_2 production and substrate oxidation by *Af*AA11B, we performed HRP competition experiments in typical "monooxygenase conditions". Linear time-course experiments were performed using 1 μM LPMO, 2 mM (GlcNAc)$_4$, 1 mM AscA, and varying concentrations of HRP, revealing that product formation decreased as the HRP concentration increased. The inverse hyperbolic curve obtained upon plotting the observed rate against the HRP concentration indicated that 95% inhibition of the monooxygenase reaction of *Af*AA11B occurred when the LPMO:HRP ratio was 1:6. These findings were strengthened by anaerobic experiments in peroxygenase reaction conditions (1 μM LPMO, 2 mM (GlcNAc)$_4$, 1 mM AscA, 300 μM H_2O_2) in which stoichiometric quantities of product were formed rapidly (within 1.5 min), indicating that the reaction is indeed dependent on the availability of H_2O_2. We also found that the reaction rate is dependent on the enzyme concentration and not, as previously observed for AA10s [101], limited by an LPMO-independent side reaction. Together, these results show that *Af*AA11B-catalyzed substrate oxidation is limited by the availability of H_2O_2 produced *in situ* (**Paper II, Figure 4**).

To characterize the peroxygenase reaction of *Af*AA11B in detail, we studied its kinetics and measured its k_{cat} and K_m values with respect to H_2O_2, (GlcNAc)$_4$, and AscA. Varying the H_2O_2 concentration in the presence of 2 mM (GlcNAc)$_4$ and 1 mM AscA yielded a k_{cat} of 4.7 ± 0.4 s^{-1} and a $K_m^{H_2O_2}$ of 8.9 ± 1.0 μM. To study the dependency on the (GlcNAc)$_4$ concentration, assays were performed in the presence of 300 μM H_2O_2 and 1 mM AscA giving a k_{cat} of 3.5 ± 0.1 s^{-1} and a $K_m^{(GlcNAc)_4}$ of 200 ± 29 μM. Finally, the reductant concentration was varied to investigate the dependency on the initial reaction rate. These experiments were performed using 1 mM H_2O_2 and 2 mM (GlcNAc)$_4$, and yielded a k_{cat} of 3.9 ± 0.2 s^{-1} and a K_m of 502 ± 35 μM. It should be noted that the K_m value for AscA is actually an apparent half-saturating concentration (K_{mR}^{app}) that depends on the H_2O_2 concentration because these two compounds participate in a side reaction. The k_{cat} value of 4.0 ± 0.6 s^{-1} we reported in the manuscript is the average of the three values reported above. In line with previous reports, the determined rate of the peroxygenase reaction is about three orders of magnitude higher than that of a typical monooxygenase reaction. (**Paper II, Figure 5, Table 3**). With the k_{cat} and K_m values in hand, we could calculate the k_{cat}/K_m values with respect to H_2O_2 and (GlcNAc)$_4$ which were $k_{cat}/K_m^{H_2O_2}$ = 4.5 • 10^5 M^{-1}s^{-1} and $k_{cat}/K_m^{(GlcNAc)_4}$ = 2.0 • 10^4 M^{-1}s^{-1}, respectively. Both of these efficiency constants are of the same order of magnitude as those previously reported for the LPMO-driven peroxygenase reaction and heme-dependent fungal peroxygenases [95], [107].

In conclusion, these findings suggest that the functions of LPMOs may extend beyond the depolymerization of recalcitrant biomass and that these enzymes may be involved in other, as yet unknown biological processes. Additionally, the study on AfAA11B showed that even when LPMOs have a classical active site architecture, their redox potentials can differ substantially from each other. We also demonstrated that the redox potential of an LPMO has important effects on the *in situ* production of H_2O_2. Finally, our data suggest that AfAA11B is a true peroxygenase because the oxidation of $(GlcNAc)_4$ depends solely on the availability of H_2O_2.

3.3 Paper III: Fast and specific peroxygenase reactions catalyzed by fungal mono-copper enzymes

LPMOs are multifaceted enzymes that catalyze the oxidation of glycosidic bonds in accessible carbohydrates via a monooxygenase/peroxygenase reaction [39], [105]. In the absence of a suitable polymer substrate, the reduced LPMO can either catalyze the *in situ* production of H_2O_2 in an oxidase reaction [58] or act as a H_2O_2 scavenger via a peroxidase-like mechanism [118]. To investigate the connection between the monooxygenase and oxidase reactions and how the reductant influences catalysis, we performed comprehensive kinetic analyses using *Nc*AA9C and *Ls*AA9A as catalysts and AscA, GA, and cysteine as external electron sources.

We started our study by investigating the consumption of 1 mM Glc_5 by *Nc*AA9C and its dependence on the three reductants under "monooxygenase conditions" (1 µM enzyme, 1 mM reductant). The enzyme's ability to oxidize Glc_5 allowed us to avoid issues previously encountered with the detection of C4-oxidized reaction products [75] because we could simply quantify the accumulation of native dimers and trimers by HPAEC-PAD chromatography. The obtained progress curves revealed significant differences between the reductants used for LPMO activation. Specifically, reactions using AscA and GA as the reductant both generated linear progress curves that were stable over 4 h, but the k_{obs} for the reaction with AscA was 0.05 ± 0.01 s^{-1}, whereas that for the reaction with GA was about 5 times lower (0.01 ± 0.00 s^{-1}). The rates observed when using cysteine as the electron source were very similar to those for AscA (0.06 ± 0.01 s^{-1}) but in this case the reaction became limited by the reductant after reaching a product concentration of ~450 µM. This was attributed to the fact that two electrons are required per turnover but, unlike AscA and GA, cysteine can only donate one electron. Thus 1 mM of cysteine can only fuel cleavage of 0.5 mM products (**Paper III, Figure 2A, Table 1**).

To investigate the potential correlation between monooxygenase activity and the *in situ* accumulation of H_2O_2, we assessed the enzyme's oxidase activity using the approach of Kittl *et al.* [58] under conditions identical to those used to study the monooxygenase reaction but in the absence of Glc_5. The obtained curves showed that the rate of H_2O_2 formation follows the trends observed for the monooxygenase reaction, resulting in similar rates for AscA (0.017 ± 0.001 s^{-1}) and cysteine (0.019 ± 0.001 s^{-1}). However, the results obtained with GA suggested that no H_2O_2 is formed under the applied conditions (**Paper III, Figure 2B, Table 1**).

A comparison of the rates showed that the monooxygenase reaction is about 5 times faster than the oxidase reaction. Since this difference is too large for self-fueling of the LPMO with H_2O_2, we measured the H_2O_2 production only in the presence of 1 mM Glc_5 and 1 mM reductant. The resulting progress curves revealed rapid accumulation of H_2O_2, with rates of 0.016 ± 0.000 s^{-1}

and 0.017 ± 0.000 s^{-1} in reactions with AscA and cysteine, respectively. This indicates the presence of free transition metals in the purchased substrate. However, the sum of the oxidase rates (enzyme + substrate) is close to the rate of the monooxygenase reaction. Still, it is important to keep in mind that the LPMO-catalyzed H_2O_2 production will be influenced by substrate-binding during turnover and thus comparison of the monooxygenase and oxidase rate is not straightforward. Once again, no H_2O_2 formation was observed in reactions with GA. This indicates that GA is incompatible with Amplex Red/HRP assays, probably because it can act as a substrate for HRP and/or coordinate free copper [127], [128].

A more recent study showed that cellulose-active AA10-type LPMOs have low rates of H_2O_2 production and that their catalysis is mainly driven by the LPMO-independent oxidation of a reductant [101]. Here we show that the AA9-type LPMOs contribute significantly to H_2O_2 formation, which is a major point of difference between the AA9 and AA10 families. To probe if the monooxygenase reaction is indeed dependent on the *in situ* generation of H_2O_2 we performed reactions with 1 µM *Nc*AA9C, 2 µM HRP and 100 µM Amplex Red in the presence of 1 mM GA as reductant as those reaction would not be biased by H_2O_2 originating from LPMO independent side reactions. The obtained results clearly showed that the in the presence of HRP the apparent monooxygenase reaction is strongly inhibited confirming the importance of H_2O_2 for Glc$_5$ oxidation (**Paper III, Figure 3**).

To assess the influence of the reductant on Glc$_5$ consumption in peroxygenase reactions with *Nc*AA9C we performed experiments with 0.25 µM enzyme, 300 µM H_2O_2, and 1 mM Glc$_5$ in the presence of 100 µM of a reductant. Three reductants were tested, namely AscA, gallic acid, and cysteine, giving apparent rate constants of ~70 s^{-1}, ~25 s^{-1}, and ~6 s^{-1}, respectively. These values are 100 – 2300 times higher than the rates observed for the apparent monooxygenase reaction. The progress curves for the reaction with AscA revealed that the reaction is limited by H_2O_2 because the ratio of added H_2O_2 to formed product was 1:1. To determine whether the reductant can be limiting, we increased its concentration 10-fold. This did indeed slightly increase the rate of reaction when using AscA as the reductant and caused a two-fold increase with GA but had no effect on reactions with cysteine (**Paper III, Figure 4A**). It is thus clear that the fast peroxygenase reaction can be limited by the availability of the reductant, which is most likely due to an increased re-oxidation frequency. In the case of cysteine, we could exclude H_2O_2 scavenging by the reductant (**Paper III, Figure 4B**), so we assume that the lower (but still high) turnover numbers are due to the formation of a relatively stable cuprous thiolate complex that limits the faster peroxygenase reaction. This inhibitory effect could be obscured in monooxygenase reactions as they are significantly slower.

We then assessed the dependency of the catalytic rate on the Glc_5 concentration in a Michaelis-Menten analysis, yielding a k_{cat} of 124 ± 27 s^{-1} and a K_m of 1.8 ± 0.2 mM for Glc_5 (**Paper III, Figure 5A**). Due to the fast reaction rates and the desire to obtain linearity in the time-window of turnover, we performed the peroxygenase reactions with 600 µM H_2O_2 and 1 mM AscA or GA at a temperature of 4 °C. The reaction with AscA as the external electron source resulted in the formation of 600 µM of product within 30 sec and the calculated initial rate was 90.8 ± 3.6 s^{-1}, based on an acceptably linear initial rate curve ($R^2=0.95$). With GA as the reductant, the reaction was slower but perfectly linear ($R^2=0.99$) and the initial rate was 10.7 ± 0.3 s^{-1}. Even though the experiments were conducted under non-saturating conditions with respect to Glc_5, these are the highest reported rates for LPMO catalysis (**Paper III, Figure 5B**).

To determine whether other members of the AA9 family behave like *Nc*AA9C, we assessed the activity of *Ls*AA9A, which is also active on Glc_5 in the same manner. Very similar trends were observed: there was a correlation between the monooxygenase and oxidase reactions, and the nature of the reductants had a significant impact on catalysis. Interestingly, with *Ls*AA9A cysteine was the reductant yielding the highest rates for the monooxygenase and oxidase reactions (0.029 ± 0.001 s^{-1} and 0.018 ± 0.000 s^{-1}, respectively) rather than AscA (0.014 ± 0.002 s^{-1}). However, AscA was the best reductant under peroxygenase conditions, giving rates of $\sim$6 s^{-1} and $\sim$24 s^{-1} in reactions with 100 µM and 1000 µM AscA, respectively. When we assessed the rate dependency of *Ls*AA9A-catalyzed oxidation on the Glc_5 concentration, we observed substrate inhibition even at rather low Glc_5 concentrations (75 µM), which made it impossible to obtain the Michaelis-Menten parameters. Still, the peroxygenase reaction is 400 to 1600 times faster than the monooxygenase reaction (**Paper III, Figure 6 A- C**).

The potential unspecific binding of the polymer to the surface of *Ls*AA9A was also indicated by a higher dependency on the reductant concentration during catalysis, which is probably indicative of elevated re-oxidation rates of the active LPMO. A more oxidation-prone copper site would also be more likely to undergo unproductive catalysis, leading to faster inactivation. This is exactly what was observed in peroxygenase reactions (1 µM LPMO, 1 mM Glc5, 1 mM AscA) with increasing H_2O_2 concentrations: *Ls*AA9A was inactivated at H_2O_2 concentrations of 250 µm whereas *Nc*AA9C could stoichiometrically convert 500 µM H_2O_2 indicating once more how important the interaction with the polymeric substrate is (**Paper III, Figure 7**).

It has previously been claimed that adding H_2O_2 to LPMO reactions results a loss in specificity and that H_2O_2 therefore cannot be the catalytic co-substrate. In this study we conducted experiments using 600 µM of H_2O_2, which *Nc*AA9C consumed stoichiometrically to convert cellopentaose into cellobiose and cellotriose (**Paper III, Figure 8**) Moreover, we incubated *Nc*AA9C and *Ls*AA9A under monooxygenase conditions and two distinct peroxygenase

conditions (high/low AscA and H_2O_2 concentrations) with xylopentaose and mannopentaose. None of the peroxygenase reactions showed any conspicuous features compared to the control reactions without added reductant or the chromatograms of the apparent monooxygenase reactions, demonstrating that LPMOs do not lose specificity in the presence of H_2O_2 (**Paper III, Figure S1- S3**).

In conclusion, the experiments performed in **Paper III** demonstrate the complexity of LPMO catalysis and how a plethora of simultaneously occurring interconnected (side) reactions can complicate the assessment of kinetic data for these enzymes. Nevertheless, we obtained new insights into LPMO catalysis by showing that LPMOs active on soluble substrates are highly specific and fast peroxygenases that both tolerate and consume high concentrations of H_2O_2 under suitable reaction conditions. Moreover, the data revealed a reductant-dependent tight connection between the *in situ* accumulation of H_2O_2 and substrate oxidation. Together with the strong inhibition observed in the presence of HRP and the high catalytic rates of the studied LPMOs, this indicates that H_2O_2 is the catalytically relevant oxygen donor for these AA9-type enzymes when oxidizing soluble substrates.

4 Concluding remarks

In conclusion, the work performed in this thesis, which includes enzyme cloning and production and comprehensive kinetic characterization of several fungal LPMOs, has considerably increased our understanding of how LPMOs catalyze carbohydrate oxidation. The newly gained insights suggest that not all LPMOs are necessarily part of the biomass degrading machinery of organisms. Moreover, we have shown that H_2O_2 is the catalytically relevant co-substrate required for substrate oxidation, at least for soluble carbohydrate oligomers. The detailed kinetic characterization of the AA9 and AA11-type LPMOs has also demonstrated the enormous complexity of LPMO reactions and the resulting importance of controlling the reaction conditions when comparing their catalytic abilities. The most important findings obtained in this work are briefly summarized below.

4.1 The LPMO-catalyzed oxidation of soluble substrates

All LPMOs studied were of fungal origin and can be considered atypical because they are all active on oligomeric substrates, unlike most previously reported LPMOs. However, the oxidation of oligomeric substrates provided a perfect starting point for detailed kinetic analysis as reaction products can be easily quantified.

To avoid limitations in the availability of LPMOs, we developed an efficient and streamlined expression platform based on *P. pastoris* that enables the production of diverse LPMOs with minimal effort. Conveniently, the resulting LPMOs can be purified to homogeneity using a single tag-less purification step. (**Paper I**)

Interestingly, all enzymes studied in this thesis have similar and rather convex surface topologies with structures protruding from the equatorial plane surrounding the active site. These protrusions are found in the area of the L3 loop in *Nc*AA9C and the L8 loop in *Ls*AA9A, and are involved in binding to oligomeric substrates [68], [71]. Similarly, the L3 loop in the homology model of *Af*AA11B has a structure that is outside the plane of the active site, potentially explaining this enzyme's activity towards soluble chitin oligomers. (**Paper II**).

Despite their similar surface topologies, the obtained kinetic data indicate that *Af*AA11B is fundamentally different to *Ls*AA9A and *Nc*AA9A as the latter two enzymes are highly active towards crystalline substrates like PASC and Avicel whereas *Af*AA11B cannot access crystalline chitin (**Paper I**, **Paper II, Paper III**). Moreover, there is a significant difference in oligosaccharide affinity between *Af*AA11B, for which the K_m value for (GlcNAc)$_4$ is ~0.2mM, and *Nc*AA9C, for which the K$_m$ value for Glc$_5$ is ~2 mM. Additionally, we found that *Ls*AA9A is subject to substrate inhibition at moderately low Glc$_5$ concentrations (**Paper II, Paper III**). Of course, it

is fair to question whether this activity towards oligomeric substates has any biological relevance. Nevertheless, it seems plausible that AfAA11B has evolved to act on short chitin moieties, suggesting that it has some biological function beyond degrading chitin.

Notwithstanding all the uncertainties about the biological relevance of the oxidation of oligomers by LPMOs, we found that their oxidation of oligomers is specific. Moreover, we showed that the LPMO-catalyzed peroxygenase reactions with such substrates can be astonishingly fast as the oxidation of Glc$_5$ by NcAA9C at 4 °C yielded observed rate constants of ~90 s^{-1} and ~10 s^{-1} when using AscA and GA as the reductant, respectively; these are the two highest turnover numbers ever reported for LPMOs (**Paper III**).

We were also able to address questions regarding LPMO inactivation in the presence of H$_2$O$_2$ and the effect of LPMO-related side reactions. Our findings indicate that inactivation of these enzymes is probably due to poor substrate interaction. Substrate binding appears to be important for LPMO stability because it confines and "cages" the reactive oxygen intermediate species. This hypothesis is consistent with previous findings (e.g. [91], [92], [105], [108]) and contradicts suggestions that the rapid inactivation of LPMOs observed in some cases is caused by H$_2$O$_2$. Moreover, our data suggest that high reaction rates during catalysis with rapidly diffusing substrates increase the frequency of enzyme re-oxidation via the unproductive LPMO pathways. The resulting loss of electrons is then compensated for through increased consumption of the reductant, which is needed to maintain the enzyme in the catalytically competent Cu(I) state (**Paper II**, **Paper III**).

4.2 The catalytically relevant co-substrate

The turnover numbers determined in our kinetic investigations clearly show that H$_2$O$_2$ is a better co-substrate for LPMOs than O$_2$, confirming previous observations [95], [105], [108], [109]. The rate constants determined in this work for monooxygenase reactions show that the rate of Glc$_5$ oxidation catalyzed by NcAA9C (~0.05 sec^{-1}) is very similar to the rate of (GlcNAc)$_4$ oxidation catalyzed by AfAA11B (~0.05 s^{-1}). The rate for LsAA9A was significantly lower (~0.001 s^{-1}), probably because of substrate inhibition (**Paper II**, **Paper III**). However, when the reactions were performed in the presence of high concentrations of H$_2$O$_2$ (i.e., under peroxygenase conditions), we saw rapid formation of stochiometric amounts of products with rates of ~90 s^{-1} for NcAA9C and ~4 s^{-1} for AfAA11B. In the case of LsAA9A, the peroxygenase reaction exhibited rates of ~24 s^{-1}; given the practical difficulties encountered during kinetic analysis of this reaction, these values are probably underestimates (**Paper II**, **Paper III**). The k_{cat} and k_{obs} values of the LPMO-catalyzed peroxygenase reaction are thus orders of magnitudes higher than those of the monooxygenase reaction, confirming that the LPMOs are stable for

thousands of peroxygenase turnovers (**Paper II**, **Paper III**). The importance of H_2O_2 is supported by the low measured K_m ($\sim$9 μM) with *Af*AA11B, which is consistent with previous reports [95] (**Paper II**).

In addition to the monooxygenase and peroxygenase reactions, we assessed the oxidase activity of the investigated LPMOs. Interestingly, we found a correlation between the redox potential of the LPMO and its oxidase activity; our data suggest that a low redox potential is beneficial for H_2O_2 production (**Paper II**). Furthermore, the measured rates suggest that *in situ* production of H_2O_2 may be the source of the H_2O_2 consumed during substrate oxidation because the rate of the oxidase reaction catalyzed by *Af*AA11B is much higher than the rate of the corresponding monooxygenase reaction (**Paper II**) and H_2O_2 production is tightly connected to substrate oxidation in the tested AA9 enzymes (**Paper III**). However, direct comparisons of these rates is not straightforward because the Amplex Red/HRP assay used to measure the *in situ* accumulation of H_2O_2 is performed under non-turnover conditions and the monooxygenase reaction is highly sensitive to free copper, which may be present in the substrate ([101], [109], **Paper III**). Our results also indicated that the oxidase activity of fungal AA9 and AA11-type LPMOs exceeds that of bacterial AA10-type LPMOs (**Paper II, Paper III,** [101]).

Most importantly our study showed that the nature of the external reductant used for LPMO activation significantly affects the rates of the monooxygenase, peroxygenase and oxidase reactions. The choice of reductant also has different effects on different reactions; for example, cysteine is a potent reductant in the monooxygenase and oxidase reactions but poor for the peroxygenase reactions (**Paper III**).

To connect the *in situ* production of H_2O_2 with substrate oxidation, we performed experiments with HRP as an H_2O_2 scavenger. Although it was previously reported that HRP does not influence LPMO-catalyzed monooxygenase reactions in the presence of soluble substrates [116], our data strongly contradict these claims: we found that HRP strongly inhibited the *Af*AA11B- and *Nc*AA9C- catalyzed oxidation of (GlcNAc)$_4$ and Glc$_5$ under monooxygenase conditions. This suggests that H_2O_2 is the reaction limiting substrate and may allow to speculate that the monooxygenase reaction is in fact a H_2O_2-limited peroxygenase reaction (**Paper II, Paper III**).

5 References

[1]   T. W. Lyons, C. T. Reinhard, and N. J. Planavsky, "The rise of oxygen in Earth's early ocean and atmosphere," *Nature*, vol. 506, pp. 307–315, 2014.

[2]   M. S. W. Hodgskiss, P. W. Crockford, Y. Peng, B. A. Wing, and T. J. Horner, "A productivity collapse to end Earth's Great Oxidation," *Proc. Natl. Acad. Sci. U. S. A.*, vol. 116, pp. 17207–17212, 2019.

[3]   P. R. Ogilby, "Singlet oxygen: There is indeed something new under the sun," *Chem. Soc. Rev.*, vol. 39, pp. 3181–3209, 2010.

[4]   J. P. Klinman, "How do enzymes activate oxygen without inactivating themselves?," *Acc. Chem. Res.*, vol. 40, pp. 325–333, May 2007.

[5]   M. Reth, "Hydrogen peroxide as second messenger in lymphocyte activation," *Nat. Immunol.*, vol. 3, pp. 1129–1134, 2002.

[6]   P. M. Wood, "The potential diagram for oxygen at pH 7," *Biochem. J.*, vol. 253, pp. 287–289, 1988.

[7]   B. Bissaro, A. Várnai, Å. K. Røhr, and V. G. H. Eijsink, "Oxidoreductases and reactive oxygen species in conversion of lignocellulosic biomass," *Microbiol. Mol. Biol. Rev.*, vol. 82, pp. e00029-18, 2018.

[8]   S. Bui and R. A. Steiner, "New insight into cofactor-free oxygenation from combined experimental and computational approaches," *Curr. Opin. Struct. Biol.*, vol. 41, pp. 109–118, 2016.

[9]   A. T. Martínez *et al.*, "Oxidoreductases on their way to industrial biotransformations," *Biotechnol. Adv.*, vol. 35, pp. 815–831, 2017.

[10]   R. Noor, S. Mittal, and J. Iqbal, "Superoxide dismutase - applications and relevance to human diseases," *Med. Sci. Monit.*, vol. 8, pp. 210–216, 2002.

[11]   R. J. DeJong, L. M. Miller, A. Molina-Cruz, L. Gupta, S. Kumar, and C. Barillas-Mury, "Reactive oxygen species detoxification by catalase is a major determinant of fecundity in the mosquito *Anopheles gambiae*," *Proc. Natl. Acad. Sci. U. S. A.*, vol. 104, pp. 2121–2126, 2007.

[12]   S. Yamamoto, "The 50th anniversary of the discovery of oxygenases," *IUBMB Life*, vol. 58, pp. 248–250, 2006.

[13]   D. Werck-Reichhart and R. Feyereisen, "Cytochromes P450: a success story," *Genome Biol.*, vol. 1, pp. 3003.1-3003.9, 2000.

[14]   J. Rittle and M. T. Green, "Cytochrome P450 compound I: Capture, characterization, and C-H bond activation kinetics," *Science*, vol. 330, pp. 933–937, 2010.

[15]   M. Hofrichter, H. Kellner, M. J. Pecyna, and R. Ullrich, "Fungal unspecific peroxygenases:

heme-thiolate proteins that combine peroxidase and cytochrome P450 properties," in *Monooxygenase, Peroxidase and Peroxygenase Properties and Mechanisms of Cytochrome P450*, E. G. Hrycay and S. M. Bandiera, Eds. Cham: Springer International Publishing, 2015, pp. 341–368.

[16]   J. H. Prestegard, J. Liu, and G. Widmalm, "Oligosaccharides and polysaccharides," in *Essentials of Glycobiology [Internet]. 3rd edition.*, 3rd ed., A. Varki, R. Cummings, and J. Esko, Eds. Cold Spring Harbor (NY): Cold Spring Harbor Laboratory Press, 2017.

[17]   H. M. C. Azeredo, H. Barud, C. S. Farinas, V. M. Vasconcellos, and A. M. Claro, "Bacterial cellulose as a raw material for food and food packaging applications," *Front. Sustain. Food Syst.*, vol. 3, 7, 2019.

[18]   J. Rytioja, K. Hildén, J. Yuzon, A. Hatakka, R. P. de Vries, and M. R. Mäkelä, "Plant-polysaccharide-degrading enzymes from basidiomycetes," *Microbiol. Mol. Biol. Rev.*, vol. 78, pp. 614–649, 2014.

[19]   V. Zargar, M. Asghari, and A. Dashti, "A review on chitin and chitosan polymers: Structure, chemistry, solubility, derivatives, and applications," *ChemBioEng Rev.*, vol. 2, pp. 204–226, 2015.

[20]   E. A. Bayer, J. P. Belaich, Y. Shoham, and R. Lamed, "The cellulosomes: Multienzyme machines for degradation of plant cell wall polysaccharides," *Annu. Rev. Microbiol.*, vol. 58, pp. 521–554, 2004.

[21]   A. E. Naas *et al.*, "Do rumen Bacteroidetes utilize an alternative mechanism for cellulose degradation?," *MBio*, vol. 5, pp. e01401-14, 2014.

[22]   J. Larsbrink *et al.*, "A discrete genetic locus confers xyloglucan metabolism in select human gut Bacteroidetes," *Nature*, vol. 506, pp. 498–502, 2014.

[23]   J. Larsbrink *et al.*, "A polysaccharide utilization locus from *Flavobacterium johnsoniae* enables conversion of recalcitrant chitin," *Biotechnol. Biofuels*, vol. 9, 260, 2016.

[24]   S. J. Horn, G. Vaaje-Kolstad, B. Westereng, and V. G. H. Eijsink, "Novel enzymes for the degradation of cellulose," *Biotechnol. Biofuels*, vol. 5, 45, 2012.

[25]   E. M. Gomez del Pulgar and A. Saadeddin, "The cellulolytic system of *Thermobifida fusca*," *Crit. Rev. Microbiol.*, vol. 40, pp. 236–247, Aug. 2014.

[26]   G. Vaaje-Kolstad, S. J. Horn, M. Sørlie, and V. G. H. Eijsink, "The chitinolytic machinery of *Serratia marcescens* - A model system for enzymatic degradation of recalcitrant polysaccharides," *FEBS J.*, vol. 280, pp. 3028–3049, 2013.

[27]   E. T. Reese, "A microbiological process report; enzymatic hydrolysis of cellulose," *Appl. Microbiol.*, vol. 4, pp. 39–45, Jan. 1956.

[28]   H. Palonen, M. Tenkanen, and M. Linder, "Dynamic interaction of *Trichoderma reesei* cellobiohydrolases Cel6A and Cel7A and cellulose at equilibrium and during hydrolysis,"

Appl. Environ. Microbiol., vol. 65, pp. 5229–5233, 1999.

[29] T. M. Lee, M. F. Farrow, F. H. Arnold, and S. L. Mayo, "A structural study of *Hypocrea jecorina* Cel5A," *Protein Sci.*, vol. 20, pp. 1935–1940, Nov. 2011.

[30] B. Synstad *et al.*, "Expression and characterization of endochitinase C from *Serratia marcescens* BJL200 and its purification by a one-step general chitinase purification method," *Biosci. Biotechnol. Biochem.*, vol. 72, pp. 715–723, 2008.

[31] D. Shallom and Y. Shoham, "Microbial hemicellulases," *Curr. Opin. Microbiol.*, vol. 6, pp. 219–228, 2003.

[32] G. Janusz, A. Pawlik, J. Sulej, U. Świderska-Burek, A. Jarosz-Wilkolazka, and A. Paszczyński, "Lignin degradation: Microorganisms, enzymes involved, genomes analysis and evolution," *FEMS Microbiol. Rev.*, vol. 41, pp. 941–962, 2017.

[33] G. R. Hemsworth, E. M. Johnston, G. J. Davies, and P. H. Walton, "Lytic polysaccharide monooxygenases in biomass conversion," *Trends Biotechnol.*, vol. 33, pp. 747–761, 2015.

[34] K. S. Johansen, "Discovery and industrial applications of lytic polysaccharide mono-oxygenases," *Biochem. Soc. Trans.*, vol. 44, pp. 143–149, 2016.

[35] D. Cannella, C. W. C. Hsieh, C. Felby, and H. Jørgensen, "Production and effect of aldonic acids during enzymatic hydrolysis of lignocellulose at high dry matter content," *Biotechnol. Biofuels*, vol. 5, 26, 2012.

[36] E. T. Reese, R. G. H. Siu, and H. S. Levinson, "The biological degradation of soluble cellulose derivatives and its relationship to the mechanism of cellulose hydrolysis," *J. Bacteriol.*, vol. 59, pp. 485–497, 1950.

[37] K.-E. Eriksson, B. Pettersson, and U. Westermark, "Oxidation: An important enzyme reaction in fungal degradation of cellulose," *FEBS Lett.*, vol. 49, pp. 282–285, 1974.

[38] G. Vaaje-Kolstad, S. J. Horn, D. M. F. Van Aalten, B. Synstad, and V. G. H. Eijsink, "The non-catalytic chitin-binding protein CBP21 from *Serratia marcescens* is essential for chitin degradation," *J. Biol. Chem.*, vol. 280, pp. 28492–28497, 2005.

[39] G. Vaaje-Kolstad *et al.*, "An oxidative enzyme boosting the enzymatic conversion of recalcitrant polysaccharides," *Science,* vol. 330, pp. 219–223, 2010.

[40] Z. Forsberg *et al.*, "Cleavage of cellulose by a cbm33 protein," *Protein Sci.*, vol. 20, pp. 1479–1483, 2011.

[41] R. J. Quinlan *et al.*, "Insights into the oxidative degradation of cellulose by a copper metalloenzyme that exploits biomass components," *Proc. Natl. Acad. Sci. U. S. A.*, vol. 108, pp. 15079–15084, 2011.

[42] C. M. Phillips, W. T. Beeson, J. H. Cate, and M. A. Marletta, "Cellobiose dehydrogenase and a copper-dependent polysaccharide monooxygenase potentiate cellulose degradation by Neurospora crassa," *ACS Chem. Biol.*, vol. 6, pp. 1399–1406, 2011.

[43]   N. Lenfant, M. Hainaut, N. Terrapon, E. Drula, V. Lombard, and B. Henrissat, "A bioinformatics analysis of 3400 lytic polysaccharide oxidases from family AA9," *Carbohydr. Res.*, vol. 448, pp. 166–174, 2017.

[44]   D. K. Paspaliari, J. S. M. Loose, M. H. Larsen, and G. Vaaje-Kolstad, "*Listeria monocytogenes* has a functional chitinolytic system and an active lytic polysaccharide monooxygenase," *FEBS J.*, vol. 282, pp. 921–936, 2015.

[45]   F. Askarian *et al.*, "The lytic polysaccharide monooxygenase CbpD promotes *Pseudomonas aeruginosa* virulence in systemic infection," *Nat. Commun.*, vol. 12, 1230, 2021.

[46]   Y. Li *et al.*, "*Magnaporthe oryzae* auxiliary activity protein *Mo*Aa91 functions as chitin-binding protein to induce appressorium formation on artificial inductive surfaces and suppress plant immunity," *MBio*, vol. 11, pp. 1–20, 2020.

[47]   Z. Wang *et al.*, "Global gene expression and focused knockout analysis reveals genes associated with fungal fruiting body development in *Neurospora crassa*," *Eukaryot. Cell*, vol. 13, no. 1, pp. 154–169, 2014.

[48]   V. Lombard, H. Golaconda Ramulu, E. Drula, P. M. Coutinho, and B. Henrissat, "The carbohydrate-active enzymes database (CAZy) in 2013," *Nucleic Acids Res.*, vol. 42, pp. D490–D495, Jan. 2014.

[49]   A. Várnai, O. A. Hegnar, S. J. Horn, V. G. H. Eijsink, and J.-G. Berrin, "Fungal lytic polysaccharide monooxygenases (LPMOs): Biological importance and applications," in *Reference Module in Life Sciences*, 2020.

[50]   G. R. Hemsworth, B. Henrissat, G. J. Davies, and P. H. Walton, "Discovery and characterization of a new family of lytic polysaccharide monooxygenases.," *Nat. Chem. Biol.*, vol. 10, pp. 122–126, 2014.

[51]   D. Wang *et al.*, "Production of functionalised chitins assisted by fungal lytic polysaccharide monooxygenase," *Green Chem.*, vol. 20, pp. 2091–2100, 2018.

[52]   L. Ma *et al.*, "Functional characterization of a novel copper-dependent lytic polysaccharide monooxygenase *Tg*AA11 from *Trichoderma guizhouense* NJAU 4742 in the oxidative degradation of chitin," *Carbohydr. Polym.*, vol. 258, p. 117708, 2021.

[53]   V. V. Vu, W. T. Beeson, E. A. Span, E. R. Farquhar, and M. A. Marletta, "A family of starch-active polysaccharide monooxygenases," *Proc. Natl. Acad. Sci. U. S. A.*, vol. 111, pp. 13822–13827, 2014.

[54]   A. Zerva, C. Pentari, S. Grisel, J. G. Berrin, and E. Topakas, "A new synergistic relationship between xylan-active LPMO and xylobiohydrolase to tackle recalcitrant xylan," *Biotechnol. Biofuels*, vol. 13, 142, 2020.

[55]   C. Filiatrault-Chastel *et al.*, "AA16, a new lytic polysaccharide monooxygenase family

identified in fungal secretomes," *Biotechnol. Biofuels*, vol. 12, 55, 2019.

[56]   G. Vaaje-Kolstad, D. R. Houston, A. H. K. Riemen, V. G. H. Eijsink, and D. M. F. Van Aalten, "Crystal structure and binding properties of the *Serratia marcescens* chitin-binding protein CBP21," *J. Biol. Chem.*, vol. 280, pp. 11313–11319, 2005.

[57]   K. E. H. Frandsen *et al.*, "The molecular basis of polysaccharide cleavage by lytic polysaccharide monooxygenases," *Nat. Chem. Biol.*, vol. 12, pp. 298–303, 2016.

[58]   R. Kittl, D. Kracher, D. Burgstaller, D. Haltrich, and R. Ludwig, "Production of four *Neurospora crassa* lytic polysaccharide monooxygenases in *Pichia pastoris* monitored by a fluorimetric assay," *Biotechnol. Biofuels*, vol. 5, 79, 2012.

[59]   F. L. Aachmann, M. Sorlie, G. Skjak-Braek, V. G. H. Eijsink, and G. Vaaje-Kolstad, "NMR structure of a lytic polysaccharide monooxygenase provides insight into copper binding, protein dynamics, and substrate interactions," *Proc. Natl. Acad. Sci.*, vol. 109, pp. 18779–18784, 2012.

[60]   K. E. H. Frandsen and L. Lo Leggio, "Lytic polysaccharide monooxygenases: A crystallographer's view on a new class of biomass-degrading enzymes," *IUCrJ*, vol. 3, pp. 448–467, 2016.

[61]   X. Li, W. T. Beeson IV, C. M. Phillips, M. A. Marletta, and J. H. D. Cate, "Structural basis for substrate targeting and catalysis by fungal polysaccharide monooxygenases," *Structure*, vol. 20, pp. 1051–1061, 2012.

[62]   B. Bissaro, I. Isaksen, G. Vaaje-Kolstad, V. G. H. Eijsink, and Å. K. Røhr, "How a lytic polysaccharide monooxygenase binds crystalline chitin," *Biochemistry*, vol. 57, pp. 1893–1906, 2018.

[63]   J. S. M. Loose, M. Arntzen, B. Bissaro, R. Ludwig, V. G. H. Eijsink, and G. Vaaje-Kolstad, "Multipoint precision binding of substrate protects lytic polysaccharide monooxygenases from self-destructive off-pathway processes," *Biochemistry*, vol. 57, pp. 4114–4124, 2018.

[64]   L. Lo Leggio *et al.*, "Structure and boosting activity of a starch-degrading lytic polysaccharide monooxygenase," *Nat. Commun.*, vol. 6, 5961, 2015.

[65]   F. Sabbadin *et al.*, "An ancient family of lytic polysaccharide monooxygenases with roles in arthropod development and biomass digestion," *Nat. Commun.*, vol. 9, 756, 2018.

[66]   J. W. Agger *et al.*, "Discovery of LPMO activity on hemicelluloses shows the importance of oxidative processes in plant cell wall degradation," *Proc. Natl. Acad. Sci. U. S. A.*, vol. 111, pp. 6287–6292, 2014.

[67]   P. Sun *et al.*, "Configuration of active site segments in lytic polysaccharide monooxygenases steers oxidative xyloglucan degradation," *Biotechnol. Biofuels*, vol. 13, 95, 2020.

[68] K. E. H. Frandsen, M. Haon, S. Grisel, B. Henrissat, L. Lo Leggio, and J.-G. Berrin, "Identification of the molecular determinants driving the substrate specificity of fungal lytic polysaccharide monooxygenases (LPMOs)," *J. Biol. Chem.*, vol. 296, 100086, 2020.

[69] T. Isaksen *et al.*, "A C4-oxidizing lytic polysaccharide monooxygenase cleaving both cellulose and cello-oligosaccharides," *J. Biol. Chem.*, vol. 289, pp. 2632–2642, 2014.

[70] T. J. Simmons *et al.*, "Structural and electronic determinants of lytic polysaccharide monooxygenase reactivity on polysaccharide substrates," *Nat. Commun.*, vol. 8, 1064, 2017.

[71] M. A. S. Kadowaki *et al.*, "Functional characterization of a lytic polysaccharide monooxygenase from the thermophilic fungus *Myceliophthora thermophila*," *PLoS One*, vol. 13, p. e0202148, 2018.

[72] B. Liu *et al.*, "Structural and molecular dynamics studies of a C1-oxidizing lytic polysaccharide monooxygenase from *Heterobasidion irregulare* reveal amino acids important for substrate recognition," *FEBS J.*, vol. 285, pp. 2225–2242, 2018.

[73] W. T. Beeson, V. V. Vu, E. A. Span, C. M. Phillips, and M. A. Marletta, "Cellulose degradation by polysaccharide monooxygenases," *Annu. Rev. Biochem.*, vol. 84, pp. 923–946, 2015.

[74] B. Westereng *et al.*, "Efficient separation of oxidized cello-oligosaccharides generated by cellulose degrading lytic polysaccharide monooxygenases," *J. Chromatogr. A*, vol. 1271, pp. 144–152, 2013.

[75] B. Westereng, M. T. Arntzen, F. L. Aachmann, A. Várnai, V. G. H. Eijsink, and J. W. Agger, "Simultaneous analysis of C1 and C4 oxidized oligosaccharides, the products of lytic polysaccharide monooxygenases acting on cellulose," *J. Chromatogr. A*, vol. 1445, pp. 46–54, 2016.

[76] M. Frommhagen, A. H. Westphal, W. J. H. van Berkel, and M. A. Kabel, "Distinct substrate specificities and electron-donating systems of fungal lytic polysaccharide monooxygenases," *Front. Microbiol.*, vol. 9, p. 1080, 2018.

[77] A. K. Chaplin *et al.*, "Heterogeneity in the histidine-brace copper coordination sphere in auxiliary activity family 10 (AA10) lytic polysaccharide monooxygenases," *J. Biol. Chem.*, vol. 291, pp. 12838–12850, 2016.

[78] M. Tanghe *et al.*, "Recombinant expression of *Trichoderma reesei* Cel61A in *Pichia pastoris*: Optimizing yield and N-terminal processing," *Mol. Biotechnol.*, vol. 57, pp. 1010–1017, 2015.

[79] G. Courtade, S. B. Le, G. I. Sætrom, T. Brautaset, and F. L. Aachmann, "A novel expression system for lytic polysaccharide monooxygenases," *Carbohydr. Res.*, vol. 448, pp. 212–219, 2017.

[80] D. M. Petrović *et al.*, "Methylation of the N-terminal histidine protects a lytic

polysaccharide monooxygenase from auto-oxidative inactivation," *Protein Sci.*, vol. 27, pp. 1636–1650, 2018.

[81]   A. Labourel *et al.*, "A fungal family of lytic polysaccharide monooxygenase-like copper proteins," *Nat. Chem. Biol.*, vol. 16, pp. 345–350, 2020.

[82]   S. Brander *et al.*, "Biochemical evidence of both copper chelation and oxygenase activity at the histidine brace," *Sci. Rep.*, vol. 10, p. 16369, 2020.

[83]   Z. Forsberg *et al.*, "Structural and functional characterization of a conserved pair of bacterial cellulose-oxidizing lytic polysaccharide monooxygenases," *Proc. Natl. Acad. Sci. U. S. A.*, vol. 111, pp. 8446–8451, 2014.

[84]   Z. Forsberg *et al.*, "Comparative study of two chitin-active and two cellulose-active AA10-type lytic polysaccharide monooxygenases," *Biochemistry*, vol. 53, pp. 1647–1656, 2014.

[85]   P. V. Harris *et al.*, "Stimulation of lignocellulosic biomass hydrolysis by proteins of glycoside hydrolase family 61: Structure and function of a large, enigmatic family," *Biochemistry*, vol. 49, pp. 3305–3316, 2010.

[86]   S. M. Jones, W. J. Transue, K. K. Meier, B. Kelemen, and E. I. Solomon, "Kinetic analysis of amino acid radicals formed in H_2O_2-driven Cu^I LPMO reoxidation implicates dominant homolytic reactivity," *Proc. Natl. Acad. Sci. U. S. A.*, vol. 117, pp. 11916–11922, 2020.

[87]   G. Vaaje-Kolstad, Z. Forsberg, J. S. Loose, B. Bissaro, and V. G. H. Eijsink, "Structural diversity of lytic polysaccharide monooxygenases," *Curr. Opin. Struct. Biol.*, vol. 44, pp. 67–76, 2017.

[88]   E. A. Span, D. L. M. Suess, M. C. Deller, R. D. Britt, and M. A. Marletta, "The role of the secondary coordination sphere in a fungal polysaccharide monooxygenase," *ACS Chem. Biol.*, vol. 12, pp. 1095–1103, 2017.

[89]   L. Ciano, G. J. Davies, W. B. Tolman, and P. H. Walton, "Bracing copper for the catalytic oxidation of C–H bonds," *Nat. Catal.*, vol. 1, pp. 571–577, 2018.

[90]   P. H. Walton and G. J. Davies, "On the catalytic mechanisms of lytic polysaccharide monooxygenases," *Curr. Opin. Chem. Biol.*, vol. 31, pp. 195–207, 2016.

[91]   B. Bissaro *et al.*, "Molecular mechanism of the chitinolytic peroxygenase reaction," *Proc. Natl. Acad. Sci. U. S. A.*, vol. 117, pp. 1504–1513, 2020.

[92]   B. Wang *et al.*, "QM/MM studies into the H_2O_2-dependent activity of lytic polysaccharide monooxygenases: Evidence for the formation of a caged hydroxyl radical intermediate," *ACS Catal.*, vol. 8, pp. 1346–1351, 2018.

[93]   S. Garajova *et al.*, "Single-domain flavoenzymes trigger lytic polysaccharide monooxygenases for oxidative degradation of cellulose," *Sci. Rep.*, vol. 6, p. 28276, 2016.

[94]   D. Kracher *et al.*, "Extracellular electron transfer systems fuel cellulose oxidative degradation," *Science*, vol. 352, pp. 1098–1101, 2016.

[95]   S. Kuusk *et al.*, "Kinetics of H_2O_2-driven degradation of chitin by a bacterial lytic polysaccharide monooxygenase," *J. Biol. Chem.*, vol. 293, pp. 523–531, 2018.

[96]   M. Frommhagen *et al.*, "Lytic polysaccharide monooxygenases from *Myceliophthora thermophila* C1 differ in substrate preference and reducing agent specificity," *Biotechnol. Biofuels*, vol. 9, p. 186, 2016.

[97]   B. Bissaro, E. Kommedal, Å. K. Røhr, and V. G. H. Eijsink, "Controlled depolymerization of cellulose by light-driven lytic polysaccharide oxygenases," *Nat. Commun.*, vol. 11, 890, 2020.

[98]   F. Filandr, P. Man, P. Halada, H. Chang, R. Ludwig, and D. Kracher, "The H_2O_2-dependent activity of a fungal lytic polysaccharide monooxygenase investigated with a turbidimetric assay," *Biotechnol. Biofuels*, vol. 13, 37, 2020.

[99]   M. Haddad Momeni *et al.*, "Discovery of fungal oligosaccharide-oxidising flavo-enzymes with previously unknown substrates, redox-activity profiles and interplay with LPMOs," *Nat. Commun.*, vol. 12, 2132, 2021.

[100]   O. Hegnar, D. Petrovic, B. Bissaro, A. Varnai, and V. G. H. Eijsink, "pH-Dependent relationship between catalytic activity and hydrogen peroxide production shown via characterization of a lytic polysaccharide monooxygenase from *Gloeophyllum trabeum*," *Appl. Environ. Microbiol.*, vol. 85, pp. e02612-18, 2019.

[101]   A. A. Stepnov *et al.*, "Unraveling the roles of the reductant and free copper ions in LPMO kinetics," *Biotechnol. Biofuels*, vol. 14, 28, 2021.

[102]   D. Kracher, M. Andlar, P. G. Furtmüller, and R. Ludwig, "Active-site copper reduction promotes substrate binding of fungal lytic polysaccharide monooxygenase and reduces stability," *J. Biol. Chem.*, vol. 293, pp. 1676–1687, 2018.

[103]   G. Courtade *et al.*, "Interactions of a fungal lytic polysaccharide monooxygenase with β-glucan substrates and cellobiose dehydrogenase," *Proc. Natl. Acad. Sci. U. S. A.*, vol. 113, pp. 5922–5927, 2016.

[104]   Z. Forsberg *et al.*, "Polysaccharide degradation by lytic polysaccharide monooxygenases," *Curr. Opin. Struct. Biol.*, pp. 54–64, 2019.

[105]   B. Bissaro *et al.*, "Oxidative cleavage of polysaccharides by monocopper enzymes depends on H_2O_2," *Nat. Chem. Biol.*, vol. 13, pp. 1123–1128, 2017.

[106]   C. Wang *et al.*, "Evidence that the fosfomycin-producing epoxidase, HppE, is a non–heme-iron peroxidase," *Science*, vol. 342, pp. 991–995, 2013.

[107]   M. Hofrichter and R. Ullrich, "Oxidations catalyzed by fungal peroxygenases," *Curr. Opin. Chem. Biol.*, vol. 19, pp. 116–125, 2014.

[108]   T. M. Hedison *et al.*, "Insights into the H_2O_2-driven catalytic mechanism of fungal lytic polysaccharide monooxygenases.," *FEBS J.*, 2021.

[109] R. Kont, B. Bissaro, V. G. H. Eijsink, and P. Väljamäe, "Kinetic insights into the peroxygenase activity of cellulose-active lytic polysaccharide monooxygenases (LPMOs)," *Nat. Commun.*, vol. 11, 5786, 2020.

[110] G. Müller, P. Chylenski, B. Bissaro, V. G. H. Eijsink, and S. J. Horn, "The impact of hydrogen peroxide supply on LPMO activity and overall saccharification efficiency of a commercial cellulase cocktail," *Biotechnol. Biofuels*, vol. 11, 209, 2018.

[111] S. Kuusk *et al.*, "Kinetic insights into the role of the reductant in H_2O_2-driven degradation of chitin by a bacterial lytic polysaccharide monooxygenase," *J. Biol. Chem.*, vol. 294, pp. 1516–1528, 2019.

[112] P. Chylenski *et al.*, "Lytic polysaccharide monooxygenases in enzymatic processing of lignocellulosic biomass," *ACS Catal.*, vol. 9, pp. 4970–4991, 2019.

[113] S. Kim, J. Ståhlberg, M. Sandgren, R. S. Paton, and G. T. Beckham, "Quantum mechanical calculations suggest that lytic polysaccharide monooxygenases use a copper-oxyl, oxygen-rebound mechanism," *Proc. Natl. Acad. Sci. U. S. A.*, vol. 111, pp. 149–154, 2014.

[114] L. Bertini *et al.*, "Catalytic mechanism of fungal lytic polysaccharide monooxygenases investigated by first-principles calculations," *Inorg. Chem.*, vol. 57, pp. 86–97, 2018.

[115] C. H. Kjaergaard *et al.*, "Spectroscopic and computational insight into the activation of O_2 by the mononuclear Cu center in polysaccharide monooxygenases," *Proc. Natl. Acad. Sci. U. S. A.*, vol. 111, pp. 8797–8802, 2014.

[116] J. A. Hangasky, A. T. Iavarone, and M. A. Marletta, "Reactivity of O_2 versus H_2O_2 with polysaccharide monooxygenases," *Proc. Natl. Acad. Sci. U. S. A.*, vol. 115, pp. 4915–4920, 2018.

[117] O. Caldararu, E. Oksanen, U. Ryde, and E. D. Hedegård, "Mechanism of hydrogen peroxide formation by lytic polysaccharide monooxygenase," *Chem. Sci.*, vol. 10, pp. 576–586, 2019.

[118] E. Breslmayr *et al.*, "A fast and sensitive activity assay for lytic polysaccharide monooxygenase," *Biotechnol. Biofuels*, vol. 11, 79, 2018.

[119] J. S. M. Loose *et al.*, "Activation of bacterial lytic polysaccharide monooxygenases with cellobiose dehydrogenase," *Protein Sci.*, vol. 25, pp. 2175–2186, 2016.

[120] D. M. Petrović *et al.*, "Comparison of three seemingly similar lytic polysaccharide monooxygenases from *Neurospora crassa* suggests different roles in plant biomass degradation," *J. Biol. Chem.*, vol. 294, pp. 15068–15081, 2019.

[121] S. Liang, C. Zou, Y. Lin, X. Zhang, and Y. Ye, "Identification and characterization of P$_{GCW14}$: A novel, strong constitutive promoter of *Pichia pastoris*," *Biotechnol. Lett.*, vol. 35, pp. 1865–1871, 2013.

[122] T. Vogl *et al.*, "A toolbox of diverse promoters related to methanol utilization:

Functionally verified parts for heterologous pathway expression in *Pichia pastoris*," *ACS Synth. Biol.*, vol. 5, pp. 172–186, 2015.

[123] C. Sygmund *et al.*, "Characterization of the two *Neurospora crassa* cellobiose dehydrogenases and their connection to oxidative cellulose degradation," *Appl. Environ. Microbiol.*, vol. 78, pp. 6161–6171, 2012.

[124] I. Fitzgerald and B. S. Glick, "Secretion of a foreign protein from budding yeasts is enhanced by cotranslational translocation and by suppression of vacuolar targeting," *Microb. Cell Fact.*, vol. 13, p. 125, 2014.

[125] J. J. Barrero, J. C. Casler, F. Valero, P. Ferrer, and B. S. Glick, "An improved secretion signal enhances the secretion of model proteins from *Pichia pastoris*," *Microb. Cell Fact.*, vol. 17, p. 161, 2018.

[126] J. L. Cereghino and J. M. Cregg, "Heterologous protein expression in the methylotrophic yeast *Pichia pastoris*," *FEMS Microbiol. Rev.*, vol. 24, pp. 45–66, 2000.

[127] X. Zhang, H. Wu, L. Zhang, and Q. Sun, "Horseradish peroxidase-mediated synthesis of an antioxidant gallic acid-g-chitosan derivative and its preservation application in cherry tomatoes," *RSC Adv.*, vol. 8, pp. 20363–20371, 2018.

[128] J. F. Severino, B. A. Goodman, T. G. Reichenauer, and K. F. Pirker, "Is there a redox reaction between Cu(II) and gallic acid?," *Free Radic. Res.*, vol. 45, pp. 123–132, 2011.

Publications

Novel molecular biological tools for the efficient expression of fungal lytic polysaccharide monooxygenases in *Pichia pastoris*

Lukas Rieder, Katharina Ebner, Anton Glieder, Morten Sørlie

Paper I

Kinetic characterization of a putatively chitin-active LPMO reveals novel LPMO functionalities and demonstrates the absence of monooxygenase activity

Lukas Rieder, Dejan M. Petrović, Priit Valjamae, Vincent G.H. Eijsink, Morten Sørlie

Paper II

Fast and specific peroxygenase reactions catalyzed by fungal mono-copper enzymes

Lukas Rieder, Anton A. Stepnov, Morten Sørlie, Vincent G.H. Eijsink

Paper III

Novel molecular biological tools for the efficient expression of fungal lytic polysaccharide monooxygenases in *Pichia pastoris*

Lukas Rieder, Katharina Ebner, Anton Glieder, Morten Sørlie

Paper I

RESEARCH   **Open Access**

Novel molecular biological tools for the efficient expression of fungal lytic polysaccharide monooxygenases in *Pichia pastoris*

Lukas Rieder[1†], Katharina Ebner[2†], Anton Glieder[3] and Morten Sørlie[1*]

Abstract

Background: Lytic polysaccharide monooxygenases (LPMOs) are attracting large attention due their ability to degrade recalcitrant polysaccharides in biomass conversion and to perform powerful redox chemistry.

Results: We have established a universal *Pichia pastoris* platform for the expression of fungal LPMOs using state-of-the-art recombination cloning and modern molecular biological tools to achieve high yields from shake-flask cultivation and simple tag-less single-step purification. Yields are very favorable with up to 42 mg per liter medium for four different LPMOs spanning three different families. Moreover, we report for the first time of a yeast-originating signal peptide from the dolichyl-diphosphooligosaccharide-protein glycosyltransferase subunit 1 (*OST1*) form *S. cerevisiae* efficiently secreting and successfully processes the N-terminus of LPMOs yielding in fully functional enzymes.

Conclusion: The work demonstrates that the industrially most relevant expression host *P. pastoris* can be used to express fungal LPMOs from different families in high yields and inherent purity. The presented protocols are standardized and require little equipment with an additional advantage with short cultivation periods.

Keywords: LPMO, *Pichia pastoris*, Signal peptide cleaving, Simplified expression

Background

Lytic polysaccharide monooxygenases (LPMOs) are mono-copper-dependent oxidoreductases that catalyze the oxidative cleavage of glycosidic bonds of recalcitrant sugar polymers such as chitin, cellulose, and hemicelluloses [1–5]. LPMOs are proposed to be major players in the efficient enzymatic conversion of bio-based materials and have become a key ingredient in commercially available products for enzymatic saccharification. Their unique and powerful oxidative abilities make them promising

candidates for the application in renewable energy technologies and interesting targets for enzyme engineering, especially in light of the large amount of carbohydrate-based waste [6–11].

Although the potential of LPMOs has been recognized a decade ago [1], research in this field still faces major challenges starting, most fundamentally, with the production of active enzymes. Since isolation from native hosts can be challenging due to low yields, secretion of enzyme cocktails, and cultivation obstacles, recombinant production in bacterial or eukaryotic model organisms is desired. Due to the extracellular biomass-degrading nature, all LPMOs are secreted from their native hosts, regardless of their origin being eukaryotic or prokaryotic, which facilitates secretion in the recombinant host systems and allows easier down-stream processing.

*Correspondence: morten.sorlie@nmbu.no
†Lukas Rieder and Katharina Ebner contributed equally to this work
[1] Faculty of Chemistry, Biotechnology, and Food Sciences, Norwegian University of Life Sciences (NMBU), Ås, Norway
Full list of author information is available at the end of the article

Rieder *et al. Biotechnol Biofuels*   (2021) 14:122

Page 2 of 17

For the recombinant expression of LPMOs of eukaryotic origin, the yeast *Pichia pastoris* (*Komagataella phaffii*) is one of the more frequently used host systems [12]. Main reasons for the use of *P. pastoris* are typical eukaryotic post-translational modifications, its capacity to secrete recombinant proteins to a high titer, and the increasing number of tools available for efficient genetic engineering [13–15]. One of the main challenges in the recombinant expression of active LPMOs lies in the correct processing of the N-terminus, as all LPMOs share a highly conserved N-terminal histidine that is directly involved in the formation of the active site by coordinating the copper center with both the imidazole ring and the backbone N-terminal amine, the so-called *histidine brace* [16]. Thus, a correctly processed N-terminus is indispensable for the catalytic activity and highlights the importance of a well-tailored expression system for LPMOs as recently addressed in several publications [17–19].

For *P. pastoris* the most commonly used expression tools are the promoter of the *P. pastoris* alcohol oxidase 1 gene (P_{AOX1}) in combination with the α-mating factor secretion signal of *Saccharomyces cerevisiae* that has successfully been applied for the recombinant expression of a multitude of proteins [20]. While the P_{AOX1}, which requires induction by toxic methanol, has been used for the expression of LPMOs, the α-mating signal is not suitable for the recombinant expression of LPMOs [18]. Thus, the production of LPMOs in *P. pastoris* is dependent on native LPMO signal peptides and the hosts ability to recognize correctly foreign leading sequences of sometimes only distantly related organisms. While the problem of the signal peptide has been addressed for the expression of bacterial LPMOs in *E. coli* [21], no one has tackled the problem for eukaryotic expression systems.

In this study, we present a LPMO-tailored expression system that allows a streamlined and efficient state-of-the-art recombination cloning and easy protein expression with a subsequent one-step purification. As an alternative to native LPMO signal peptides, we present a yeast-originating signal peptide that facilitates secretion of the correctly processed LPMOs of fungal origin.
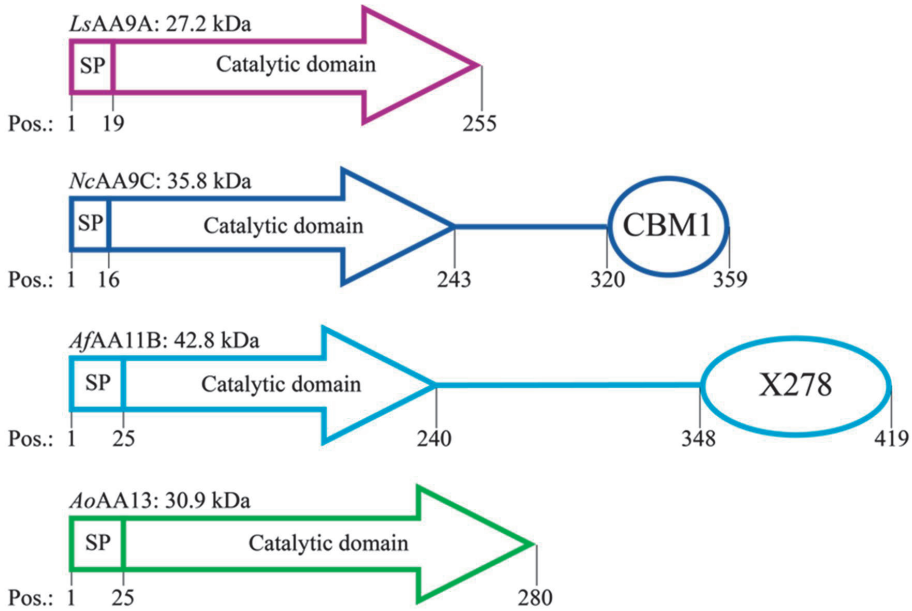
Results and discussion
Evaluation of the expression system, LPMO expression and purification

We opted to use two well-described LPMOs of the auxiliary activity (AA) family 9 that have previously been expressed in *P. pastoris* [22, 23] to evaluate the applicability of the Bisy platform strain BSYBG11 (Bisy GmbH, Hofstätten a. d. Raab, Austria) in combination with the integrative *E. coli/P. pastoris* shuttle vectors pBSYP$_{GCW14}$Z or pBSY3Z for the functional expression of LPMOs. The tested plasmids are almost identical but employ either the strong constitutive promoter of the uncharacterized *Chr1-4_0586* gene (P_{GCW14}) [24, 25] or the 500-bp fragment of the derepressed promoter of the *CAT1* gene (P_{DC}) [15] to control the transcription of the gene of interest (GOI). If not explicitly mentioned otherwise, the LPMOs were expressed with their native signal peptide (SP) to facilitate secretion to the extra-cellular environment. Despite belonging into the same family, the chosen genes originating from *Lentinus similis* (*Ls*AA9A) and *Neurospora crassa* (*Nc*AA9C) are encoding for LPMOs with a fundamental different domain architecture. *Ls*AA9A is a single-domain protein with only a catalytic domain whereas *Nc*AA9C is a multidomain protein with a catalytic domain and a CBM1 domain which is attached via a long threonine and serine-rich linker region (Fig. 1). Nonetheless, both genes were successfully cloned into the two tested plasmids and efficiently secreted by the *P. pastoris* BSYBG11 strain.

Following transformation, selection, initial cultivation in micro-scale, and analysis based on titer of secreted protein, we chose the best producing clone for each construct for medium-scale enzyme production. This was performed in 500 ml YPD in 2-L baffled shake flasks and expression of the LPMOs was confirmed by SDS-PAGE. The predicted masses of *Ls*AA9A and *Nc*AA9C are 27.1 kDa and 35.8 kDa, respectively. In silico studies of the proteins via the online tools NetNGlyc and NetOGlyc (http://www.cbs.dtu.dk/services) indicated that the catalytic domain of both enzymes and the linker region of *Nc*AA9C are prone to be N- and O-glycosylated (Fig. 1). This prediction was confirmed by SDS-PAGE analysis showing the protein band of *Ls*AA9A at ~35 kDa and *Nc*AA9C at ~50 kDa, respectively (Fig. 2A).

After 60 h of cultivation, the total amount of secreted protein from 500 mL culture ranged from 21 to 76 mg for the different strains (Bradford assay). Interestingly, the strain carrying the pBSYP$_{GCW14}$Z-*Nc*AA9C construct showed significantly higher expression levels (76 ± 7 mg) compared to the other three selected expression strains (~ 25 mg). It has been noted that this clone carrying the pBSYP$_{GCW14}$Z-*Nc*AA9C construct was already an outlier in the initial screening and all other transformants carrying this construct showed significantly lower amounts of secreted protein. Therefore, the extraordinary performance of this strain is presumed to be due to integration effects (locus, copy number) of the expression cassette and not caused by regulatory features (promoter) or related to the GOI. Nonetheless, this observation stresses the importance of assessing the secretion capacity of the different transformants prior expression clone selection as multicopy integration and locus effects seem to be the key for an extraordinary LPMO production strain.

Rieder *et al. Biotechnol Biofuels* (2021) 14:122

Page 3 of 17

Fig. 1 Schematic representation of the domain architecture of the LPMOs expressed in this study (top) including a table showing potential N- and O-linked glycosylation sites found on the catalytic domain, linker region and (potential) CBM (bottom) of the individual enzymes

SDS-PAGE analysis of the expression supernatant displayed a clean secretome with mainly recombinant LPMO. Thus, we saw the opportunity to use a single-step purification approach using size exclusion chromatography (SEC) to keep purification fast and efficient. For this purpose, 10 ml of the fivefold concentrate, corresponding to 2–7 mg of protein, were concentrated, and loaded onto SEC column. The chromatograms obtained from the SEC purification revealed that *Nc*AA9C and *Ls*AA9A elute in single peaks corresponding to their mass difference at 50 and 60 ml, respectively. Analysis by SDS-PAGE showed a homogenous appearance of the purified enzyme solution underlying the power of this one-step purification system (Fig. 2A).

The performance of the strains was evaluated by assessing the yield of pure protein we could obtain from the one-step SEC purification. From 50 mL cultivation broth, which was concentrated prior to loading onto the SEC column, 0.61 ± 0.01 and 0.60 ± 0.03 mg of pure *Ls*AA9A and 0.39 ± 0.02 and 2.08 ± 0.06 mg pure *Nc*AA9C could be achieved with pBSY3Z and the pBSYP$_{GCW14}$Z, respectively (Table 1). The shown yields correspond to 8—42 mg of pure LPMO per liter culture supernatant.

Since it was the aim to make the production of LPMOs efficient it is interesting to compare the yields obtained with the here presented expression platforms to yields reported in literature. It appears the most frequently used regulatory sequences for the transcription of
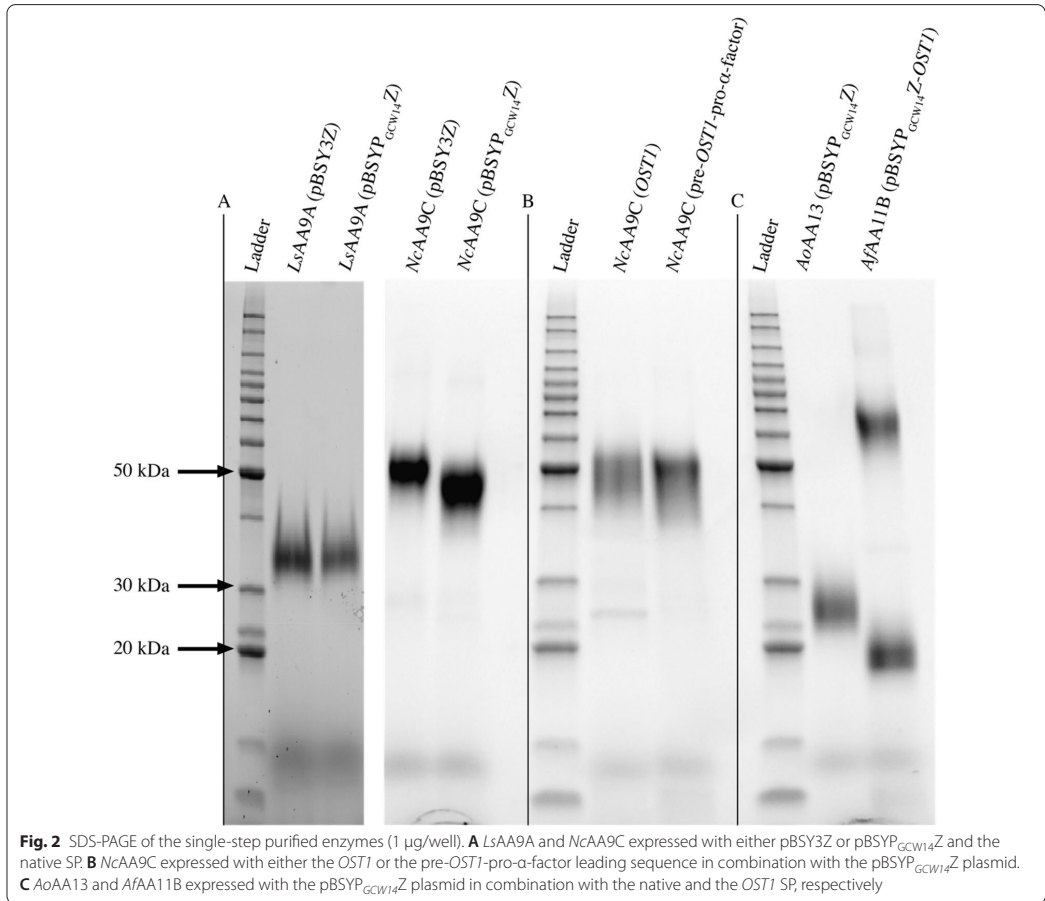
Rieder *et al. Biotechnol Biofuels*   (2021) 14:122

Page 4 of 17

Fig. 2 SDS-PAGE of the single-step purified enzymes (1 µg/well). **A** *Ls*AA9A and *Nc*AA9C expressed with either pBSY3Z or pBSYP$_{GCW14}$Z and the native SP. **B** *Nc*AA9C expressed with either the *OST1* or the pre-*OST1*-pro-α-factor leading sequence in combination with the pBSYP$_{GCW14}$Z plasmid. **C** *Ao*AA13 and *Af*AA11B expressed with the pBSYP$_{GCW14}$Z plasmid in combination with the native and the *OST1* SP, respectively

Table 1 Overview on the protein concentration (mg/ml) and total amount of protein (mg) of each step along the purification process of *Ls*AA9A and *Nc*AA9C expressed with either the pBSY3Z or the pBSY$_{PGCW14}$Z expression plasmid and the native LPMO SP, from the crude supernatant to the pure protein

Enzyme	Plasmid + SP	Supernatant		Fivefold concentrated		Purified (obtained from 50 ml cultivation supernatant)		Recovered protein
		mg	mg/ml	mg	mg/ml	mg	mg/ml	%
*Ls*AA9A	pBSY3Z + native	21 ± 5	0.042 ± 0.010	22.5 ± 0.4	0.225 ± 0.004	0.61 ± 0.01	1.2 ± 0.02	27
	pBSYP$_{GCW14}$Z + native	28 ± 2	0.056 ± 0.004	24.7 ± 1.7	0.247 ± 0.017	0.6 ± 0.03	1.4 ± 0.05	24
*Nc*AA9C	pBSY3Z + native	22.5 ± 1.5	0.045 ± 0.003	20.7 ± 2.3	0.207 ± 0.023	0.39 ± 0.02	0.8 ± 0.05	18
	pBSYP$_{GCW14}$Z + native	76 ± 7	0.153 ± 0.014	70.5 ± 0.5	0.705 ± 0.005	2.08 ± 0.06	2.9 ± 0.03	29

For precise measurements, the volume of the supernatant and the fivefold concentrate was adjusted to 500 ml and 100 ml, respectively. Please note that the values reported in the column labeled with "purified" were obtained from 50 ml cultivation supernatant

Rieder *et al. Biotechnol Biofuels*   (2021) 14:122

Page 5 of 17

recombinant LPMO in *P. pastoris* are the strong methanol-dependent promoter of the alcohol oxidase 1 gene (P_{AOX1}) or the strong constitutive glyceraldehyde-3-phosphate dehydrogenase promotor (P_{GAP}) in combination with the native LPMO SP. Unfortunately, most publications that describe LPMO characterization using *P. pastoris* as host system and medium-scale cultivation using shake flasks, do not provide any data about expression or purification yields [23, 26–28].

The few works stating LPMO production titers were usually done on bioreactor scale using defined medium, methanol induction and cultivation times far exceeding 60 h, which makes comparisons with our system difficult. These often tediously optimized advanced expression approaches result in much higher extra cellular protein titers (up to 3 g) per liter of cultivation media [22, 29, 30] and consequently also in a higher titer of LPMO, up to 0.79 g, per liter culture supernatant before purification [22].

Although we report lower total yields (up to 150 mg), it has be noted that cultivations were done in shake flasks in standard YPD over 60 h without any optimization of cultivation conditions or media, we presume much higher titers can be achieved with our strains on larger scale. Nonetheless, this system was tested on medium scale with simple cultivation techniques to make it applicable for a broad range of end users without the need for specialized equipment. Additionally, the here presented system employs regulatory sequences that circumvent

the need for methanol as inducer of protein production and are superior to the so far reported systems either in strength (P_{GCW14}) [25] or regulatory qualities (P_{DC}) [15]. However, it has be noted, that for the P_{DC} to reach its full potential a longer cultivation time would be advised, since this promoter's strength of separating culture growth and protein production was not realized to the fullest in this work.

To summarize, the herein presented expression system allows simplified protein production in YPD media without the necessity of induction which can be performed over a relatively short time without the need for specialized equipment or expertise, but at this scale its productivity is not comparable with an optimized bioreactor system. Therefore, we propose the most feasible comparison of productivity is done based on the amount of pure LPMO recovered from the total amount of secreted protein. Like for the expression several methods are described for the purification of LPMOs in literature.

One strategy for the purification of LPMOs is purification tags. For LPMO purification, the use of N-terminal tags is generally not possible due to the N-terminal histidine that is involved in the formation of the active site. Thus, a C-terminal His-tag is most commonly used for the production of LPMOs. This strategy has been shown to result in yields of ~500 mg pure protein per liter cultivation broth [30] which is much higher than the yields obtained with standard chromatography techniques (Table 2). Nonetheless, the use of His-tags is

Table 2 Comparison of expression constructs, cultivation and purification methods and the thereof resulting yields of different LPMO production protocols found in literature

Enzyme	Plasmid	Promoter	Signal peptide	Cultivation method	Purification steps	Total protein per liter culture media prior purification	Total protein per liter culture media after purification	Reference
*Tr*Cel61A	pPpT4	AOX1	Native	2-L fed-batch reactor	N.A	>400 mg	N.A	[18]
*Nc*AA9J	pPICZαA	AOX1	Native	7-L fed-batch reactor	Three chromatographic steps	1574 mg[a]	24 mg[a]	[22]
*Nc*AA9C	pPICZαA	AOX1	Native	7-L fed-batch reactor	Two chromatographic steps	2762 mg	67 mg[a]	[22]
*Nc*AA9F	pPICZαA	AOX1	Native	7-L fed-batch reactor	Three chromatographic steps	1818 mg[a]	2.4 mg[a]	[22]
*Nc*AA9E	pPICZαA	AOX1	Native	7-L fed-batch reactor	Three chromatographic steps	1327 mg[a]	2.2 mg[a]	[22]
*Nc*AA9C	pPICZαA	AOX1	Native	500-mL fed-batch reactor	Two chromatographic steps	1370 mg[a]	90 mg[a]	[29]
AaAA16	pPICZαA	AOX1	Native	1.3-L fed-batch reactor	IMAC[b], IEC	N.A	500 mg after IMAC	[30]
Several AA9s	pPICZT	AOX1	Native	2-L shake flask	IMAC	34 mg per 100 g cell wet weight	N.A	[31]

[a] Yield was adjusted to 1 L culture supernatant

[b] Resulted in LPMO inactivation

problematic as histidines can bind free metal ions that lead to complications during analysis of the enzyme action. Additionally, it has been shown that His-tag purification causes severe damage to the active site resulting a lower enzyme activity [30]. To avoid metal coordination by the tag, a cleavable version of the His-tag using the TEV protease was engineered and used by Kadowaki et al. [31]. However, this approach requires overnight incubation at room temperature and two purification rounds to separate tagged and untagged LPMOs and in the end the enzyme still contains an overhang at the C-terminus at the TEV cleavage site.
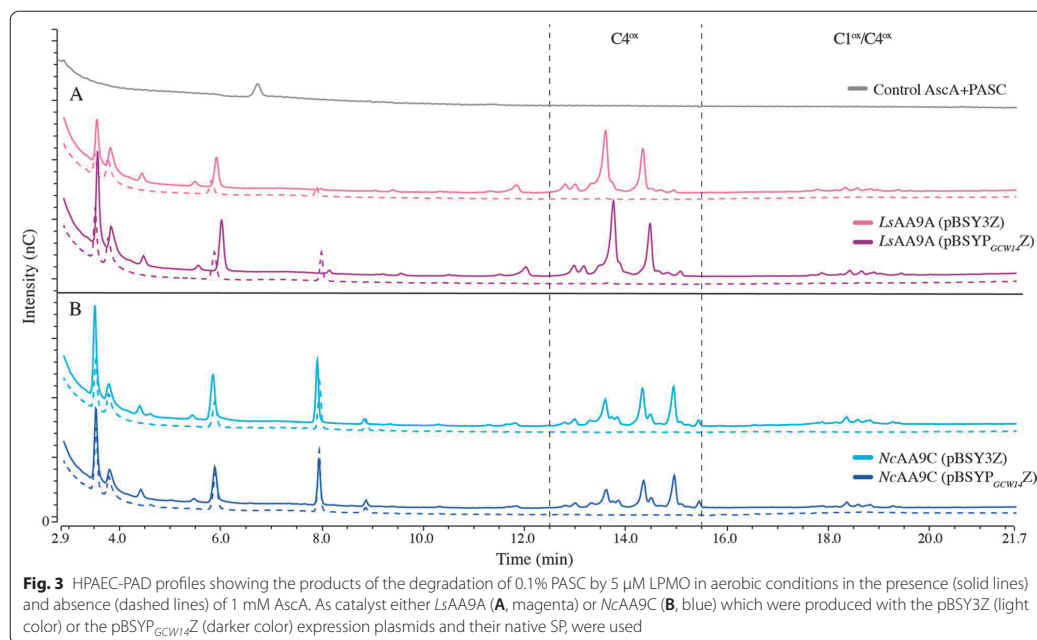
Another possibility to purify LPMOs that helps to avoid the earlier mentioned complications, is the use of standard chromatography approaches as outlined by Kittl et al. and Sygmund et al. [22, 29]. Depending on the enzyme they report two or three chromatography steps to obtain the pure LPMO which results in low enzyme recovery rates (< 8%) and final protein yields of 2–90 mg from bioreactor cultivation. Interestingly, the herein presented expression and purification strategy results in higher protein recovery rates (< 25%) and, as we think, in very competitive yields of pure LPMO (8–42 mg) keeping in mind the much simpler shake-flask cultivation.

Substrate oxidation

To assess LPMO catalysis, we incubated 5 μM of the enzymes, produced either with pBSY3Z (light color) or the pBSYP$_{GCW14}$Z (dark color), with 0.1% PASC in the presence (solid lines) and absence (dashed lines) of 1 mM L-ascorbic acid (AscA) over night (Fig. 3). Analysis via HPAEC-PAD chromatography confirmed the oxidation of PASC by *Ls*AA9A and *Nc*AA9C in the presence of reductant shown through the formation of C4 and C1/C4-oxidized products in accordance with previous published studies [32, 33]. Furthermore, the identical product profiles confirm that the expression vectors and therefore the differently regulated LPMO transcription and expression in different growth phases, has no influence on the mode of action of the enzymes.

Moreover, the results equals those by Frandsen et al. showing that *Ls*AA9A does not require the methylation at the N-terminal histidine, which occurs upon expression in higher eukaryotic fungal expression hosts (e.g., *Aspergillus* species [16]) but not in *P. pastoris*, to perform substrate oxidation [23]. This finding however is not surprising as the posttranslational methylation is proposed to have no direct influence on the catalytic activity and is solely related to enzyme stability [26].

Interestingly, the results demonstrate the differences in activity between the two LPMOs as can be seen in the

Fig. 3 HPAEC-PAD profiles showing the products of the degradation of 0.1% PASC by 5 μM LPMO in aerobic conditions in the presence (solid lines) and absence (dashed lines) of 1 mM AscA. As catalyst either *Ls*AA9A (**A**, magenta) or *Nc*AA9C (**B**, blue) which were produced with the pBSY3Z (light color) or the pBSYP$_{GCW14}$Z (darker color) expression plasmids and their native SP, were used

C4-oxidized product area of the chromatograms between 12- and 16-min retention time. Whereas *Nc*AA9C releases products ranging from DP2^{ox}-DP4^{ox}, *Ls*AA9A produces mainly DP2^{ox} and DP3^{ox}, which demonstrates the ability of *Ls*AA9A to oxidatively cleave small oligomers in accordance with the study of Frandsen et al. [33].

Hydrolytic background activity and product profile

The HPLC analysis shows the presence of native (non-oxidized) products in the absence of the reductant needed to initiate LPMO catalysis (Fig. 3). We wanted to confirm that product formation (native and oxidized) derives directly from LPMO catalysis and not from minor concentrations of endogenous secreted hydrolases that could not be removed by SEC. The following study was only done with enzymes produced with pBSYP$_{GCW14}$Z plasmid, since previous analysis showed that LPMO quality was independent of the expression vector. Reactions were set up with 1 mM oligomeric substrates (DP3-6) in the presence of i) 1 μM LPMO and 1 mM reductant, ii) 1 μM LPMO and no reductant and iii) 1 mM reductant and no LPMO and incubated for 6 h prior quenching and analysis via HPAEC-PAD chromatography For product quantification we prepared standard curves for each oligomer ranging from DP2-DP6 and used linear regression to calculate the concentration of each native oligomer that was released from LPMO catalysis as they would increase proportionally with the oxidized products. The total amount of released product was obtained by summing up the concentration found for each oligomer (Fig. 4).

The results displayed in Fig. 4 confirm that only the presence of LPMO and reductant lead to the formation of product in the form of shorter oligomers. In both control reactions which were either without reductant or enzyme (experiments ii and iii), similar product levels were detected which would not be the case if the enzyme preparation would contain cellulases as they are reductant independent. Thus, the detected shorter oligomers most certainly originate from the purchased substrate which is in accordance with the > 95% purity pledged by the producer. Comparing the amount of released product after 6 h, it appears that *Nc*AA9C outperforms *Ls*AA9A on the oxidation of oligomers with DP6 and DP5. However, *Ls*AA9A has higher activity with DP4 compared to *Nc*AA9C. This confirms the observations made in the experiments with PASC that indicate that *Ls*AA9A is able to bind and oxidize shorter oligomers. These findings are in line with previous studies of *Nc*AA9C and *Ls*AA9A that showed the oxidation of oligomeric carbohydrates and indicated that *Ls*AA9A is active on shorter oligomers than *Nc*AA9C [23, 32].
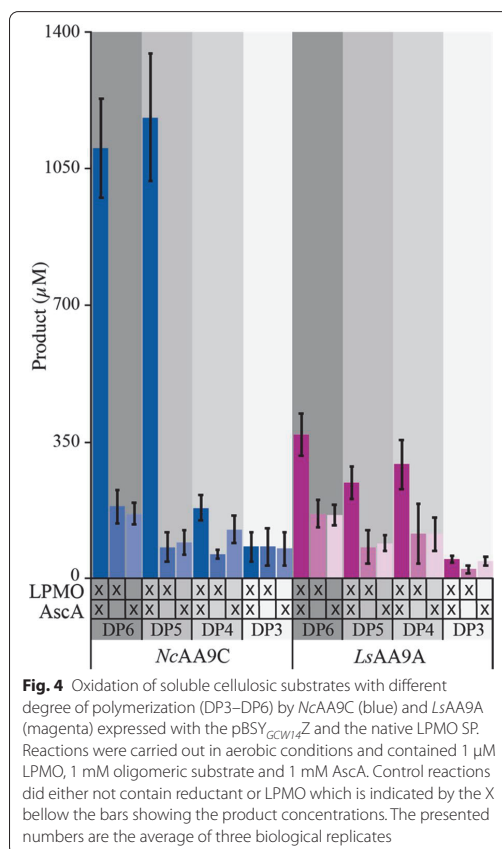

Fig. 4 Oxidation of soluble cellulosic substrates with different degree of polymerization (DP3–DP6) by *Nc*AA9C (blue) and *Ls*AA9A (magenta) expressed with the pBSY$_{GCW14}$Z and the native LPMO SP. Reactions were carried out in aerobic conditions and contained 1 μM LPMO, 1 mM oligomeric substrate and 1 mM AscA. Control reactions did either not contain reductant or LPMO which is indicated by the X bellow the bars showing the product concentrations. The presented numbers are the average of three biological replicates

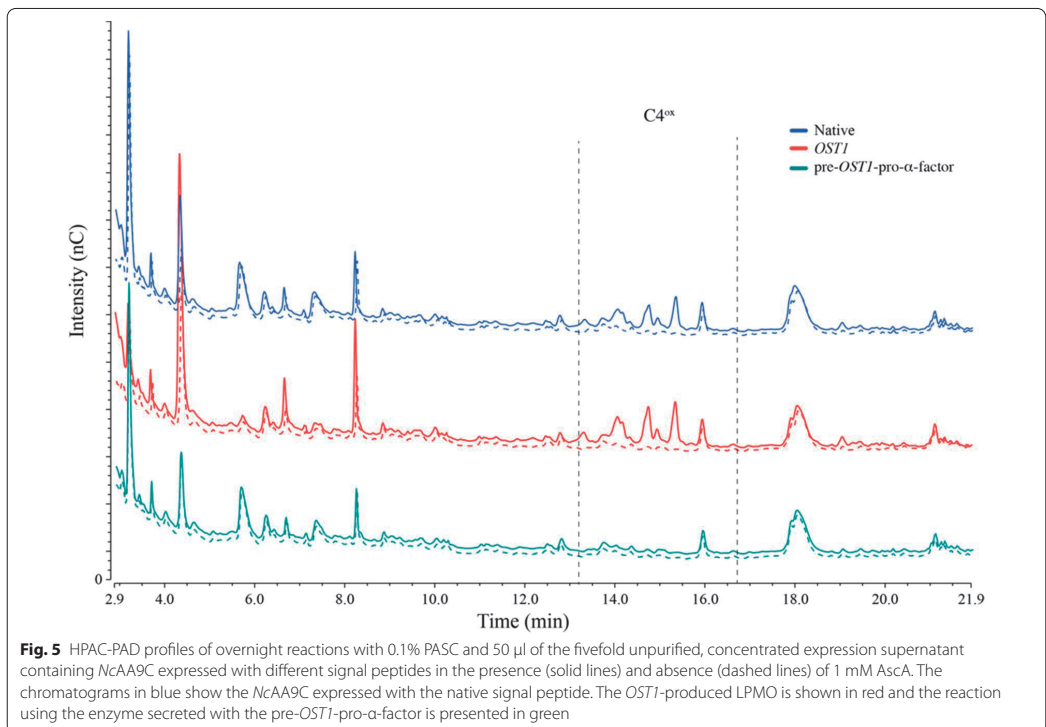**A new signal peptide for the secretion of active recombinant LPMOs**

In 2014, Fitzgerald and Glick were the first ones to use the signal peptide of the dolichyl-diphosphooligosaccharide-protein glycosyltransferase subunit 1 (*OST1*) from *S. cerevisiae* for secretion of a model protein in *P. pastoris* [34]. Four years later, Barrero et al. created an artificial hybrid secretion signal the pre-*OST1*-pro-α-factor, which combines the pre-*OST1* sequence and the pro-region of the α-mating factor, they were able to successfully secrete a tetrameric far-red fluorescent protein (E2-Crimson) [35]. In contrast to most cleavable signal peptides the pre-*OST1* facilitates co-translational translocation to the ER as a way for mature proteins to enter the secretion pathway (opposed to post-translational translocation promoted for example by the pre-pro-α-mating factor) which can be beneficial for the secretion of aggregation-prone proteins [34].

Trying to simplify and improve recombinant LPMO expression, we not only targeted transcriptional regulation by different promoters, but also the topic of heterologous signal peptides for the secretion of active recombinant LPMOs. Since it is known that the most frequently used heterologous signal peptide for protein secretion with *P. pastoris*, the pre-pro-α-mating factor of *S. cerevisiae*, does not yield active enzyme [18] we searched for suitable alternatives that have previously achieved satisfying titers secreting recombinant proteins with *P. pastoris*. Therefore, we assessed the applicability of the pre-*OST1* signal peptide and its hybrid, for the expression of active LPMO. For this purpose, the native signal peptide of *Nc*AA9C was exchanged against the *OST1* and the pre-*OST1*-pro-α-factor and were used for protein production with *P. pastoris*. Expression and secretion could be confirmed for both LPMO-signal peptide constructs by SDS-PAGE (Fig. 2B). Single step purification from 50 mL broth yielded 1.38 ± 0.06 and 0.93 ± 0.1 mg of protein with *OST1* and the pre-*OST1*-pro-α-factor, respectively, which is less than the 2.08 ± 0.06 mg protein we obtained earlier with the same plasmid but with the native LPMO SP (Table 1).

Nonetheless, it must be noted that it is not possible to directly compare the effect of the signal peptides with respect to obtained protein quantity as the most active clones of the landscape (clonal outliers) were chosen for LPMO production, which resulted in high protein titers, but brings the bias of locus and copy number effects [36, 37]. However, the data suggests that the expression of LPMOs is independent of the translocation process and therefore, the place of translation, as recombinant protein was obtained from both constructs.

To obtain active recombinant LPMOs, correct cleavage and processing of the enzymes N-terminus is essential since the conserved N-terminal histidine is part of the active site and plays an important role in the enzymes ability to catalyze substrate oxidation. To assess the applicability of the different recombinant fungal signal peptides to efficiently secret active functional LPMOs, HPAEC-PAD analysis was undertaken to determine oxidized products resulting from enzymes activity.

Due to good expression levels, 50 μL of the fivefold concentrated, unpurified expression supernatant was directly incubated with 0.1% PASC in the presence (solid lines) and absence (dashed lines) of 1 mM AscA (Fig. 5). HPLC

Fig. 5 HPAC-PAD profiles of overnight reactions with 0.1% PASC and 50 μl of the fivefold unpurified, concentrated expression supernatant containing *Nc*AA9C expressed with different signal peptides in the presence (solid lines) and absence (dashed lines) of 1 mM AscA. The chromatograms in blue show the *Nc*AA9C expressed with the native signal peptide. The *OST1*-produced LPMO is shown in red and the reaction using the enzyme secreted with the pre-*OST1*-pro-α-factor is presented in green

Rieder *et al. Biotechnol Biofuels*   (2021) 14:122

Page 9 of 17

analyses clearly shows, that only reactions with *Nc*AA9C secreted with either the native or the *OST1* signal peptide contain C4-oxidized degradation products from PASC. In the reaction with the LPMO that was secreted with the pre-*OST1*- pro-α-factor, we could not observe any difference to the control reaction without reductant which implies that no substrate oxidation occurred indicating that the enzyme is inactive.

Moreover, regarding enzyme activity, two further observations were made when the concentrated culture supernatant was used as catalyst: firstly, no external $CuSO_4$ had to be added to the reactions. This indicates that the enzyme naturally contains sufficient amounts of copper in their active site for reactivity, which is advantageous when thinking about industrial use of LPMOs or screening processes during enzyme engineering. Secondly, an external reductant was needed to obtain substrate oxidation. This suggests that no reductant powerful enough to prime the copper center is present once the cells were separated from the expression broth and the initial concentration step was performed which is highly beneficial as the likelihood of damage to the enzymes active center due to auto-oxidation during storage of the crude enzyme sample until purification is drastically reduced.

To confirm that inactivity of the LPMO secreted with the pre-*OST1*-pro-α-factor relates to incorrect processing of the N-terminus, a MALDI-ToF MS analysis was performed on trypsin digested LPMOs expressed with the different signal peptides. Based on in silico trypsin digestions (Table 5), a correctly processed N-terminus results in a peptide with the sequence: "**H**TIFQK", having a mass of 773. Non-correctly processed N-termini would have increased masses due to additional amino acids N-terminal of the terminal histidine as the downstream located trypsin cleavage site would not be affected. The resulting peptides of proteins with incorrectly processed N-termini would have m/z values of 1986, 3104 and 1173, for the *Nc*AA9C native, the *OST1* and the pre-*OST1*-pro-α-factor signal peptide, respectively.

In the spectra of the *Nc*AA9C samples with the native and the *OST1* signal peptide peaks at the mass of 773 could be identified (Fig. 6, red and blue trace). In both spectra, no peaks, at m/z values of 1986 and 3104 corresponding to wrongly processed N-termini could be detected (small inlaid boxes in Fig. 6). In the spectra of *Nc*AA9C samples secreted with the *OST1*-pro-α-factor, a peak at a m/z value of 1173 could be found, which corresponds to a peptide with the sequence: "EAEA**H**TIFQK" (Fig. 6, green trace). Therefore, we presume that the previously observed missing functionality of this sample is due to incorrect signal peptide cleavage, which resulted in a wrongly processed N-terminus and loss of enzyme

activity. The "EAEA" found N-terminal of the terminal histidine is part of the Ste13 cleavage site, which is notoriously problematic in terms of N-terminal processing [20].

In summary, the data confirm that the *OST1* signal peptide both successfully secrets *Nc*AA9C and is correctly recognized and cleaved by *P. pastoris*, which results in a homogenously processed N-terminus and full enzymatic functionality. In contrast, the pre-*OST1*-pro-α-factor is incorrectly processed, which leads to a loss of activity of *Nc*AA9C and makes this signal peptide unsuitable for recombinant production of LPMOs. This finding is in line with reports of Tanghe et al. [18], who reported the unsuitability of the α-factor for secretion of LPMOs, as the pre-*OST1*-pro-α-factor and the native α-factor signal peptide share the same pro- sequence, which is adjacent to the N-terminus of the mature protein.

Expanding to other LPMO families

To further investigate the applicability of the presented novel expression tools for recombinant production of LPMOs, we expanded the testing to other LPMO families. Additionally, to the already presented LPMOs *Ls*AA9A and *Nc*AA9A, we produced a single-domain AA13 from *Aspergillus oryzae* (*Ao*AA13) and a multi-domain AA11 from *Aspergillus fumigatus* (*Af*AA11B) using pBSYP$_{GCW14}$Z and pBSYP$_{GCW14}$Z-*OST1*, respectively. For *Ao*AA13 this is, to our best knowledge, the first report of a successful recombinant expression of active enzyme using *P. pastoris* as all published articles refer to the same patent that describes the expression in *A. oryzae* [38].

Expression and purification of *Ao*AA13 was done as described above. Again, expression analysis by SDS-PAGE indicated a rather clean expression broth with mainly recombinant, LPMO which allowed us to use one single SEC step for purification which yielded in pure enzyme (Fig. 2C). The enzyme is on the gel visible as a band at ~25 kDa which is in accordance with the expected theoretical calculated mass of 27.8 kDa (Fig. 1). For the *Ao*AA13 we got 1.58 ± 0.11 mg of protein from 50 ml expression broth corresponding to ~30 mg pure LPMO from 1 L culture supernatant which is comparable to the yields we obtained for other LPMOs.

For *Af*AA11B protein expression was lower than for the other tested LPMOs. To ensure complete isolation of secreted *Af*AA11B of the expression supernatant, a hydrophobic interaction chromatography (HIC) step was introduced to bind the protein on the column and elute it in a small volume to reduce the time required for concentration prior SEC. The SEC purification was executed as described for the other LPMOs, and *Af*AA11B eluted in a single peak off the column. In the subsequent SDS-PAGE
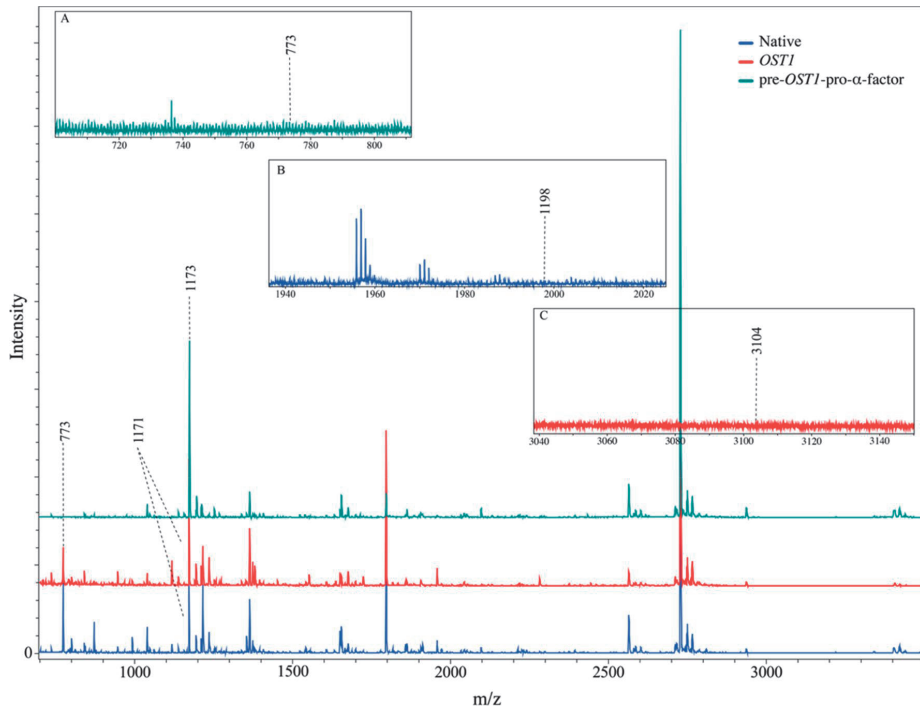
Fig. 6 MALDI-ToF spectra of the trypsin digested *Nc*AA9C expressed with the different signal peptides. The different colors present the different constructs. The spectrum of the LPMO expressed with the native signal peptide is shown in blue whereas the enzyme expressed with *OST1* is presented in red and the one produced with the pre-*OST1*-pro-α-factor in green. The inlaid boxes show the spectra in the areas in which the masses of the correctly processed N-terminus in case of the pre-*OST1*-pro-α-factor (**A**) or the wrongly processed N-termini of the other two constructs (**B**, **C**), would be expected

analysis a double band was observed (Fig. 2C) with the LPMO at ~60 kDa and a contamination at ~20 kDa. Based on the previous in silico analysis we expected heavy glycosylation (Fig. 1) of *Af*AA11B which is confirmed by SDS-PAGE analyzes as the enzyme appears to be about 17 kDa bigger than the theoretical calculated molecular weight (42.8 kDa).

Repeating the SEC purification step with a fraction of the purified LPMO did not change the composition of the protein solution (double band on SDS gel), which indicates that the second band is not from a native *P. pastoris* protein. We presume, that the LPMO linker region with the CBM separates from the catalytic domain during the preparation of the sample prior to the SDS-PAGE analysis or in the analysis, we do not know exactly how, which results in the second protein form. From the process we obtained 1.38 ± 0.00 mg of pure protein from 500 mL cultivation broth, which is about 10 times less in comparison to the other tested LPMOs.

The substrate oxidation ability of 1 μM *Ao*AA13 was tested by incubation with 0.1% starch, maltopentaose, panose, maltotriosyl-maltotriose or ismaltotriose (1 mM each) in the presence and absence of 1 mM reductant overnight. From none of these substrates oxidized products could be detected, which is in agreement with published results of this particular LPMO on starch [39]. To confirm functional expression of *Ao*AA13, the oxidase activity assay described by Kittl et al. [22] was used, which is based on the enzymes ability to produce H_2O_2 from a reduced copper center. To ensure that the observed H_2O_2 does not origin from unbound copper, control reactions with $CuSO_4$ were included. From the progress curves (Fig. 7A) H_2O_2 production rates of 0.03 ± 0.003 μM*s^{-1} and 0.01 ± 0.001 μM*s^{-1} for the reaction with LPMO and $CuSO_4$ were calculated, respectively, which confirms the structural integrity of the active site and indicates that we lack the correct carbohydrates to detect the formation of oxidized products.
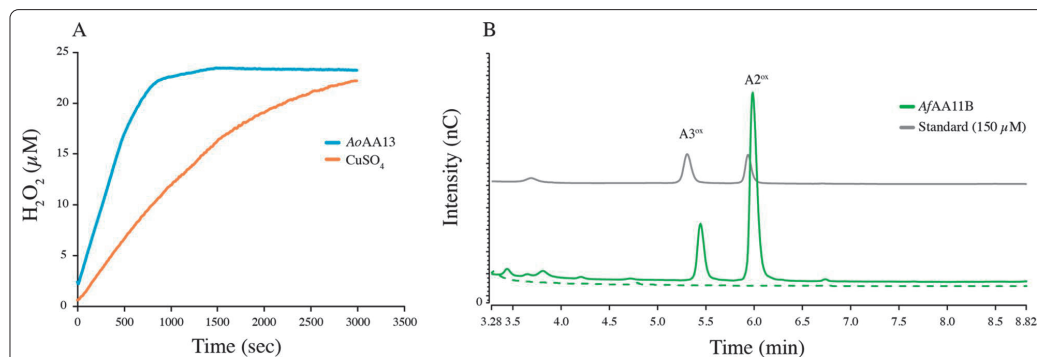
Fig. 7 H2O2 production curve (**A**) and HPEAC-PAD profile (**B**) to confirm the functional expression of *Ao*AA13 and *Af*AA11B by using either the pBSYP$_{GCW14}$Z or the pBSYP$_{GCW14}$Z-*OST1* expression plasmid. **A** For the H2O2 production curve 3 μM *Ao*AA13/CuSO4, 100 μM Amplex Red and 0.025 mg/ml HRP were used, and the reaction was initiated by the addition of 50 μM AscA (all final concentrations). Control reactions did not contain catalyst. The presented curves represent the average of three independent replicates. **B** To assess the substrate oxidation ability of *Af*AA11B standard aerobic reactions (green) with 1 μM LPMO, 1 mM (GlcNAc)4 in the presence (solid lines) and absence (dashed lines) of 1 mM AscA were made. To show that peaks correspond to oxidized products, a standard containing 150 μM oxidized chitobiose and chitotriose is shown (grey)

To confirm the substrate oxidation ability of *Af*AA11B and therefore its functional secretion using the *OST1* as a leader sequence, the enzyme was incubated with (Glc-NAc)4 in the presence and absence of AscA (1 mM) over night. Reaction products were analyzed by HPAEC-PAD and the chromatograms (Fig. 7B) confirm the release of oxidized products from *Af*AA11B in the presence of reductant (solid lines) and the absence of products in the control reaction without reductant (dashed lines) confirming the correct processing of the N-terminus.

Conclusion

The presented study gives novel insights into the expression of fungal LPMOs using the industrially most relevant expression host *P. pastoris*. The presented data show the successful and active expression of four LPMOs from three different fungal LPMO families, one of which (*Ao*AA13) has, to our best knowledge, never before been expressed in a lower eukaryotic host.

The implementation of advanced molecular biology tools for the genetic manipulation of *P. pastoris* made cloning, expression and downstream processing as effortless as possible. Our data demonstrate that both tested vectors that employ differently regulating promoters (pBSY3Z and pBSYP$_{GCW14}$Z) in combination with the *Pichia pastoris* strain BSYBG11 are suitable for the expression of LPMOs. The presented protocols are standardized, require little equipment, short cultivation periods and result in up to 42 mg of pure LPMO per liter of cultivation supernatant with the limited effort of a medium-scale cultivation. The use of medium-scale shake flasks with subsequent tag-less single-step purification

makes the production of valuable LPMOs no longer tedious and time consuming and abolishes enzyme production as limiting factor in this field of science.

To expand the toolbox for LPMO-tailored expression further we report, for the first time, a non-LPMO-originating signal peptide that facilitates secretion of active LPMOs. The *OST1* signal peptide in combination with the presented regulatory tools, facilitates an efficient way for LPMO discovery, as cloning is streamlined, and the achieved protein concentrations are high enough to determine substrate oxidation activity from crude supernatant. Here, the *OST1* presents an interesting alternative to using an LPMOs native signal peptide, as it provides a way to express bacterial LPMOs in *P. pastoris* or to overcome potential inactivation caused by incorrectly processed N-termini.

Moreover, this is, to our best knowledge, only the fourth time the *OST1* signal peptide has been reported for secretion of proteins with *P. pastoris* and the second time the secretion of an enzyme is reported [34, 35, 40]. Additionally, we are the first ones to investigate N-terminal processing of this signal peptide by MS. The fact that this N-terminal leading sequence is cleaved perfectly makes it an interesting candidate for the production of proteins that require a largely homogenous N-terminus, i.e., pharmaceutically relevant proteins.

Material and methods

Chemicals, microorganisms and media

All chemicals were purchased from Carl Roth (Karlsruhe, Germany), VWR or Sigma-Aldrich. Oligonucleotides were ordered from Integrated DNA Technologies

(Leuven, Belgium) and BioXP® regents from SGI-DNA, Inc. (San Diego, CA, USA). Kits used for plasmid isolation (Wizard® Plus SV Minipreps DNA Purification Systems) and purification of agarose gel slices, PCRs and restriction digests (Wizard® SV Gel and PCR Clean-Up System) were purchased from Promega (Fitchburg, WI, USA). For cloning by Gibson isothermal assembly, Gibson Assembly® HiFi 1-Step Kit (SGI-DNA, Inc., San Diego, CA, USA) was used, all other enzymes and Phusion DNA polymerase were obtained from Thermo Fisher Scientific (Waltham, MA, USA).

For standard cloning procedures and plasmid propagation, self-made chemically competent *Escherichia coli* XL1-Blue were used (Mix & Go! *E. coli* Transformation Kit and Buffer Set, Zymo research, Irivine, CA, USA). For amplification of BioXP synthesized plasmids, NEB® 5-alpha Competent *E. coli* (High Efficiency) cells (New England Biolabs, Ipswich, MA, USA) were used and transfection was performed according to the manual for high efficiency transformation. As an eukaryotic expression host Bisy GmbH provided the killer plasmid-free *P. pastoris* strain BSYBG11(Δ*AOX1*, Mut^S), which originates from BG08 (BioGrammatics Inc., Carlsbad, CA, USA) and is a NRRL Y-11,430 derivative [41].

E. coli strains were cultivated in/on LB-medium (Luria/Miller) supplemented with Zeocin to a final concentration of 25 µg/mL (Life Technologies, Carlsbad, CA, USA).

For selection and expression of *P. pastoris* strains YPD containing 1% (w/v) yeast extract, 2% (w/v) peptone and 2% (w/v) glucose) was used. For selection following transformation and re-streaking of transformants and expression clones YPD agar plates were supplemented with100 µg/ml Zeocin.

Assembly of the novel vector backbone

Throughout this study, we used the commercially available *P. pastoris/E. coli* shuttle vector pBSY3Z (Bisy GmbH, Hofstätten a. d. Raab, Austria) and the newly assembled pBSYP$_{GCW14}$Z. The pBSYP$_{GCW14}$Z plasmid is except of the promotor that controls the expression of the GOI identical to the pBSY3Z plasmid. To exchange the promoter (P$_{DC}$), we digested the pBSY3Z plasmid with *Eco*RI and *Smi*I and inserted the PCR-amplified P$_{GCW14}$ promoter [25, 41] that contained 5´ and 3´ homologous regions to the vector backbone by Gibson assembly® upstream of the multiple cloning site (MCS) (Fig. 8A). The sequence of the newly assembled pBSYP$_{GCW14}$Z was verified by Sanger sequencing (Microsynth AG, Balgach, Switzerland).

LPMO construct assembly

Molecular biological in silico design of the expression plasmids was performed using SnapGene (Chicago, IL, USA). De novo synthesis of the LPMO genes and
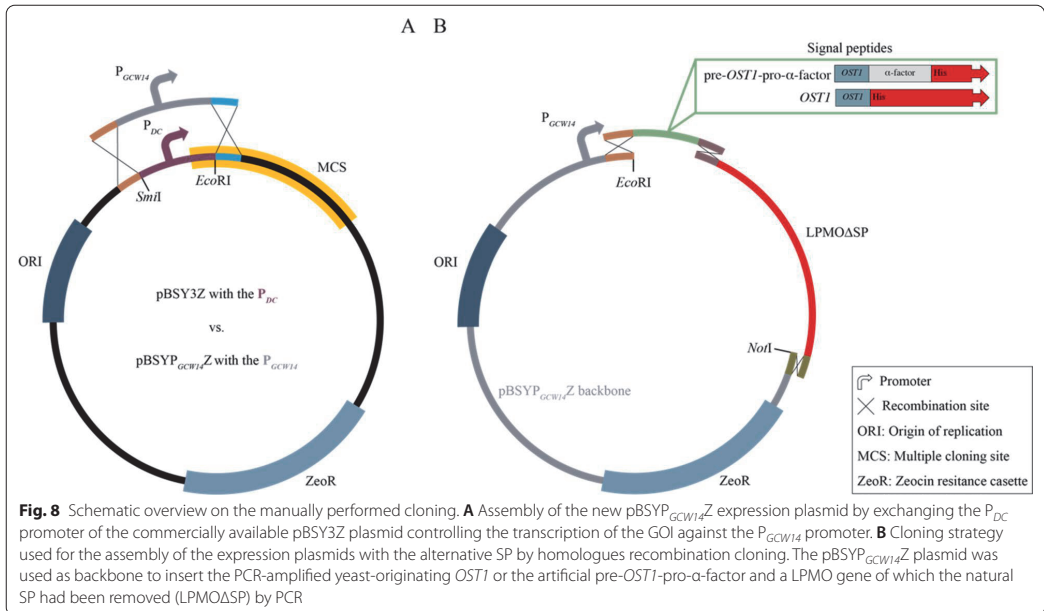

Fig. 8 Schematic overview on the manually performed cloning. **A** Assembly of the new pBSYP$_{GCW14}$Z expression plasmid by exchanging the P$_{DC}$ promoter of the commercially available pBSY3Z plasmid controlling the transcription of the GOI against the P$_{GCW14}$ promoter. **B** Cloning strategy used for the assembly of the expression plasmids with the alternative SP by homologues recombination cloning. The pBSYP$_{GCW14}$Z plasmid was used as backbone to insert the PCR-amplified yeast-originating *OST1* or the artificial pre-*OST1*-pro-α-factor and a LPMO gene of which the natural SP had been removed (LPMOΔSP) by PCR

Rieder *et al. Biotechnol Biofuels*   (2021) 14:122

Page 13 of 17

cloning were performed using the BioXP 3000 system (SGI-DNA, Inc., San Diego, CA, USA). Since the BioXP-mediated cloning is based on homologous recombination cloning, the 5′ and 3′-ends of the codon-optimized genes of *Ls*AA9A (AN: ALN96977), *Nc*AA9C (AN: XP_965598), *Af*AA11B (AN: XP_748042) and *Ao*AA13 (AN: XP_023092053) that included the native LPMO SP were designed to have a 30 bp overhang to the promoter and terminator region of the target vector backbone. The BioXP 3000 system was set up according to the manual and the cloning strip of the instrument was filled with 23 µl of 20 ng/µl *Sap*I linearized pBSY3Z and pBSYP$_{GCW14}$Z, respectively. The output of the BioXP run was in total eight plasmids with either the pBYSP$_{GCW14}$Z or the pBYS3Z expression plasmid into which one of the four LPMO genes had been cloned.

Expression plasmids with the alternative SP are based on the pBYSP$_{GCW14}$Z backbone. Assembly was done using three DNA fragments, one was the linearized vector backbone pBYSP$_{GCW14}$Z, one the respective LPMO without its native signal sequence and the last one the novel alternative signal sequence. The native signal peptides of *Nc*LPMO9C and *Af*AA11B were removed by PCR employing primer pair one or two (Table 4) using the newly synthesized LPMO expression plasmids as template resulting in *Nc*AA9CΔSP and *Af*AA11BΔSP, which

are for now on referred to as LPMOΔSP. The *OST1* and pre-*OST1*-pro-α-factor signal sequence (SP) (Table 3) were amplified from the commercially available plasmid pBSY3S2Z (Bisy GmbH, Hofstätten a. d. Raab, Austria) which contains the pre-*OST1*-pro-α-factor by using primer pair three and four, respectively (Table 4). Since our cloning strategy is based on homologous recombination cloning, we introduced 5′ and 3′ overhangs to the flanking DNA regions during amplification. This means that the 5′-ends of the PCR-amplified SP were overlapping with the promoter region of the pBSYP$_{GCW14}$Z plasmid and the 3′-end overlapped with the 5′-end of the LPMOΔSP genes. Similarly, the PCR-amplified LPMOΔSP gene had a homologous region to the SP fragment at the 5′-end and an overhang to terminator region of the plasmid backbone at the 3′-end. Prior to Gibson isothermal assembly the pBSYP$_{GCW14}$Z plasmid was digested with *Not*I and *Eco*RI which resulted in a linear DNA fragment that contained the required homologous region to the signal peptide fragment at the promotor region and the correct overlap to the LPMOΔSP fragment at the terminator region.

For the final plasmid construction, we followed the manual provided with the Gibson assembly® kit. The pBSYP$_{GCW14}$Z-*OST1*-*Nc*AA9C construct was assembled by incubation of the linearized pBSYP$_{GCW14}$Z

Table 3 DNA sequence of the tested yeast-originating *OST1* and the artificial pre-*OST1*-pro-α-factor secretion signal

Signal peptide	DNA sequence 5` 3`
OST1	atgaggcaggtttggttctcttggattgtgtgggattgttcctatgttttttcaacgtgtcttctgct
pre-*OST1*-pro-α-factor	atgaggcaggtttggttctcttggattgtgtgggattgttcctatgttttttcaacgtgtcttctgctgcccctgttaacactaccactgaagacgagactgctcaaattccagctgaagcagttatcggttactctgaccttgagggtgatttcgacgtcgctgttttgcctttctctgcttccattgctgctaaggaagagggtgtctctctcgagaagagagaggccgaagct

Table 4 Primer pairs used for DNA amplification

#	Construct	DNA sequence 5`→3`
1	*Nc*AA9CΔSP	
	FWD	catacaattttttcagaaggtgtcagtcaacg
	REV	tggcattctgacatcctcttgagc
2	*Af*AA11BΔSP	
	FWD	catatgaagatgagacaacccactccatattc
	REV	tggcattctgacatcctcttgagc
3	*OST1*	
	FWD	gtcactcgcttcactcaacaacaaaaatgaggcaggtttggttctcttgg
	REV	ccgttgactgacaccttctgaaaaattgtatgagcagaagacacgttgaaaaaacataggaac
4	pre- *OST1*-pro-α-factor	
	FWD	gtcactcgcttcactcaacaacaaaaatgaggcaggtttggttctcttgg
	REV	ccgttgactgacaccttctgaaaaattgtatgagcttcggcctctctcttctcg

backbone with the *OST1* and *Nc*AA9CΔSP fragment. The pBSYP_{GCW14}Z-pre-*OST1*-pro-α-factor-*Nc*AA9C and the pBSYP_{GCW14}Z-*OST1*-*Af*AA11B constructs were assembled identically but instead of the *OST1* we used the pre-*OST1*-pro-α-factor fragment and instead of the NcAA9CΔSP we used the *Af*AA11BΔSP fragment, respectively (Fig. 8B). Sequence of the plasmids was verified by Sanger sequencing (Microsynth AG, Balgach, Switzerland).

Pichia pastoris transformation and screening

The expression plasmids were *Smi*I linearized prior to transformation of the eukaryotic host. Transformation of the *Pichia pastoris* BSYBG11 one-shot ready competent cells (Bisy GmbH, Hofstätten a. d. Raab, Austria) was done according BSY *Pichia pastoris* transformation protocol.

Following 48 h of growth and antibiotic selection on agar plates, 24 transformants of each construct were randomly selected for expression analysis. Microscale cultivation (96 deep-well plate cultures) of *P. pastoris* cells carrying constructs based on pBSY3Z was done according to the BSY high-throughput screening protocol, which is based on the work of R. Weis et al. [42]. Microscale cultivation (96 deep-well plate cultures) of *P. pastoris* cells carrying constructs based on pBSYP_{GCW14}Z was performed in YPD media over 60 h due to the P_{GCW14}, which facilitates methanol-independent constitutive expression.

At the end of the cultivation, optical cell density of each microscale culture was determined as absorbance at 600 nm (OD_{600}). Additionally, total protein amount secreted by each culture was determined by Bradford protein assay after harvesting the culture medium by centrifugation at 4000 rpm, 4 °C for 10 min. For each culture, we normalized the protein amount by the corresponding OD_{600} and corrected by the wild-type secretion. This allowed us to select the highest secreting clone for further characterization and evaluate the average expression for each construct. Additionally, expression of the target protein by selected clones was confirmed by sodium dodecyl sulphate–polyacrylamide gel electrophoresis (SDS-PAGE). If not mentioned different protein samples were reduced and denatured prior SDS-PAGE analysis.

Expression, purification, and copper loading

500 ml YPD (1% (w/v) yeast extract, 2% (w/v) peptone and 2% (w/v) glucose) in a 2-L baffled shake flask was inoculated with a fresh single yeast colony and incubated for 60 h at 28 °C and 120 rpm. Cells and supernatant were separated by centrifugation at 10,000x*g* and 4 °C for 15 min. The protein containing supernatant was filtered by a 0.22 µM Steritop® bottle-top filter (Merck Millipore,

Burlington, MA, USA) and concentrated fivefold by a VivaFlow 200 tangential crossflow concentrator (molecular weight cut-off, MWCO 10 kDa, Sartorius Stedim Biotech Gmbh, Germany).

For size exclusion chromatography (SEC), we used a HiLoad 16/60 Superdex 75 size exclusion column (GE Healthcare Life Sciences, Uppsala, Sweden) that was equilibrated with 50 mM BisTris/HCl buffer (pH 6.5) containing 150 mM NaCl and operated with an Äkta purifier (GE Healthcare Life Sciences, Uppsala, Sweden). Prior to loading of the samples onto the column, the expression supernatant was concentrated tenfold. We typically applied small volumes (< 1 mL) to column to ensure good separation and the isolation of pure protein. The protein was eluted and fractionated using a flow rate of 1 ml/min. Fractions containing the pure enzyme were identified using SDS-PAGE, pooled, and concentrated using Amicon Ultra centrifugal filters (MWCO 10 kDa, Merck Millipore, Burlington, MA, USA).

When a hydropic interaction chromatography (HIC) step was performed prior SEC, we added ammonium sulfate to a final concentration of 2.4 M to the protein containing supernatant. Here, we used a 5 mL HiTrap Phenyl FF column (GE Healthcare Life Sciences, Uppsala, Sweden) equilibrated with 50 mM BisTris/HCl buffer (pH 6.5), containing 2.4 M ammonium sulfate. To elute the protein from the column, a 35 ml linear gradient from 2.4 M to 0 M ammonium sulfate in 50 mM BisTris/HCl buffer (pH 6.5) using a flowrate of 1.8 ml/min was used. The collected fractions were analyzed by SDS-PAGE and pooled if the target protein was present. Prior to isolation by SEC, the protein containing solution was concentrated using Amicon Ultra centrifugal filters (MWCO 10 kDa, Merck Millipore, Burlington, MA, USA).

Copper saturation of the purified LPMO was ensured by adding a 1:3 molecular ratio of enzyme to CuSO₄ and left for incubation for 1 h at $t = 4$ °C. Remaining copper and salt were removed by exchanging the total volume to 50 mM BisTris/HCl buffer (pH 6.5) four times using Amicon Ultra centrifugal filters (MWCO 10 kDa, Merck Millipore, Burlington, MA, USA). The homogeneity of the enzymes was evaluated by SDS-PAGE and concentration was measured by the Bradford assay. The purified and copper-saturated proteins were stored at 4 °C until further use.

LPMO reactions

Standard LPMO reactions contained 1-5 µM enzyme, 0.1% phosphoric acid-swollen cellulose (PASC) or 1 mM oligomeric substrates (95% purity; Megazyme, Wicklow, Ireland) in 50 mM BisTris/HCl buffer (pH 6.5) and were incubated at $t = 37$ °C and 750 rpm (Thermomixer C, Eppendorf, Hamburg, Germany). Reactions were

Rieder *et al. Biotechnol Biofuels*   (2021) 14:122

Page 15 of 17

initiated by the addition of 1 mM AscA and either terminated by boiling (crystalline substrates) or by the addition of 7 reaction volumes of 200 mM NaOH (soluble substrates).

Reaction products were detected using high-performance anion exchange chromatography with pulsed amperometric detection (HPAEC-PAD). For the analyses, a Dionex ICS5000 system, equipped with a CarboPac PA200 analytical column and a CarboPac PA200 guard column, with a 26 min gradient for cellulose and an 18 min gradient for chitin containing samples [43].

The activity of the cellulose-active LPMOs was assessed by quantification of the native products that would proportionally increase upon oxidation of soluble substrates. For the confirmation of oxidized chitin products, in-house made standards were used as described elsewhere [44]. Chromatograms were recorded and analyzed with Chromeleon.

H$_2$O$_2$ production assay

The formation of H$_2$O$_2$ was measured to determine the LPMOs oxidase activity as described previously by Kittl et al. [22]. The reaction was carried out in 50 mM Bis-Tris/HCl buffer (pH 6.5) and contained 3 µM LPMO, 100 µM Amplex Red and 0.025 mg/ml HRP. The reaction

was initiated by the addition of AscA (final concentration 50 µM) after 5 min preincubation at $t = 30$ °C. The formation of resorufin was monitored at 540 nm. Blank reaction did not contain LPMO and standards had AscA added to capture potential interactions between the substrate/product and the reductant.

MALDI-ToF analysis

Matrix-assisted laser desorption/ionization time of flight mass spectrometry (MALDI-ToF MS) analyses were performed on an Ultraflex MALDI-ToF/ToF instrument (Bruker Daltonik GmbH, Bremen, Germany) equipped with a Nitrogen 337 nm laser applying suitable preinstalled instrument methods.

To investigate the homogeneity of our protein stocks, the purified protein was mixed in a 1:1 ratio with a 2% TFA solution. As matrix a solution containing 3.8 mg/ml 2,5-DHAP and 4.5 mg/ml DAC in 75% ethanol was used. Prior analysis the protein solution and matrix were mixed in a 1:1 ratio and spotted on a ground steel plate.

The correct processing of the N-terminus was examined by trypsin fragmentation of the LPMOs with subsequent MALDI-ToF analysis. MS sample preparation followed the protocol described by Tuveng et al. [45]. For reduction and acetylation of the protein sample, 30 µg of the purified

Table 5 List with the theoretical peptide masses of the trypsin digested *Nc*AA9C expressed with the different signal peptides

Fragment	Masses expected if the signal peptide is cleaved correctly	Masses expected of a wrongly processed N-terminus		
	Independent of SP	Native	OST1	pre- *OST1*-pro-α-factor
1	**773.4304**	**1986.1018**	**3104.5855**	6754.3264
2	1215.6328	1215.6328	1215.6328	890.4465
3	2505.1782	2505.1782	2505.1782	**1173.5898**
4	1171.6317	1171.6317	1171.6317	1215.6328
5	2725.2865	2725.2865	2725.2865	2505.1782
6	991.5645	991.5645	991.5645	1171.6317
7	1234.6273	1234.6273	1234.6273	2725.2865
8	945.4999	945.4999	945.4999	991.5645
9	3347.5322	3347.5322	3347.5322	1234.6273
10	5926.898	5926.898	5926.898	945.4999
11	6678.2651	6678.2651	6678.2651	3347.5322
12	1020.5142	1020.5142	1020.5142	5926.898
13	1469.7091	1469.7091	1469.7091	6678.2651
14	1038.5037	1038.5037	1038.5037	1020.5142
15	1355.5718	1355.5718	1355.5718	1469.7091
16	1359.5674	1359.5674	1359.5674	1038.5037
17				1355.5718
18				1359.5674

The second column shows the expected masses of a correctly processed enzyme and is therefore independent of the leading sequence. In the columns 3 to 5 the expected masses of wrongly processed N-termini of the different signal peptides are listed. Highlighted in bold are the masses of the peptides containing the N-terminal histidine

Rieder *et al. Biotechnol Biofuels*   (2021) 14:122

Page 16 of 17

enzyme was mixed with dithiothreitol (DTT, final concentration 10 mM) in Eppendorf LoBind tubes and incubated for 30 min. Subsequently, indole-3-acetic acid (IAA, final concentration of 15 mM) was added and incubated another 30 min in the dark before digestion of the enzymes with 0.75 µg trypsin (Sequencing Grade Modified Trypsin, Promega) over night at 37 °C. The reaction was quenched with trifluoroacetic acid (TFA, final concentration of 1%) and concentrated by C_{18} solid phase extraction ZipTips (Merck Millipore, Cork, Ireland). The peptides were eluted in 10 µl 70% ACN with 0.1% TFA and dried under vacuum. The peptide pellet was suspended in 10 µL of 2% ACN with 0.1% TFA. Prior to analysis, the protein samples, and the matrix (HCCA saturated in TA30) were mixed in a 1:1 ratio and spotted on a ground steel plate. The peptide mass lists (Table 5) for the different LPMO constructs were generated using the ExPASy online tool PeptideMass (https://web.expasy.org/peptide_mass/). The peptides containing the N-terminal histidine are highlighted in bolt.

Authors' contributions
LR and KE designed the experiments, performed research, and wrote the manuscript. MS carried out supervision, helped to design experiments, provided feedback on the results, and carried out refining of the manuscript. AG provided supervision for plasmid design and gave feedback on results. All authors read and approved the final manuscript.

Availability of data and materials
All data generated or analyzed during this study are included in this published article.

Declarations

Ethics approval and consent to participate
Not applicable.

Consent for publication
Not applicable.

Competing interests
The authors declare no competing interest.

Author details
[1] Faculty of Chemistry, Biotechnology, and Food Sciences, Norwegian University of Life Sciences (NMBU), Ås, Norway. [2] Bisy GmbH, Hofstätten a. d. Raab, Austria. [3] Institute of Molecular Biotechnology, Graz University of Technology, Petersgasse 14, Graz, Austria.

References
1. Vaaje-Kolstad G, et al. An oxidative enzyme boosting the enzymatic conversion of recalcitrant polysaccharides. Science. 2010;330:219–23.
2. Forsberg Z, et al. Cleavage of cellulose by a cbm33 protein. Protein Sci. 2011;20(9):1479–83.
3. Agger JW, et al. Discovery of LPMO activity on hemicelluloses shows the importance of oxidative processes in plant cell wall degradation. Proc Natl Acad Sci U S A. 2014;111(17):6287–92.
4. Vu VV, Beeson WT, Span EA, Farquhar ER, Marletta MA. A family of starch-active polysaccharide monooxygenases. Proc Natl Acad Sci U S A. 2014;111(38):13822–7.
5. Frommhagen M, et al. Discovery of the combined oxidative cleavage of plant xylan and cellulose by a new fungal polysaccharide monooxygenase. Biotechnol Biofuels. 2015;8:101.
6. Vaaje-Kolstad G, Horn SJ, Van Aalten DMF, Synstad B, Eijsink VGH. The non-catalytic chitin-binding protein CBP21 from *Serratia marcescens* is essential for chitin degradation. J Biol Chem. 2005;280(31):28492–7.
7. Harris PV, et al. Stimulation of lignocellulosic biomass hydrolysis by proteins of glycoside hydrolase family 61: Structure and function of a large, enigmatic family. Biochemistry. 2010;49(15):3305–16.
8. Cannella D, Hsieh CWC, Felby C, Jørgensen H. Production and effect of aldonic acids during enzymatic hydrolysis of lignocellulose at high dry matter content. Biotechnol Biofuels. 2012;5:26.
9. Hemsworth GR, Johnston EM, Davies GJ, Walton PH. Lytic polysaccharide monooxygenases in biomass conversion. Trends Biotechnol. 2015;33(12):747–61.
10. Johansen KS. Discovery and industrial applications of lytic polysaccharide mono-oxygenases. Biochem Soc Trans. 2016;44:143–9.
11. Müller G, Chylenski P, Bissaro B, Eijsink VGH, Horn SJ. The impact of hydrogen peroxide supply on LPMO activity and overall saccharification efficiency of a commercial cellulase cocktail. Biotechnol Biofuels. 2018;11:209.
12. Eijsink VGH, et al. On the functional characterization of lytic polysaccharide monooxygenases (LPMOs). Biotechnol Biofuels. 2019;12:58.
13. L. Rieder, N. Teuschler, K. Ebner, and A. Glieder, "Eukaryotic expression systems for industrial enzymes," in *Industrial Enzyme Applications*, Wiley-VCH Verlag, 2019, pp. 47–69.
14. Fischer JE, Glieder A. Current advances in engineering tools for *Pichia pastoris*. Curr Opin Biotechnol. 2019;59:175–81.
15. Vogl T, et al. A toolbox of diverse promoters related to methanol utilization: functionally verified parts for heterologous pathway expression in *Pichia pastoris*. ACS Synth Biol. 2015;5(2):172–86.
16. Quinlan RJ, et al. Insights into the oxidative degradation of cellulose by a copper metalloenzyme that exploits biomass components. Proc Natl Acad Sci U S A. 2011;108(37):15079–84.
17. Nakagawa YS, et al. A small lytic polysaccharide monooxygenase from S*treptomyces griseus* targeting α- And β-chitin. FEBS J. 2015;282(6):1065–79.
18. Tanghe M, et al. Recombinant expression of *Trichoderma reesei* Cel61A in *Pichia pastoris*: Optimizing yield and N-terminal processing. Mol Biotechnol. 2015;57:1010–7.
19. Labourel A, et al. A fungal family of lytic polysaccharide monooxygenase-like copper proteins. Nat Chem Biol. 2020;16:345–50.
20. Cereghino JL, Cregg JM. Heterologous protein expression in the methylotrophic yeast *Pichia pastoris*. FEMS Microbiol Rev. 2000;24(1):45–66.
21. Courtade G, Le SB, Sætrom GI, Brautaset T, Aachmann FL. A novel expression system for lytic polysaccharide monooxygenases. Carbohydr Res. 2017;448:212–9.
22. Kittl R, Kracher D, Burgstaller D, Haltrich D, Ludwig R. Production of four *Neurospora crassa* lytic polysaccharide monooxygenases in *Pichia pastoris* monitored by a fluorimetric assay. Biotechnol Biofuels. 2012;5:79.
23. Frandsen KEH, Haon M, Grisel S, Henrissat B, LoLeggio L, Berrin JG. Identification of the molecular determinants driving the substrate specificity of fungal lytic polysaccharide monooxygenases (LPMOs). J Biol Chem. 2020;296:100086.
24. Tolstorukov I, Cregg JM. Yeast promoters from *Pichia pastoris*, US2016/0097053A1, 2016.

25. Liang S, Zou C, Lin Y, Zhang X, Ye Y. Identification and characterization of PGCW14: A novel, strong constitutive promoter of *Pichia pastoris*. Biotechnol Lett. 2013;35(11):1865–71.
26. Petrović DM, et al. Methylation of the N-terminal histidine protects a lytic polysaccharide monooxygenase from auto-oxidative inactivation. Protein Sci. 2018;27(9):1636–50.
27. Kojima Y, et al. A lytic polysaccharide monooxygenase with broad xyloglucan specificity from the brown-rot fungus Gloeophyllum trabeum and its action on cellulose-xyloglucan complexes. Appl Environ Microbiol. 2016;82(22):6557–72.
28. Petrović DM, et al. Comparison of three seemingly similar lytic polysaccharide monooxygenases from *Neurospora crassa* suggests different roles in plant biomass degradation. J Biol Chem. 2019;294(41):15068–81.
29. Sygmund C, et al. Characterization of the two *Neurospora crassa* cellobiose dehydrogenases and their connection to oxidative cellulose degradation. Appl Environ Microbiol. 2012;78(17):6161–71.
30. Filiatrault-Chastel C, et al. AA16, a new lytic polysaccharide monooxygenase family identified in fungal secretomes. Biotechnol Biofuels. 2019;12:55.
31. Kadowaki MAS, Magri S, de Godoy MO, Monclaro AV, Zarattini M, Cannella D. A fast and easy strategy for lytic polysaccharide monooxygenase-cleavable 6His-tag cloning, expression and purification. Enzyme Microb Technol. 2020;143:109704.
32. Isaksen T, et al. A C4-oxidizing lytic polysaccharide monooxygenase cleaving both cellulose and cello-oligosaccharides. J Biol Chem. 2014;289(5):2632–42.
33. Frandsen KEH, et al. The molecular basis of polysaccharide cleavage by lytic polysaccharide monooxygenases. Nat Chem Biol. 2016;12(4):298–303.
34. Fitzgerald I, Glick BS. Secretion of a foreign protein from budding yeasts is enhanced by cotranslational translocation and by suppression of vacuolar targeting. Microb Cell Fact. 2014;13:125.
35. Barrero JJ, Casler JC, Valero F, Ferrer P, Glick BS. An improved secretion signal enhances the secretion of model proteins from *Pichia pastoris*. Microb Cell Fact. 2018;17:161.
36. Vogl T, Gebbie L, Palfreyman RW, Speight R. Effect of plasmid design and type of integration event on recombinant protein expression in *Pichia pastoris*. Appl Environ Microbiol. 2018;84(6):e02712-e2717.
37. Schwarzhans JP, Wibberg D, Winkler A, Luttermann T, Kalinowski J, Friehs K. Integration event induced changes in recombinant protein productivity in *Pichia pastoris* discovered by whole genome sequencing and derived vector optimization. Microb Cell Fact. 2016;15:84.
38. PV Harris and M Wogulis, Polypetides having amylolytic enhancing activity and polynucleotides encoding same WO 2010/059413, 2010.
39. Leggio LL, et al. Structure and boosting activity of a starch-degrading lytic polysaccharide monooxygenase. Nat Commun. 2015;6:5961.
40. Barrero JJ, Pagazartaundua A, Glick BS, Valero F, Ferrer P. Bioreactor-scale cell performance and protein production can be substantially increased by using a secretion signal that drives co-translational translocation in *Pichia pastoris*. N Biotechnol. 2021;60(September):85–95.
41. Sturmberger L, et al. Refined *Pichia pastoris* reference genome sequence. J Biotechnol. 2016;235:121–31.
42. Weis R, Luiten R, Skranc W, Schwab H, Wubbolts M, Glieder A. Reliable high-throughput screening with *Pichia pastoris* by limiting yeast cell death phenomena. FEMS Yeast Res. 2004;5(2):179–89.
43. Westereng B, et al. Efficient separation of oxidized cello-oligosaccharides generated by cellulose degrading lytic polysaccharide monooxygenases. J Chromatogr A. 2013;1271(1):144–52.
44. Loose JSM, Forsberg Z, Fraaije MW, Eijsink VGH, Vaaje-Kolstad G. A rapid quantitative activity assay shows that the *Vibrio cholerae* colonization factor GbpA is an active lytic polysaccharide monooxygenase. FEBS Lett. 2014;588(18):3435–40.
45. Tuveng TR, Arntzen MØ, Bengtsson O, Gardner JG, Vaaje-Kolstad G, Eijsink VGH. Proteomic investigation of the secretome of *Cellvibrio japonicus* during growth on chitin. Proteomics. 2016;16(13):1904–14.

Publisher's Note

Kinetic characterization of a putatively chitin-active LPMO reveals novel LPMO functionalities and demonstrates the absence of monooxygenase activity

Lukas Rieder, Dejan M. Petrović, Priit Valjamae, Vincent G.H. Eijsink, Morten Sørlie

Paper II

Kinetic characterization of a putatively chitin-active LPMO reveals novel LPMO functionalities and absence of monooxygenase activity

Lukas Rieder[1], Dejan Petrović[1], Priit Väljamäe[2], Vincent G.H. Eijsink[1], Morten Sørlie[1*]

[1]Faculty of Chemistry, Biotechnology, and Food Sciences, Norwegian University of Life Sciences (NMBU), N-1432 Ås, Norway

[2]Institute of Molecular and Cell Biology, University of Tartu, Tartu, Estonia

* Corresponding author:

Morten Sørlie Tel: + 47 67 23 25 62, morten.sorlie@nmbu.no

Abstract

Enzymes known as Lytic Polysaccharide Monooxygenases (LPMOs) are recognized as important contributors to aerobic enzymatic degradation of recalcitrant polysaccharides such as chitin and cellulose. LPMOs are remarkably abundant in Nature, with some fungal species possessing more than 50 LPMO genes, and the biological implications of this diversity remain enigmatic. For example, chitin-active LPMOs have been encountered in biological niches where chitin conversion does not seem to take place. We have carried out an in-depth kinetic characterization of a putatively chitin-active LPMO from *Aspergillus fumigatus* (*Af*AA11B), which, as we show here, has multiple unusual properties, such as a low redox potential and high oxidase activity. Furthermore, *Af*AA11B is hardly active on chitin, while being very active on soluble oligomers of *N*-acetylglucosamine. The unique properties of *Af*AA11B allowed experiments showing that it is a strict peroxygenase and does not catalyze a monooxygenase reaction. This study shows that Nature uses LPMOs for breaking glycosidic bonds in non-polymeric substrates in reactions that depend on H_2O_2. The quest for the true substrates of these enzymes, possibly carbohydrates in the cell wall of the fungus or its competitors, will be of major interest.

Introduction

Lytic polysaccharide monooxygenases (LPMOs) are receiving massive attraction due their ability to degrade recalcitrant polysaccharides, such as cellulose and chitin, in biomass conversion (1–7). Through the use of powerful redox chemistry, LPMOs are able to selectively activate C-H bonds that requires overcoming an energy barrier of ~100 kcal/mol (3, 8–11). LPMOs are abundant in Nature and categorized, based on their sequences, in seven distinct families (AA9-AA11 and AA13-AA16), within the class of auxiliary activities (AA) in the CAZy database (12). Central to LPMO action is a unique mononuclear copper active site made up of two histidines, where the N-terminal histidine coordinates with both the imidazole ring and the N-terminal amine (8, 13). When reduced to Cu(I), LPMOs can activate O_2 (3, 14) or H_2O_2 (11, 15, 16) to create a reactive oxygen-containing intermediate that catalyzes the oxidation of glycosidic bonds in chitin (3), cellulose (17) and other plant-based polysaccharides (18–20) (EC 1.14.99.53 - 1.14.99.56).

In the oxygen-driven mechanism, a fundamental challenge is the thermodynamically unfavorable formation of superoxide through reduction of O_2 by Cu(I), a barrier that is potentially lowered by binding of the substrate (14, 21, 22). The formed superoxide may react as the oxidant or can be further reduced to create a Cu(II)-oxyl or Cu(III) hydroxide (9, 10, 23, 24). Several catalytic scenarios have been proposed for the H_2O_2-driven peroxygenase reaction (25). Accumulating data from experiments and modelling indicate that the peroxygenase reaction entails homolytic cleavage of H_2O_2 by the reduced LPMO, leading to the formation of a hydroxyl radical that may react directly the with substrate or generate a Cu(II)-oxyl species (11, 15, 25).

While there is some debate in the field as to the relative importance of the monooxygenase and peroxygenase reaction in Nature, it is evident that the peroxygenase reaction is orders of magnitude faster (26–29). For example, the first kinetic characterization with respect to O_2 showed an apparent oxidative rate of 0.02 s^{-1} for a bacterial chitin-active AA10 (3). An in-depth kinetic analysis of the same LPMO revealed that the k_{cat} for chitin oxidation increased to 6.7 s^{-1} when H_2O_2 was used as the co-substrate (30). Furthermore, with a Michaelis constant (K_m) for H_2O_2 in the low μM range (2.8 μM), the enzyme has an efficiency constant (k_{cat}/K_m) of ~10^6 M^{-1}s^{-1}, which is similar to efficiency constants reported for heme-dependent peroxygenases (30, 31).

LPMOs are widespread in Nature, in particular in fungi, some of which contain up to > 50 LPMO genes (32). While the role of some of these LPMOs in biomass conversion is well established, supported by both enzymological and expression data as well as successful use in industrial biomass conversion (33), the biological roles of many of these (putative) LPMOs remain enigmatic. It is noteworthy that the majority of characterized bacterial LPMOs is active on chitin, whereas several of these enzymes come from bacteria whose ecological niches do not suggest involvement in chitin degradation (34). This may be taken to suggest that chitin is not the true substrate of some of these enzymes. A considerable fraction of LPMOs contain one or more additional domains. While in some

2

67 cases these domains are known to be involved in chitin- or cellulose-binding, several are predicted to
68 be involved in binding other materials or have unknown functions (35). The discovery of a starch-
69 active LPMO cleaving α-glycosidic bonds (19) gave one glimpse of a larger functional diversity that
70 may exist among LPMOs. Functional diversity is also suggested by variation in the shapes of the
71 substrate-binding surfaces that vary from being flat and having aromatic surface residues, matching
72 well with binding crystalline polysaccharide substrates, to being more rugged and/or polar (36–38)
73 (Figure S1).

74   In search for functional diversity, we turned our attention to putatively chitin-active AA11
75 LPMOs. The substrate-binding surface of the only structurally characterized member of this family,
76 *Ao*AA11 from *Aspergillus oryzae* (36), is more convex compared to bacterial chitin-active LPMOs
77 (AA10s) (Figure S1) and is free of aromatic residues, where the latter are known to be important for
78 substrate binding in chitin-active AA10s (39, 40). Secretome data for *Aspergillus fumigatus* show that
79 at least three AA11s are expressed (41). The catalytic domains of one of these, *Af*AA11B, shares 72.6
80 % sequence identity with *Ao*AA11 (Figure 1B), whereas the other two, *Af*AA11A and *Af*AA11C are
81 less similar to *Ao*AA11, with 39.6% and 37.5% identity, respectively. In-depth functional
82 characterization of *Af*AA11B revealed multiple unusual LPMO features, such as a low redox potential,
83 high oxidase activity and a strong preference for soluble substrates, suggesting involvement of this
84 AA11 in processes other than chitin degradation. Furthermore, competition experiments with
85 horseradish peroxidase (HRP) showed that monooxygenase activity of this LPMO is essentially non-
86 existing.

87
88

89 **Material and Methods**

90 **Cloning.** Cloning of *Af*AA11B was done as described before (42). Briefly, the synthetic *Af*AA11B
91 gene (NCBI accession number XP_748042.1) including its native signal sequence was codon
92 optimized for *Pichia pastoris* (GenScript, NY, USA), excised from the pUC57 vector and ligated into
93 the pPINK-GAP vector (43), yielding in the pPINK-GAP_ *Af*AA11B plasmid.

94   The pPINK-GAP_ *Af*AA11B was transformed to *P. pastoris* PichiaPink™ Strain 4 cells,
95 following the manufacturer's instructions (Invitrogen, CA, USA). Transformants were screened for
96 protein production in BMGY medium (containing 1% (v/v) glycerol), which was prepared according
97 to the manufacturer's instructions (Invitrogen, CA, USA). The best-producing transformant was used
98 for the expression of recombinant *Af*AA11B used in the presented study.

99

100 **Expression and purification.** A single yeast colony was used to inoculate 25 ml BMGY (1% (v/v)
101 glycerol), in a 100 ml baffled shake flask and the culture was incubated at 30 °C and 150 rpm for 24
102 h. 12.5 ml of this pre culture was used to inoculate 500 ml buffered minimal medium containing 1.34
103 % YNB, 0.00004 % biotin, 100 mM potassium phosphate (pH 6.0), 0.5 % (w/v) glucose and 0.5 %

104 (v/v) glycerol in a 2 l baffled shake flask. The culture was incubated at 30 °C and 150 rpm for 48 h.

105 After 24 h 0.25 % (v/v) glycerol and 0.25 % (w/v) glucose were added.

106   Cells and debris were removed by centrifugation at 10000 x *g* for 15 min at 4 °C. The protein-

107 containing supernatant was filtered with a 45 μm Steritop® bottle-top filter (Merck Millipore,

108 Burlington, MA, USA) and concentrated five-fold by using a VivaFlow 200 tangential crossflow

109 concentrator (molecular weight cut-off, MWCO 10 kDa, Sartorius Stedim Biotech Gmbh, Germany),

110 prior to protein purification.

111   Ammonium sulfate was added to the concentrated culture supernatant to a final concentration

112 of 2.4 M before loading onto a 5 mL HiTrap Phenyl FF column (GE Healthcare Life Sciences,

113 Uppsala, Sweden), which was equilibrated with 50 mM BisTris/HCl buffer (pH 6.5), containing 2.4

114 M ammonium sulfate. The protein was eluted from the column by applying a 35 ml linear gradient

115 from 2.4 M to 0 M ammonium sulfate in 50 mM BisTris/HCl buffer (pH 6.5) using a flowrate of 1.8

116 ml/min. The collected fractions were analyzed by sodium dodecyl sulfate polyacrylamide gel

117 electrophoresis (SDS-PAGE) and fractions showing a protein band of the correct size were pooled.

118 Prior to subsequent purification steps, the buffer was exchanged to 20 mM Tris/HCl (pH 8.4) by using

119 Amicon Ultra centrifugal filters (MWCO 10 kDa, Merck Millipore, Burlington, MA, USA).

120   The salt free protein solution was loaded onto a 5-ml HiTrap DEAE FF column (GE

121 Healthcare Life Sciences, Uppsala, Sweden) that was equilibrated with 20 mM Tris/HCl (pH 8.4). The

122 protein was eluted by applying a 100 mL linear gradient from 0 to 30 % 0.5 M NaCl in 20 mM

123 Tris/HCl (pH 8.4) using a flowrate of 1.8 ml/min.

124

125 **LPMO reactions.** For analysis of enzyme activity, 200 μl reaction mixtures were prepared in 1.5 ml

126 reaction tubes with conical bottom. Standard LPMO reactions contained 1 μM LPMO, 2 mM *N*-acetyl-

127 chitooligosaccharides (Megazyme; 95% purity) or 15 g/l crystalline chitin. As reductant 1 mM of L-

128 ascorbic acid (AscA; Sigma-Aldrich) was used. All reactions were carried out in 50 mM BisTris/HCl

129 (pH 6.5) and incubated at 37 °C and 750 rpm in a Thermomixer C (Eppendorf, Hamburg, Germany).

130 Standard reactions with hydrogen peroxide (37% (v/v) stock solution, Merck) contained 300 μM

131 H_2O_2. Stock solutions of AscA and H_2O_2 with concentrations of 50 mM and 10 mM, respectively were

132 prepared in pure water (TraceSELECT®, Fluka) and stored at -20 °C. Prior to use the concentration of

133 the H_2O_2 stock solution was verified by measuring absorbance at 240 nm and using a molar extinction

134 coefficient of 43.6 $M^{-1}cm^{-1}$. The conditions used in non-standard activity assays are described in the

135 Results section, in the corresponding Figure texts.

136   Anaerobic experiments were performed inside an anaerobic chamber (Whitley A95

137 Workstation, Don Whitley Scientific Limited, UK). To ensure oxygen free reactions, each reactant

138 solution was separately prepared in an airtight GC-vial (1.5 ml) and degassed by successive placing

139 vacuum over the solution followed by addition of oxygen free nitrogen using a Schlenk-Line.

140 Subsequently, reactant solutions were incubated inside the anaerobic chamber for at least 30 min prior
141 setting up the reactions.

142 For time course experiments with soluble substrates, reaction conditions and timing were such
143 that the substrate concentration in the samples would not go below 80% of the starting concentration.
144 For sampling product formation, 25 µl aliquots were withdrawn from the reaction and mixed with
145 three volumes of 200 mM NaOH to quench the reaction. Reactions with crystalline chitin were
146 terminated by a 10 min boiling step prior to degradation of the remaining solid chitin with a mixture
147 of recombinantly produced purified chitinolytic enzymes from *Serratia marcescens* [(44–46); final
148 concentrations: 2.5 µM Chitinase A, 2.5 µM Chitinase C and 2 µM Chitobiase], for 24 hours at 37 °C
149 and 150 rpm. Prior to product analysis, the reaction volumes were adjusted with 200 mM NaOH to
150 quench the reaction and achieve a four to one dilution. Product solutions were obtained by filtering
151 using a 96-well 0.45 µm filter plate (Merck Millipore, Billerica, MA) that was operated with a vacuum
152 manifold. All experiments shown were done in at least three independent replicates.

153

154 **Detection of oxidized products.** High-performance anion exchange chromatography with pulsed
155 amperometric detection (HPAEC-PAD) and matrix-assisted laser desorption ionization–time of flight
156 mass spectrometry (MALDI-ToF MS) were used to analyze oxidized products. HPAEC-PAD was
157 conducted using a Dionex ICS5000 system, equipped with a CarboPac PA1 analytical column (2 ×
158 250 mm) and a CarboPac PA1 guard column (2 × 50 mm). Product separation was achieved by
159 applying a 29 min gradient as preciously described for cello-oligosaccharides (47). Oxidized products
160 were quantified by using in-house made standards as described elsewhere (46). Chromatograms were
161 recorded and analyzed with Chromeleon and plot preparation was done in Microsoft Excel. MALDI-
162 ToF MS was performed on an Ultraflex MALDI-ToF/ToF instrument (Bruker Daltonik GmbH,
163 Bremen, Germany) equipped with a Nitrogen 337 nm laser, as described previously (18).

164

165 **Determination of the redox potential.** The cell potential of the LPMO-Cu^{2+}/LPMO-Cu^{+} redox
166 couple was determined from the reaction between reduced N,N,N′,N′-tetramethyl-1,4-
167 phenylenediamine (TMP_{red}) and LPMO-Cu^{2+}, as described previously (40, 48). The concentrations of
168 *Af*AA11B and TMP were 31 µM and 500 µM, respectively.

169

170 **H_2O_2 production assay.** The capability of *Af*AA11B, *Sm*AA10A and free copper to generate H_2O_2
171 was assessed as described by Kittl *et al*. (49). The total reaction volume of 100 µl contained 1 µM
172 LPMO or $CuSO_4$, 100 µM Amplex Red and 0.55 µM HRP in 50 mM BisTris/HCl (pH 6.5). After 5
173 min preincubation at 37 °C the reactions were started by the addition of AscA to final concentrations
174 of 50, 250 or 1000 µM. The generation of resorufin was measured by monitoring absorbance at 595
175 nm every 10 sec over 3000 sec in a plate reader. Blank reactions did not contain LPMO or $CuSO_4$ and

176 the calibration curves included AscA to incorporate the influence of the reductant on resorufin

177 formation. The data shown was obtained from three independent replicates.

178

179

180 **Results**

181 **Heterologous expression of *Af*AA11B.** The gene encoding for *Af*AA11B (NCBI accession number

182 XP_748042.1) consists of 1257 base pairs encoding a secretion signal, the catalytic domain and a

183 linker region with an attached X278 module of unknown function (Figure 1A).

184   The *Af*AA11B enzyme was recombinantly expressed in *Pichia pastoris* (*Komagataella*

185 *phaffii*). SDS-PAGE analysis of the purified protein, obtained after several chromatographic steps,

186 indicated a mass of approximately 60 kDa (Figure S2). As the theoretical calculated mass of *Af*AA11B

187 is 42.8 kDa, it seems that the recombinant protein carries N- and/or O-glycosylations. The NetNGlyc

188 and NetOGlyc online tools (http://www.cbs.dtu.dk/services) showed three potential N- glycosylation

189 sites, at positions Asn116, Asn134 and Asn228, and seven potential O- glycosylation sites, at positions

190 Ser174, Ser175, Ser192, Ser230, Ser241 and Thr143, in the catalytic domain. Another 47 potential O-

191 glycosylation sites were identified for the linker region and the X278 module.

192   To obtain a structural impression of *Af*AA11B the online tool SWISSMODEL

193 (https://swissmodel.expasy.org) was used to generate a homology model of the catalytic domain,

194 based on the crystal structure of *Ao*AA11 (PDB: 4mah; (36)), with 72.6 % sequence identity (Figure

195 1B). The resulting structural model (Figure 1C) had a QMEAN value of 0.34, indicating that the model

196 generally was of good quality (50). The model contains two less reliable regions due to incompleteness

197 of the template, which is lacking structural information for residues 118–128 and 170–188 (36),

198 corresponding to residues 121-131 and 173-193 in *Af*AA11B, respectively. These regions are

199 highlighted in pink in both the alignment (Figure 1B) and the homology model (Figure 1C).

200

201

6
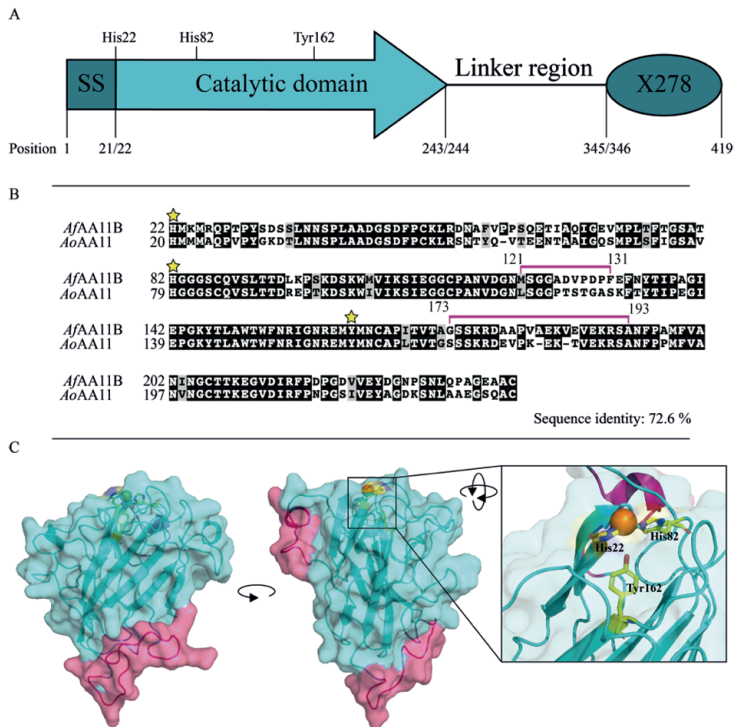
Figure 1. Overview of sequence and structure of *Af*AA11B. (A) Domain structure of *Af*AA11B. The region connecting the catalytic domain and the X278 module comprises residues 244 to 345 and was assigned as a "linker" because it was predicted to be disordered by the PredictProtein server (https://predictprotein.org) server. (B) Sequence alignment of the catalytic domains of *Af*AA11B and *Ao*AA11 performed with the T-Coffee online server. Identical residues appear in black boxes, whereas similar residues appear in grey boxes. The two histidines and a tyrosine that shape the copper site are marked with yellow stars. The pink brackets indicate the areas that are missing in the X-ray structure of *Ao*AA11. (C) Three-dimensional homology model in cartoon representation showing the immunoglobulin like β-sheet core and the surface-exposed histidine brace. The pink areas indicate unreliable areas of the model due to an incomplete structure of the template. The image to the far right shows a close-up of the histidine brace with the copper coordinating histidines and the tyrosine in the axial position shown as yellow sticks. The copper atom is displayed as orange sphere. Protein images were prepared with PyMOL.

Notwithstanding uncertainties related to the two highlighted loop regions, the homology model of *Af*AA11B shows the classical immunoglobulin like β-sheet core and the surface-exposed copper coordinating histidine brace formed by the N-terminal histidine (His22) and the second histidine at position 82 in the mature protein. The model suggests a rugged and somewhat convex

222 surface, which is also observed for *Ao*AA11 (36), This contrasts the flat, and more extended, surfaces

223 typically observed in bacterial chitin-active AA10-type LPMOs and cellulose-active LPMOs (Figure

224 S1).

225

226 **Screening for LPMO activity.** Initial screening for LPMO activity included incubation of *Af*AA11B

227 with α -chitin, β -chitin, cell walls of different yeast strains grown in different conditions (obtained

228 from in-house fermentation processes), mannan from *Saccharomyces cerevisiae*, β-glucans from

229 barley, Na- alginate, and cellopentaose, in the presence of molecular oxygen and 1 mM ascorbic acid.

230 Products were only observed for the reactions with α and β -chitin. MALDI-TOF-MS spectra showed

231 signals corresponding to oxidized chito-oligomers of varying lengths (DP3-DP7 with a mass

232 difference of 203). The dominating signals corresponded to aldonic acids in the mono and double

233 sodium adduct form (Figure S3), showing that *Af*AA11B cleaves the glycosidic bonds by oxidizing

234 the C1 position. It is noteworthy that the mass spectrum contains multiple additional signals that reflect

235 unknown compounds as well as partially deacetylated oxidized chito-oligosaccharides. Most of these

236 additional signals did not appear in MS analysis of products generated in a control reaction with the

237 well-studied bacterial LPMO, *Sm*AA10A (3).

238   Time course analyses of the degradation of α and β -chitin under conditions typically used for

239 LPMO characterization, i.e., in the presence of O_2 and 1 mM ascorbic acid, showed non-linear product

240 formation curves and yielded approximately 50 μM of oxidized products after 60 min incubation, for

241 both substrates. (Figure 2A, B). Reactions with the addition of 20 or 100 μM H_2O_2 and containing

242 only priming amounts of AscA (20 μM) showed early cessation of product formation, with ~15 μM

243 product being formed within the first 10 min of the experiment (Figure 2A, B). Of note, the chitin

244 concentration used in these experiments corresponds to a tetramer concentration of approximately 18

245 mM, meaning that only a tiny fraction of the chitin was oxidized. Under similar standard conditions

246 (O_2, 1 mM AscA) chitin-active AA10 LPMOs may produce in the order of 1 mM of oxidized products

247 (51).

248   In stark contrast to the results above, a standard reaction of *Af*AA11B with 2 mM soluble

249 (GlcNAc)$_4$ yielded a linear progress curve, reaching ~200 μM of oxidized product after 60 minutes

250 (Figure 2C). The use of H_2O_2 (100 μM) in the presence of a priming amount of AscA (20 μM) led to

251 an increased rate of oxidation and formation of ~100 μM oxidized product within 10 min (Figure 2C).

252 These observations suggest that soluble (GlcNAc)$_4$ is a better substrate than solid chitin for *Af*AA11B

253 and that, in reactions with the more preferred substrate, (GlcNAc)$_4$, H_2O_2 is a better co-substrate than

254 O_2. The data for the reaction with H_2O_2 suggest that H_2O_2 was stoichiometrically converted to oxidized

255 product.

256   The inability of *Af*AA11B to catalyze oxidation of α and β -chitin in the presence of O_2 or

257 H_2O_2 can either be due to enzyme inactivation or to limitations in substrate access. To assess this,

258 we set up a standard reaction with β -chitin (aerobic, 1 mM AscA) as well as an aerobic reaction

8

with 300 μM H_2O_2 and 20 μM AscA. After 10 minutes of incubation, $(GlcNAc)_4$, to 2 mM, H_2O_2, to 300 μM, and AscA, to 1mM, were added to both reaction mixtures. In the reaction with H_2O_2 as the initial co-substrate, no newly formed oxidized products were observed after adding $(GlcNAc)_4$ (Figure 2D), suggesting that AfAA11B had been deactivated under these conditions because of non-productive reactions with H_2O_2. Interestingly, in the standard reaction with O_2 as the co-substrate, the formation of oxidized products drastically accelerated after adding the soluble substrate (Figure 2D), indicating that under these standard conditions access to the insoluble chitin was limiting the AfAA11B reaction.
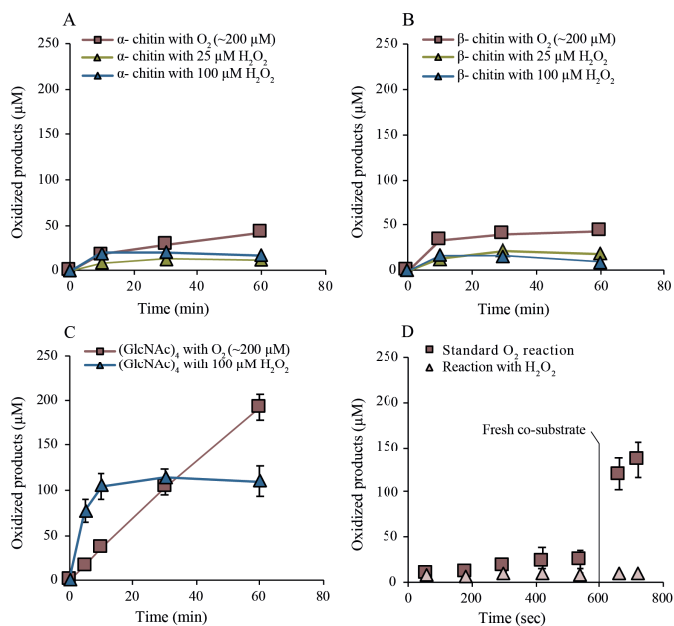
Figure 2. Time course experiments showing the formation of oxidized products by AfAA11B in different reactions (see Materials and Methods for details). In (A) and (B) α and β -chitin (15 g/l) were used as substrate, respectively. Boxes show data from standard reactions, whereas triangles show data from reactions which were supplemented with different H_2O_2 concentrations in the presence of 20 μM AscA, as indicated in the Figure. (C) Reactions with $(GlcNAc)_4$; one standard reaction (boxes) and one reaction with 100 μM H_2O_2 and 20 μM AscA. (D) Standard aerobic reaction with β-chitin and 1 mM AscA (boxes) and an aerobic reaction in the presence of 300 μM H_2O_2 and 20 μM AscA (triangles). After 10 min (line) fresh H_2O_2, $(GlcNAc)_4$ and AscA were added to final concentrations of 300 μM, 2mM and 1 mM, respectively. The data points represent average values of at least two independent experiments; vertical lines, which sometimes are hidden by the data points, indicate standard deviations.

281   To further asses the ability of *Af*AA11B to catalyze the oxidation of soluble substrates, the
282 enzyme was incubated with chitin oligomers (2 mM) with different degrees of polymerization (DP)
283 ranging from three to six in the presence of H_2O_2 (100 µM) and AscA (20 µM). The rate of reaction
284 was determined from linear progress curves for the formation of oxidized products over time. The
285 enzyme was active on all tested substrates and the highest observed rate constant (k_{obs}) was measured
286 for $(GlcNAc)_4$ with a value of 0.245 ± 0.007 s^{-1} (Table 1).

287   To investigate the mode of binding, *Af*AA11B was incubated in the presence of 2 mM chitin
288 oligomers with varying DP (DP2-DP6) in the presence of H_2O_2 (100 µM) and AscA (20 µM). After
289 30 seconds turnover the reaction was quenched and analyzed by HPAEC-PAD and the relative
290 abundance of the different oxidized products was calculated based on the recorded chromatograms.
291 The results showed that the oxidized dimer is the dominant oxidized product, regardless of the length
292 of the oligomeric substrate (Table 1). This suggests that all substrates bind strongly to subsites -2 and
293 -1 [imaginary subsites numbered by analogy to glycoside hydrolases (52)] and that binding to these
294 subsites is essential for productive substrate binding (Table 1). Based on the relative appearance of
295 each oxidized product it was possible to establish a rudimentary overview of preferred binding modes
296 (Table 1). Of note, multiple cleavages of the longer substrates cannot be excluded, and the preferred
297 binding modes given in Table 1 may thus differ from reality. However, the product peaks together
298 corresponded to as little as ~10-15 µM of oxidized product (at an initial substrate concentration of 2
299 mM and H_2O_2 concentration of 100 µM), which shows that initial rate conditions were met.

300

301 **Table 1.** Observed oxidation rates and binding modes for *Af*AA11B acting on chitin oligomers (2
302 mM) with different degrees of polymerization (DP) in the presence of 100 µM H_2O_2 and 20 µM AscA.
303 Rates were determined by measuring the generation of oxidized products over time. Note that kinetic
304 analysis described further below show that the rates reported in this Table are far below maximum
305 rates, due to a sub-saturating reductant concentration. The binding modes were determined by
306 calculation of the relative rates of appearance of oxidized products of the different lengths. The
307 numbers in the "Mode of binding" columns refer to subsites, - subsites interact with the non-reducing
308 end of the substrate.

	k_{obs} (s^{-1})	Mode of binding			
DP3	0.145 ± 0.005	-2 → +1			
		100 %			
DP4	0.245 ± 0.007	-2 → +2	-3 → +1		
		82 %	18 %		
DP5	0.169 ± 0.013	-2 → +3	-3 → +2	-4 → +1	
		58 %	28 %	14 %	
DP6	0.154 ± 0.006	-2 → +4	-3 → +3	-4 → +2	-5 → +1
		47 %	23 %	24 %	6 %

309

310

A detailed kinetic analysis of *Af*AA11B catalyzed oxidation of (GlcNAc)$_4$. The interesting observations that *Af*AA11B prefers soluble chitinous substrates and works more efficiently in the presence of added H$_2$O$_2$ prompted us to undertake a detailed kinetic analysis of (GlcNAc)$_4$ oxidation. *Af*AA11B turnover under standard conditions, i.e., in the presence of atmospheric O$_2$, (GlcNAc)$_4$ (2 mM), and AscA (1 mM) yielded an observed rate constant (k_{obs}) of 0.052 ± 0.004 s^{-1} (calculated from data shown in Figure 2C), which is about five times lower than the k_{obs} for the reaction with 100 μM H$_2$O$_2$ and 20 μM AscA (Table 1).

It is well known that H$_2$O$_2$ accumulates in reactions that contain an LPMO and a reductant, but no LPMO substrate (49, 53). It has been suggested that this H$_2$O$_2$ -generating oxidase activity also plays a role in reactions with substrate, where LPMOs could generate their own co-substrate (25). Whereas, it seems certain that reduced LPMOs react with oxygen (11, 14, 22), there is debate in the field regarding the occurrence and kinetic relevance of a true monooxygenase reaction, i.e. a reaction where the substrate-oxidizing reactive oxygen species is generated directly from O$_2$, in the active site of the substrate-bound LPMO. To gain more insight into these issues, we first assessed the H$_2$O$_2$ -generating ability of *Af*AA11B.

In the presence of 50 μM AscA, the observed initial rate of H$_2$O$_2$ production by 1 μM *Af*AA11B was 0.017 ± 0.001 μM*s^{-1}, which is higher than the H$_2$O$_2$ production rate for 1 μM free Cu(II) under the same conditions (0.008 ± 0.001 μM*s^{-1}; Figure 3, Table 2). Upon increasing the AscA concentration to 1000 μM, the rates increased to 0.183 ± 0.016 and 0.080 ± 0.002 μM*s^{-1} for *Af*AA11B and free Cu(II), respectively. It is noteworthy that the rate of the standard LPMO reaction (0.052 ± 0.004 μM*s^{-1}; Fig 2C) is lower than the rate of H$_2$O$_2$ production (0.183 ± 0.016 μM*s^{-1}; Table 2). It is plausible that the LPMO generates less H$_2$O$_2$ because the oxidase reaction is inhibited by interactions with the substrate, or that the produced H$_2$O$_2$ is at such low concentration that V_{max} is not achieved (49, 53).

Since the first step in H$_2$O$_2$ production, formation of O$_2^{\cdot-}$, is endergonic, it is interesting to compare the redox potentials to see if there is a correlation between these potentials and the ability to produce H$_2$O$_2$. In accordance with the high apparent oxidase activity, the redox potential of the *Af*AA11B-Cu(II)/ *Af*AA11B-Cu(I) redox couple, determined as described previously (40, 48), was found to be of 114 ± 1 mV, i.e. lower that the literature value for the Cu(II)/Cu(I) redox couple of 160 mV. In comparison, chitin-active *Sm*AA10A has a redox potential for the *Sm*AA10A-Cu(II)/ *Sm*AA10A-Cu(I) redox couple of 275 mV (40) and reactions containing 1 μM *Sm*AA10A showed very low H$_2$O$_2$ production rates of 0.001 ± 0.001 μM*s^{-1}, at both the tested AscA concentrations of 50 and 1000 μM, respectively (Figure 3, Table 2). These data show a correlation between the redox potential and the H$_2$O$_2$ production rate; the high oxidase activity of *Af*AA11B (0.18 s^{-1} in the presence of atmospheric O$_2$ and 1 mM AscA) is associated with an exceptionally low redox potential.

346

347

Table 2. Observed rate constants for production of H_2O_2 by AfAA11B, SmAA10A and CuSO$_4$, all at

1 µM concentration, in the presence of different reductant concentrations. The redox potentials for the

Cu(II)/Cu(I) redox couples are indicated in the column headers. The signals obtained in the Amplex

Red signal were corrected for the effect of ascorbic acid (28) and the rates were corrected for the rate

in reactions with only ascorbic acid.

[AscA]	AfAA11B ($E_0 = 0.114$ V)	CuSO$_4$ ($E_0 = 0.160$ V)	SmAA10A ($E_0 = 0.275$ V)
µM	Observed rate ($\mu M*s^{-1}$)		
50	0.017 ± 0.001	0.008 ± 0.001	0.001 ± 0.001
250	0.091 ± 0.006	0.034 ± 0.002	0.002 ± 0.001
1000	0.183 ± 0.016	0.080 ± 0.002	0.001 ± 0.001

353

354

355
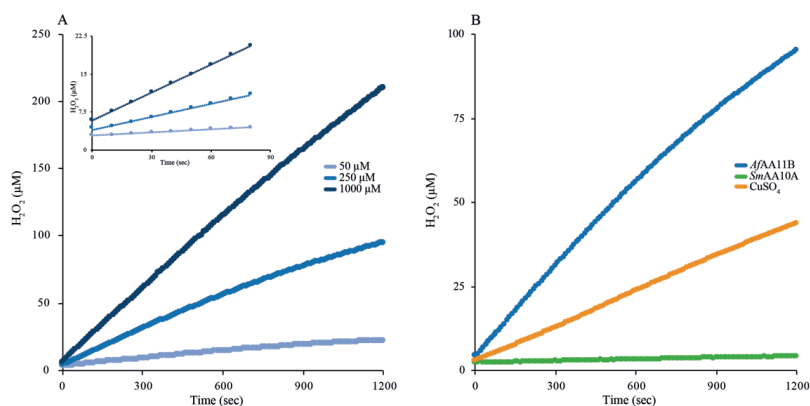
Figure 3. H_2O_2 production curves. (A) H_2O_2 production by 1 µM AfAA11B in the presence of 50,

250, or 1000 µM AscA. The insert shows data for the first 80 s of the reaction. (B) Comparison of

H_2O_2 production by 1 µM of AfAA11B, SmAA10A or CuSO$_4$ in the presence of 250 µM reductant.

H_2O_2 levels were calculated after correcting for side reactions involving AscA and Amplex Red by

using a H_2O_2 standard curve that was prepared in the presence of the same amount of reductant (no

LPMO/CuSO$_4$).

362

363

The connection between the generation of H_2O_2 and substrate oxidation by AfAA11B was

investigated by studying the ability of HRP to inhibit substrate oxidation. Standard oxygen reactions

with high concentrations of soluble substrate (2 mM) and varying concentrations of HRP resulted in

12

linear progress curves showing that the rate of substrate oxidation decreased with increasing HRP concentration. (Figure 4A). Importantly, the linearity of the progress curves shows that depletion of AscA by HRP is not responsible for the inhibition of AfAA11B under these conditions. Plotting of the reaction rates against the HRP concentration gave a reversed hyperbolic curve showing 50 % inhibition of LPMO activity at an LPMO:HRP ratio of 1:0.5 and 95% inhibition at a 1:6 ratio (Figure 4B).

Determination of the rate of $(GlcNAc)_4$ oxidation in the presence of O_2 at atmospheric pressure and AscA (1 mM) at varying LPMO concentrations showed a linear correlation between the enzyme concentration and product yields, indicating that LPMO-catalyzed production of H_2O_2 limits the reaction (Figure 4C). Importantly, the rate at the intercept (0 µM LPMO) was significant (0.0184 µM*s^{-1}). Of note, this "LPMO-independent" background level of substrate conversion is effectively inhibited by HRP (Figure 4A, B), which shows that this conversion involves H_2O_2 generated in solution, likely resulting from autooxidation of ascorbic acid (54) and is not due to, e.g., a true monooxygenase reaction that would not involve H_2O_2.

To confirm that H_2O_2 generation, and not the peroxygenase reaction, limits the AfAA11B reaction, an anaerobic reaction was set up with $(GlcNAc)_4$ (2 mM) AscA (1 mM) and a large amount of H_2O_2 (300 µM). This set-up led to the rapid formation of 300 µM oxidized products within 1.5 min demonstrating that the peroxygenase activity is much higher than AscA oxidase activity (Table 2; Figure 4D). This confirms that the reactions shown in Figure 4A-C indeed were H_2O_2-limited and further shows that AfAA11B, on average, is stable for a minimum of 300 peroxygenase turnovers.
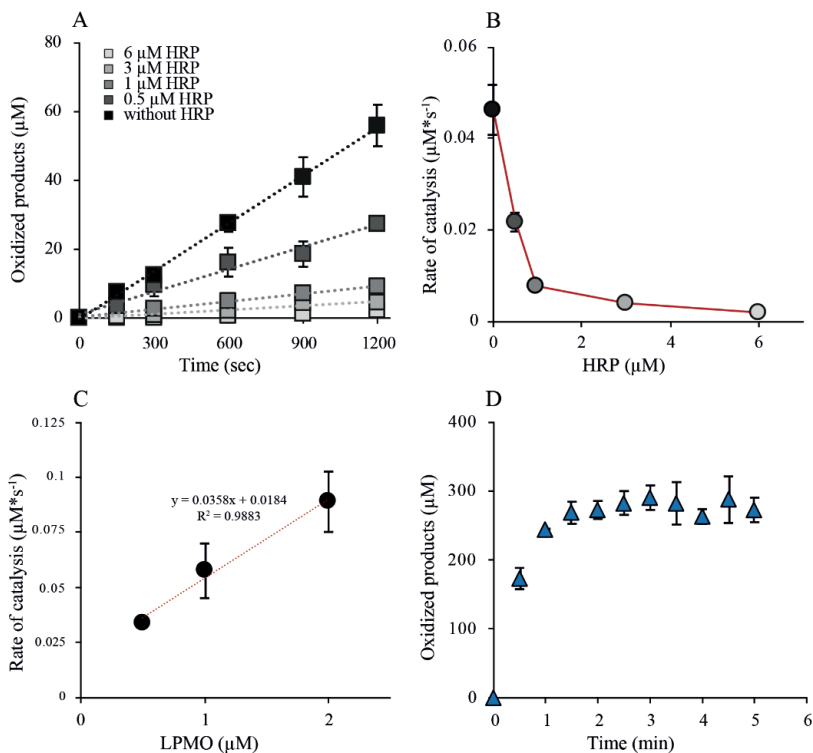
Figure 4 Inhibition of substrate oxidation by HRP. (A) Progress curves for reactions with 1 μM LPMO, 1 mM AscA, 2 mM (GlcNAc)$_4$, 100 μM Amplex Red and different concentrations of HRP. (B) Plot of the reaction rates obtained from (A) against the HRP concentration showing that the reaction rate approaches zero at high HRP concentrations. (C) Observed rates of standard reactions as in (A), using different LPMO concentrations. (D) Anaerobic time course experiment with 1 μM LPMO in the presence of 300 μM H$_2$O$_2$, (GlcNAc)$_4$ (2 mM), and AscA (1 mM).

To assess the peroxygenase activity of AfAA11B in detail, we determined the dependency of the initial enzyme rate on the concentration of (GlcNAc)$_4$, H$_2$O$_2$ and AscA, and the data were analyzed using the Michaelis-Menten equation (Figure 5 and Table 3). All experiments were performed in aerobic conditions as the data above show that, under the used reaction conditions, the *in situ* generation of H$_2$O$_2$ from O$_2$ ($\leq 0.183 \pm 0.016$ μM*s^{-1}, likely in the order of 0.052 ± 0.004 μM*s^{-1}) in the presence of 2 mM (GlcNAc)$_4$ is much lower than the rate of the peroxygenase reaction (in the order of 4 μM*s^{-1}, Fig. 4D).

Varying the H$_2$O$_2$ concentration in the presence of 2 mM (GlcNAc)$_4$ and 1 mM AscA yielded a k_{cat} of 4.7 ± 0.4 s^{-1} and a $K_m^{H_2O_2}$ of 8.9 ± 1.0 μM. The assays for studying the dependency on the concentration of (GlcNAc)$_4$ were performed in the presence of 300 μM H$_2$O$_2$ and 1 mM AscA and

14

408   yielded a k_{cat} of 3.5 ± 0.1 s^{-1} and $K_m^{(GlcNAc)_4}$ of 200 ± 29 µM. Finally, the dependency of the initial

409   enzyme rate on reductant concentration was determined using reactions with 1 mM H_2O_2 and 2 mM

410   (GlcNAc)$_4$ and yielded a k_{cat} of 3.9 ± 0.2 s^{-1} and a K_m value of 502 ± 35 µM. The k_{cat} value reported in

411   Table 3 (4.0 ± 0.6 s^{-1}) is the average of the three values reported above. Of note the K_m value for AscA

412   should be viewed as an apparent half-saturating concentration (K_{mR}^{app}) (55) and will depend on the

413   H_2O_2 concentration, because the two compounds will react in what is a side reaction. Having access

414   to k_{cat} and K_m values, efficiency constants (k_{cat} / K_m) for H_2O_2 and (GlcNAc)$_4$ were calculated, yielding

415   a $k_{cat}/K_m^{H_2O_2}$ of $4.5 \cdot 10^5$ M^{-1}s^{-1} and a $k_{cat}/K_m^{(GlcNAc)_4}$ of $2.0 \cdot 10^4$ M^{-1}s^{-1}, respectively.

416

417
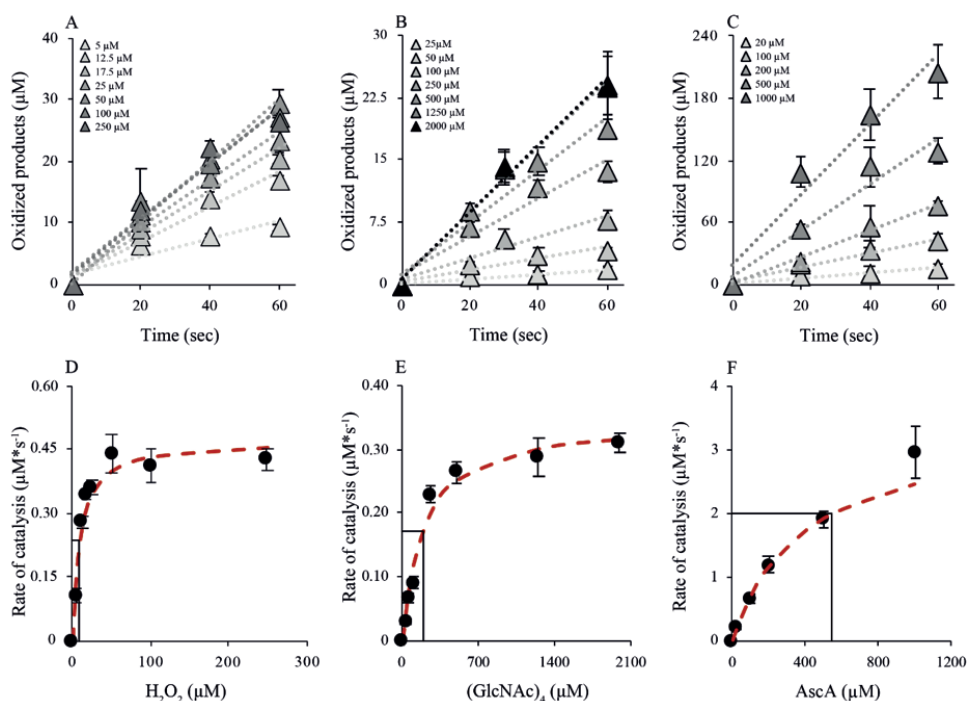
418

419   **Figure 5**. Michaelis Menten kinetic analysis of *Af*AA11B. Panels (A-C) show progress curves,

420   whereas panels (D-F) show the determined rates (black dots) as a function of the varied reaction

421   parameter, with the fit to the Michaelis-Menten equation (red dashed line). All experiments were done

422   in aerobic conditions. Conditions: panel (A/D), 0.1 µM LPMO, 1 mM AscA, 2 mM (GlcNAc)$_4$,

423   varying H_2O_2 concentrations, as indicated; panel (B/E), 0.1 µM LPMO, 1 mM AscA, 300 µM H_2O_2,

424   varying (GlcNAc)$_4$ concentrations, as indicated; panel (C/F), 1 µM LPMO, 1 mM H_2O_2, 2 mM

425   (GlcNAc)$_4$, and varying AscA concentrations, as indicated.

426

427

Table 3. Kinetic parameters of *Af*AA11B.

$k_{\text{cat}}^{\text{a}}$	$K_{\text{m}}^{\text{H}_2\text{O}_2\ \text{b}}$	$k_{\text{cat}}/K_{\text{m}}^{\text{H}_2\text{O}_2\ \text{c}}$	$K_{\text{m}}^{\text{(GlcNAc)}_4\ \text{b}}$	$k_{\text{cat}}/K_{\text{m}}^{\text{(GlcNAc)}_4\ \text{c}}$	$K_{\text{mR}}^{\text{app}\ \text{b}}$
4.0 ± 0.6	8.9 ± 1.0	$4.5 \cdot 10^5$	200 ± 29	$2.0 \cdot 10^4$	502 ± 35

429   [a] s^{-1} (average value of three values; see text); [b] μM, [c] M^{-1}s^{-1}

430

431

Discussion

Due to their importance in modern biorefineries and capability of catalyzing powerful redox chemistry, there is a vast interest in discovering and characterizing new LPMO activities. *Aspergillus fumigatus* expresses at least three AA11s where *Af*AA11B has low sequence identity with the other two, suggesting different biological roles. Previous work on *Ao*AA11, with similar domain structure and 72.6 % sequence identity in the catalytic domain, suggested that this enzyme is involved in chitin degradation (36), but functional characterization of *Ao*AA11 was limited in this previous study. The present data clearly show that chitin is not a bona fide substrate of *Af*AA11B. Product release from chitin by *Af*AA11B was minimal compared to well-known bacterial chitin-active LPMOs such as *Sm*AA10A (3, 51). Importantly, the enzyme became rapidly deactivated by H_2O_2 in reactions with chitin (Figure 2D) but not in reactions with (GlcNAc)$_4$ (Figure 4D). This supports the notion of chitin not being a true substrate, since it is well known that binding to the substrate protects LPMOs from oxidative damage (25, 30, 56).

At the same time, the ability of *Af*AA11B to stably turnover (GlcNAc)$_4$ in the presence of large initial amounts of H_2O_2 suggests that this oligomer is a good substrate. This is further supported by the kinetic analyses of the peroxygenase reaction with (GlcNAc)$_4$, which yielded kinetic parameters that are in the same order of magnitude as those found for chitin-active LPMOs (30), cellulose-active LPMOs (28) and various haem peroxygenases (31).

We found that *Af*AA11B has additional functional features that makes it stand out from other LPMOs. *Af*AA11B has the lowest redox potential observed for an LPMO so far (0.114 V). Existing data indicate that cellulose-active AA9s have redox potentials in the range from 0.19 V to 0.22 V, cellulose-active AA10s have a redox potential near 0.25 V, and chitin active AA10s have a redox potential around 0.28 V (40, 57–59). The low redox potential of *Af*AA11B is reflected in a high oxidase rate: Whereas AA9 LPMOs (60) and, even more so, AA10 LPMOs (Figure 3, (54)) produce less H_2O_2 compared to free copper in reactions with ascorbic acid, H_2O_2 production in the reaction with *Af*AA11B clearly surpassed H_2O_2 production in the reaction with free Cu(II). From the difference in redox potential, one can deduce that the thermodynamically unfavorable and likely rate-limiting reduction of O_2 to superoxide will be accompanied by a 7.8 kcal/mol lesser energetic penalty in a reaction with *Af*AA11B, compared to *Sm*AA10A.

461   The observed rate constant for oxidase activity of 0.18 s^{-1} for AfAA11B (atmospheric O$_2$

462   pressure and 1 mM AscA) is higher than the observed rate constant for (GlcNAc)$_4$ oxidation (k_{obs} =

463   0.052 s^{-1}) in the presence of same amount of O$_2$ and AscA. This may be taken to suggest that the

464   oxidase activity of AfAA11B can support the apparent monooxygenase reaction in what, *de facto*, is

465   a peroxygenase reaction. However, direct comparison of these rates is not valid because the oxidase

466   activity of AfAA11B will likely be inhibited by the presence of the (GlcNAc)$_4$ substrate. Further

467   insight in this matter was obtained from the HRP inhibition experiments. Most importantly, with this

468   LPMO, it was possible to show that HRP completely inhibits LPMO activity, in conditions that are

469   typically considered "monooxygenase" conditions (1 mM AscA, atmospheric O$_2$). Thus, the apparent

470   monooxygenase reaction is fueled only by H$_2$O$_2$ generated in solution (i.e., accessible to HRP) and

471   not by O$_2$ directly or by H$_2$O$_2$ that is formed in the enzyme-substrate complex but never leaves the

472   active site (as has been suggested for an AA9 LPMO based on modelling studies; (23)). We would

473   thus argue that the monooxygenase reaction does not occur for this catalytically perfectly competent

474   LPMO.

475   An interesting observation is the relatively high amount of AscA needed to keep AfAA11B

476   half-saturated in the Cu(I) state during (GlcNAc)$_4$ oxidation (K_{mR}^{app} = 502 μM) resulting in an

477   efficiency constant k_{cat}/K_{mR}^{app} of 8.0 • 10^3 M^{-1}s^{-1}. In comparison, the same values were 2 μM and

478   1.6 • 10^6 M^{-1}s^{-1}, respectively, for the peroxygenation reaction of SmAA10A with insoluble chitin (55).

479   This high value of K_{mR}^{app} aligns well with the low redox potential of AfAA11B. On the one hand, the

480   low redox potential will reduce the propensity of the reduction of the active site copper by AscA while,

481   on the other hand, it would promote oxidation of reduced LPMOs by O$_2$ (oxidase activity) or H$_2$O$_2$

482   (peroxidase activity) in solution. The propensity of LPMOs to become re-oxidized in between

483   subsequent peroxygenase reactions, and the resulting increased need for reductant, likely depends on

484   substrate affinity.

485   The results described above demonstrate that a fungal LPMO in the auxiliary activity

486   family 11, which deviates in active site architecture from chitin-active bacterial LPMOs in the

487   auxiliary activity family 10, shows a high peroxygenase activity towards oligomeric GlcNAc in

488   soluble form, but is not capable of catalyzing oxidation of insoluble chitin. The unique functional

489   properties of this LPMO combined with observations from the bacterial world that link LPMOs to

490   virulence (34) makes one wonder about the true function of AfAA11B. Transcriptome data for

491   *Neurospora crassa* showed the upregulation of an AA11 with an X278 module in the final stage of

492   spore formation in the fruiting body (61), suggesting a role in cellular development. The cell wall of

493   the producing fungus, as well as the cell walls of competing species, are full of polysaccharide co-

494   polymeric structures. Thus, it is conceivable that AfAA11B acts on such structures, for example during

495   remodeling of the host cell wall or when attacking other cells. Interestingly, a recent study of

496   *Magnaporthe oryzae* showed that an AA9-type LPMOs plays a role in cellular development (62). In

497   preliminary experiments, we tested AfAA11B on a range of substrates, including chitin-containing

498 cell walls, but were not able to detect oxidized products. Further studies into this direction are
499 warranted.

500   It is worth considering whether the high oxidase activity of *Af*AA11B, facilitated by its low
501 redox potential, could serve a biological purpose of its own. It is not easy for organisms to harness the
502 chemical potential of copper, because copper is rare, may easily precipitate (especially in its reduced
503 form), and can engage in potentially damaging redox reactions (e.g., Fenton chemistry) if not properly
504 controlled. Indeed, it has been proposed that LPMOs provide organisms with the opportunity to
505 harness and control the power of Fenton chemistry in biomass degradation (25). It is conceivable that
506 *Af*AA11B provides the organism with a tool to produce H_2O_2 in a process that would be controlled by
507 the delivery of reducing equivalents. Its low redox potential could make *Af*AA11B particularly
508 suitable for this purpose. The produced H_2O_2 could fuel a multitude of enzymes, including LPMOs
509 and other peroxygenases. Interestingly, stimulation of the activity of a lignin-degrading versatile
510 peroxidase by H_2O_2 produced by an AA9 LPMO from *Pleurotus ostreatus* has recently been reported
511 (63).

512   In conclusion, the present results clearly show that there is more to LPMOs than conversion
513 of recalcitrant polysaccharides and that the roles of these peroxygenases may extend to other areas of
514 biology that remain to be discovered. Furthermore, our data lead to the conclusion that the *Af*AA11B
515 LPMO is a true peroxygenases and not a monooxygenase. This lends support to (disputed) claims
516 made by some that the apparent monooxygenase activity of LPMOs in general is not only slow but,
517 in fact, essentially non-existent. Importantly, we also show that, despite the conserved copper histidine
518 brace, LPMOs show considerable variation in redox potential. Unraveling the molecular basis and
519 biological implications of these differences may bring important novel insights into copper
520 biochemistry.

521

522 **Authors' contribution:**
523 LR designed the experiments, performed research, and wrote the first draft of the manuscript. DP
524 performed cloning and helped to design experiments. PV interpreted results and contributed to writing
525 the manuscript. MS and VE initiated the research, carried out supervision, helped to design
526 experiments, interpreted results, and contributed to writing the manuscript.
527

References

540   1.   G. Vaaje-Kolstad, S. J. Horn, D. M. F. Van Aalten, B. Synstad, V. G. H. Eijsink, The non-
541   catalytic chitin-binding protein CBP21 from *Serratia marcescens* is essential for chitin
542   degradation. *J. Biol. Chem.* **280**, 28492–28497 (2005).

543   2.   P. V. Harris, *et al.*, Stimulation of lignocellulosic biomass hydrolysis by proteins of glycoside
544   hydrolase family 61: Structure and function of a large, enigmatic family. *Biochemistry* **49**,
545   3305–3316 (2010).

546   3.   G. Vaaje-Kolstad, *et al.*, An oxidative enzyme boosting the enzymatic conversion of
547   recalcitrant polysaccharides. *Science* **330**, 219–223 (2010).

548   4.   D. Cannella, C. W. C. Hsieh, C. Felby, H. Jørgensen, Production and effect of aldonic acids
549   during enzymatic hydrolysis of lignocellulose at high dry matter content. *Biotechnol. Biofuels*
550   **5**:26 (2012).

551   5.   G. R. Hemsworth, E. M. Johnston, G. J. Davies, P. H. Walton, Lytic polysaccharide
552   monooxygenases in biomass conversion. *Trends Biotechnol.* **33**, 747–761 (2015).

553   6.   K. S. Johansen, Discovery and industrial applications of lytic polysaccharide mono-
554   oxygenases. *Biochem. Soc. Trans.* **44**, 143–149 (2016).

555   7.   G. Müller, P. Chylenski, B. Bissaro, V. G. H. Eijsink, S. J. Horn, The impact of hydrogen
556   peroxide supply on LPMO activity and overall saccharification efficiency of a commercial
557   cellulase cocktail. *Biotechnol. Biofuels* **11**:209 (2018).

558   8.   R. J. Quinlan, *et al.*, Insights into the oxidative degradation of cellulose by a copper
559   metalloenzyme that exploits biomass components. *Proc. Natl. Acad. Sci. U. S. A.* **108**, 15079–
560   15084 (2011).

561   9.   P. H. Walton, G. J. Davies, On the catalytic mechanisms of lytic polysaccharide
562   monooxygenases. *Curr. Opin. Chem. Biol.* **31**, 195–207 (2016).

563   10.   P. Chylenski, *et al.*, Lytic polysaccharide monooxygenases in enzymatic processing of
564   lignocellulosic biomass. *ACS Catal.* **9**, 4970–4991 (2019).

565   11.   B. Bissaro, *et al.*, Molecular mechanism of the chitinolytic peroxygenase reaction. *Proc. Natl.*
566   *Acad. Sci. U. S. A.* **117**, 1504–1513 (2020).

567   12.   V. Lombard, H. Golaconda Ramulu, E. Drula, P. M. Coutinho, B. Henrissat, The carbohydrate-
568   active enzymes database (CAZy) in 2013. *Nucleic Acids Res.* **42**, D490–D495 (2014).

569   13.   L. Ciano, G. J. Davies, W. B. Tolman, P. H. Walton, Bracing copper for the catalytic oxidation
570   of C–H bonds. *Nat. Catal.* **1**, 571–577 (2018).

571   14.   C. H. Kjaergaard, *et al.*, Spectroscopic and computational insight into the activation of O_2 by
572   the mononuclear Cu center in polysaccharide monooxygenases. *Proc. Natl. Acad. Sci. U. S. A.*
573   **111**, 8797–8802 (2014).

574   15.   S. M. Jones, W. J. Transue, K. K. Meier, B. Kelemen, E. I. Solomon, Kinetic analysis of amino

575 acid radicals formed in H_2O_2-driven CuI LPMO reoxidation implicates dominant homolytic
576 reactivity. *Proc. Natl. Acad. Sci. U. S. A.* **117**, 11916–11922 (2020).

577 16. T. M. Hedison, *et al.*, Insights into the H_2O_2 -driven catalytic mechanism of fungal lytic
578 polysaccharide monooxygenases. *FEBS J.* (2020) https:/doi.org/10.1111/febs.15704.

579 17. Z. Forsberg, *et al.*, Cleavage of cellulose by a cbm33 protein. *Protein Sci.* **20**, 1479–1483
580 (2011).

581 18. J. W. Agger, *et al.*, Discovery of LPMO activity on hemicelluloses shows the importance of
582 oxidative processes in plant cell wall degradation. *Proc. Natl. Acad. Sci. U. S. A.* **111**, 6287–
583 6292 (2014).

584 19. V. V. Vu, W. T. Beeson, E. A. Span, E. R. Farquhar, M. A. Marletta, A family of starch-active
585 polysaccharide monooxygenases. *Proc. Natl. Acad. Sci. U. S. A.* **111**, 13822–13827 (2014).

586 20. M. Frommhagen, *et al.*, Discovery of the combined oxidative cleavage of plant xylan and
587 cellulose by a new fungal polysaccharide monooxygenase. *Biotechnol. Biofuels* **8**:101 (2015).

588 21. K. E. H. Frandsen, *et al.*, The molecular basis of polysaccharide cleavage by lytic
589 polysaccharide monooxygenases. *Nat. Chem. Biol.* **12**, 298–303 (2016).

590 22. G. Courtade, *et al.*, Mechanistic basis of substrate-O_2 coupling within a chitin-active lytic
591 polysaccharide monooxygenase: An integrated NMR/EPR study. *Proc. Natl. Acad. Sci. U. S.*
592 *A.* **117**, 19178–19189 (2020).

593 23. B. Wang, P. H. Walton, C. Rovira, Molecular mechanisms of oxygen activation and hydrogen
594 peroxide formation in lytic polysaccharide monooxygenases. *ACS Catal.* **9**, 4958–4969 (2019).

595 24. E. D. Hedegård, U. Ryde, Molecular mechanism of lytic polysaccharide monooxygenases.
596 *Chem. Sci.* **9**, 3866–3880 (2018).

597 25. B. Bissaro, *et al.*, Oxidative cleavage of polysaccharides by monocopper enzymes depends on
598 H_2O_2. *Nat. Chem. Biol.* **13**, 1123–1128 (2017).

599 26. B. Bissaro, I. Isaksen, G. Vaaje-Kolstad, V. G. H. Eijsink, Å. K. Røhr, How a lytic
600 polysaccharide monooxygenase binds crystalline chitin. *Biochemistry* **57**, 1893–1906 (2018).

601 27. B. Bissaro, A. Várnai, Å. K. Røhr, V. G. H. Eijsink, Oxidoreductases and reactive oxygen
602 species in conversion of lignocellulosic biomass. *Microbiol. Mol. Biol. Rev.* **82**:e00029-18
603 (2018).

604 28. R. Kont, B. Bissaro, V. G. H. Eijsink, P. Väljamäe, Kinetic insights into the peroxygenase
605 activity of cellulose-active lytic polysaccharide monooxygenases (LPMOs). *Nat. Commun.*
606 **11**:5786 (2020).

607 29. F. Filandr, *et al.*, The H_2O_2-dependent activity of a fungal lytic polysaccharide monooxygenase
608 investigated with a turbidimetric assay. *Biotechnol. Biofuels* **13**:37 (2020).

609 30. S. Kuusk, *et al.*, Kinetics of H_2O_2-driven degradation of chitin by a bacterial lytic
610 polysaccharide monooxygenase. *J. Biol. Chem.* **293**, 523–531 (2018).

611 31. M. Hofrichter, R. Ullrich, Oxidations catalyzed by fungal peroxygenases. *Curr. Opin. Chem.*

612   *Biol.* **19**, 116–125 (2014).

613   32.   N. Lenfant, *et al.*, A bioinformatics analysis of 3400 lytic polysaccharide oxidases from family
614   AA9. *Carbohydr. Res.* **448**, 166–174 (2017).

615   33.   T. H. F. Costa, *et al.*, Demonstration-scale enzymatic saccharification of sulfite-pulped spruce
616   with addition of hydrogen peroxide for LPMO activation. *Biofuels, Bioprod. Biorefining* **14**,
617   734–745 (2020).

618   34.   D. K. Paspaliari, J. S. M. Loose, M. H. Larsen, G. Vaaje-Kolstad, *Listeria monocytogenes* has
619   a functional chitinolytic system and an active lytic polysaccharide monooxygenase. *FEBS J.*
620   **282**, 921–936 (2015).

621   35.   S. J. Horn, G. Vaaje-Kolstad, B. Westereng, V. G. H. Eijsink, Novel enzymes for the
622   degradation of cellulose. *Biotechnol. Biofuels* **5**:45 (2012).

623   36.   G. R. Hemsworth, B. Henrissat, G. J. Davies, P. H. Walton, Discovery and characterization of
624   a new family of lytic polysaccharide monooxygenases. *Nat. Chem. Biol.* **10**, 122–126 (2014).

625   37.   L. Lo Leggio, *et al.*, Structure and boosting activity of a starch-degrading lytic polysaccharide
626   monooxygenase. *Nat. Commun.* **6**:5961 (2015).

627   38.   K. E. H. Frandsen, L. Lo Leggio, Lytic polysaccharide monooxygenases: A crystallographer's
628   view on a new class of biomass-degrading enzymes. *IUCrJ* **3**, 448–467 (2016).

629   39.   G. Vaaje-Kolstad, D. R. Houston, A. H. K. Riemen, V. G. H. Eijsink, D. M. F. Van Aalten,
630   Crystal structure and binding properties of the *Serratia marcescens* chitin-binding protein
631   CBP21. *J. Biol. Chem.* **280**, 11313–11319 (2005).

632   40.   F. L. Aachmann, M. Sorlie, G. Skjak-Braek, V. G. H. Eijsink, G. Vaaje-Kolstad, NMR
633   structure of a lytic polysaccharide monooxygenase provides insight into copper binding,
634   protein dynamics, and substrate interactions. *Proc. Natl. Acad. Sci.* **109**, 18779–18784 (2012).

635   41.   R. P. Vivek-Ananth, *et al.*, Comparative systems analysis of the secretome of the opportunistic
636   pathogen *Aspergillus fumigatus* and other *Aspergillus* species. *Sci. Rep.* **8**:6617 (2018).

637   42.   L. Nekiunaite, *et al.*, *Fg*LPMO9A from *Fusarium graminearum* cleaves xyloglucan
638   independently of the backbone substitution pattern. *FEBS Lett.* **590**, 3346–3356 (2016).

639   43.   A. Várnai, *et al.*, Expression of endoglucanases in *Pichia pastoris* under control of the GAP
640   promoter. *Microb. Cell Fact.* **13**:57 (2014).

641   44.   M. B. Brurberg, V. G. H. Eijsink, I. F. Nes, Characterization of a chitinase gene (*chiA*) from
642   *Serratia marcescens* BJL200 and one-step purification of the gene product. *FEMS Microbiol.*
643   *Lett.* **124**, 399–404 (1994).

644   45.   B. Synstad, *et al.*, Expression and characterization of endochitinase C from *Serratia*
645   *marcescens* BJL200 and its purification by a one-step general chitinase purification method.
646   *Biosci. Biotechnol. Biochem.* **72**, 715–723 (2008).

647   46.   J. S. M. Loose, Z. Forsberg, M. W. Fraaije, V. G. H. Eijsink, G. Vaaje-Kolstad, A rapid
648   quantitative activity assay shows that the *Vibrio cholerae* colonization factor GbpA is an active

| | | lytic polysaccharide monooxygenase. *FEBS Lett.* **588**, 3435–3440 (2014). |

649		lytic polysaccharide monooxygenase. *FEBS Lett.* **588**, 3435–3440 (2014).
650	47.	B. Westereng, *et al.*, Efficient separation of oxidized cello-oligosaccharides generated by cellulose degrading lytic polysaccharide monooxygenases. *J. Chromatogr. A* **1271**, 144–152 (2013).
653	48.	M. Sørlie, L. C. Seefeldt, V. D. Parker, Use of stopped-flow spectrophotometry to establish midpoint potentials for redox proteins. *Anal. Biochem.* **287**, 118–25 (2000).
655	49.	R. Kittl, D. Kracher, D. Burgstaller, D. Haltrich, R. Ludwig, Production of four *Neurospora crassa* lytic polysaccharide monooxygenases in *Pichia pastoris* monitored by a fluorimetric assay. *Biotechnol. Biofuels* **5**:79 (2012).
658	50.	P. Benkert, M. Biasini, T. Schwede, Toward the estimation of the absolute quality of individual protein structure models. *Bioinformatics* **27**, 343–350 (2011).
660	51.	J. S. M. Loose, *et al.*, Activation of bacterial lytic polysaccharide monooxygenases with cellobiose dehydrogenase. *Protein Sci.* **25**, 2175–2186 (2016).
662	52.	G. Davies, B. Henrissat, Structures and mechanisms of glycosyl hydrolases. *Structure* **3**, 853–859 (1995).
664	53.	T. Isaksen, *et al.*, A C4-oxidizing lytic polysaccharide monooxygenase cleaving both cellulose and cello-oligosaccharides. *J. Biol. Chem.* **289**, 2632–2642 (2014).
666	54.	A. A. Stepnov, *et al.*, Unraveling the roles of the reductant and free copper ions in LPMO kinetics. *Biotechnol. Biofuels* **14**:28 (2021).
668	55.	S. Kuusk, *et al.*, Kinetic insights into the role of the reductant in H_2O_2-driven degradation of chitin by a bacterial lytic polysaccharide monooxygenase. *J. Biol. Chem.* **294**, 1516–1528 (2019).
671	56.	J. S. M. Loose, *et al.*, Multipoint precision binding of substrate protects lytic polysaccharide monooxygenases from self-destructive off-pathway processes. *Biochemistry* **57**, 4114–4124 (2018).
674	57.	D. M. Petrović, *et al.*, Methylation of the N-terminal histidine protects a lytic polysaccharide monooxygenase from auto-oxidative inactivation. *Protein Sci.* **27**, 1636–1650 (2018).
676	58.	A. S. Borisova, *et al.*, Structural and functional characterization of a lytic polysaccharide monooxygenase with broad substrate specificity. *J. Biol. Chem.* **290**, 22955–22969 (2015).
678	59.	Z. Forsberg, *et al.*, Structural and functional characterization of a conserved pair of bacterial cellulose-oxidizing lytic polysaccharide monooxygenases. *Proc. Natl. Acad. Sci. U. S. A.* **111**, 8446–8451 (2014).
681	60.	S. Brander, *et al.*, Biochemical evidence of both copper chelation and oxygenase activity at the histidine brace. *Sci. Rep.* **10**:16369 (2020).
683	61.	Z. Wang, *et al.*, Global gene expression and focused knockout analysis reveals genes associated with fungal fruiting body development in *Neurospora crassa*. *Eukaryot. Cell* **13**, 154–169 (2014).

686 62. Y. Li, *et al.*, *Magnaporthe oryzae* Auxiliary activity protein *Mo*Aa91 functions as chitin-
687   binding protein to induce appressorium formation on artificial inductive surfaces and suppress
688   plant immunity. *MBio* **11**:e03304-19 (2020).

689 63. F. Li, *et al.*, A lytic polysaccharide monooxygenase from a white-rot fungus drives the
690   degradation of lignin by a versatile peroxidase. *Appl. Environ. Microbiol.* **85**:e02803-18
691   (2019).

692 64. X. Li, W. T. Beeson IV, C. M. Phillips, M. A. Marletta, J. H. D. Cate, Structural basis for
693   substrate targeting and catalysis by fungal polysaccharide monooxygenases. *Structure* **20**,
694   1051–1061 (2012).

695

Supplementary Information for

Kinetic characterization of a putatively chitin-active LPMO reveals novel LPMO functionalities and absence of monooxygenase activity

Lukas Rieder[1], Dejan Petrović[1], Priit Väljamäe[2], Vincent G.H. Eijsink[1], Morten Sørlie[1*]

[1]Faculty of Chemistry, Biotechnology, and Food Sciences, Norwegian University of Life Sciences (NMBU), N-1432 Ås, Norway
[2] Institute of Molecular and Cell Biology, University of Tartu, Tartu, Estonia

* Corresponding author:
Morten Sørlie Tel: + 47 67 23 25 62, morten.sorlie@nmbu.no

Table of contents

Materials and Methods

Eyring analysis. To obtain the activation parameters for the peroxygenase reaction of *Af*AA11B with (GlcNAc)$_4$, two forms of the Eyring equation were used (Equation (1) and Equation (2)):

$$\Delta G^{\#} = -RT\ln\left(\frac{k_{cat}h}{k_B T}\right) \tag{1}$$

$$\ln\left(\frac{k_{cat}}{T}\right) = \ln\left(\frac{k_B}{h}\right) + \frac{\Delta S^{\#}}{R} - \frac{\Delta H^{\#}}{RT} \tag{2}$$

where k_{cat} is the measured rate of the reaction, $\Delta G^{\#}$ is the change in activation free energy, $\Delta S^{\#}$ is the change in activation entropy, $\Delta H^{\#}$ is the change in activation enthalpy, h is Planck's constant, k_B is Boltzmann's constant, R is the gas constant, and T is the absolute temperature. The determined k_{cat} values were fitted to the linear form of the Eyring equation (2) using linear regression (ln k_{cat}/T vs. $1/T$) that was performed using OriginPro 2018 (OriginLab Corporation, Northampton, Massachusetts, USA). $\Delta H^{\#}$ was determined from the slope of the resulting straight line ($-\Delta H^{\#}/R$). $-T\Delta S^{\#}$ was determined from the relationship described in Equation (3):

$$\Delta G^{\#} = \Delta H^{\#} - T\Delta S^{\#} \tag{3}$$

To obtain the activation energy (E_a) and the frequency factor (A) of the reaction, the Arrhenius equation was used, Equation (4).

$$\ln k_{cat} = \ln A - \frac{E_a}{RT} \tag{4}$$

The determined k_{cat} values were fitted to the linear form of the Arrhenius equation (4) and linear regression (ln k_{cat} vs. $1/T$) was performed using OriginPro 2018 (OriginLab Corporation, Northampton, Massachusetts, USA).
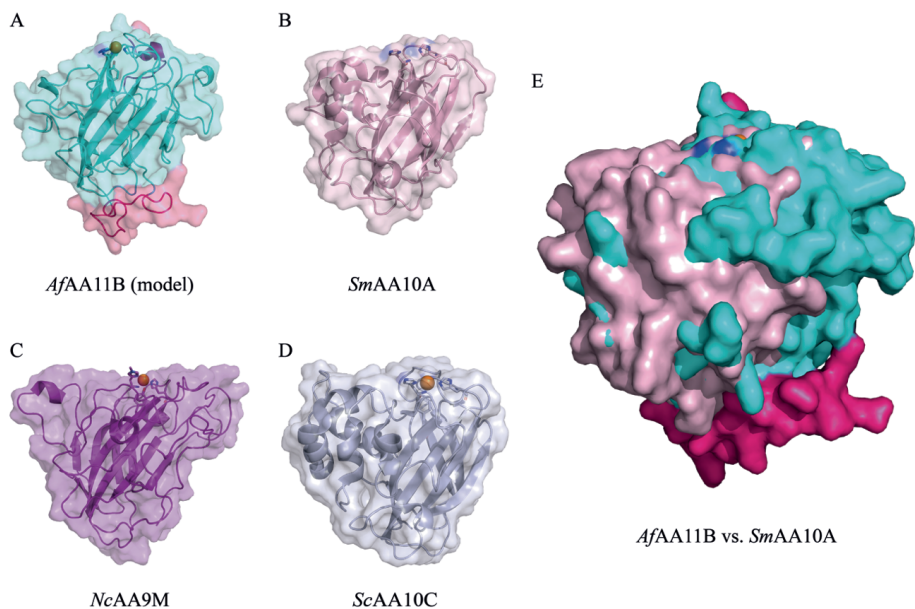
Figure S1. Comparison of the surface topology of the putatively chitin-active *Af*AA11B (A, homology model), the well characterized chitin-active *Sm*AA10A (B, PDB: 2BEM (1)) and the cellulose active LPMOs *Nc*AA9M (C; PDB: 4EIS (2)) and *Sc*AA9C (D; PDB: 4OY7 (3)). All structures are shown in cartoon representation with a transparent surface (60%). The side chains of the N-terminal histidine, the second histidine in the active site and the aromatic amino acid in the proximal axial copper coordination position are shown as sticks. All structures are oriented identically with the N-terminal histidine facing to the left. In panel A, two lesser reliable parts of the model (see main text) are colored in magenta. Panel (E) shows a superposition of *Af*AA11B (blue) and *Sm*AA10A (pink), illustrating differences in surface topology near the active site. The enzymes structures used for the superposition are angled like in illustrations (A) and (B), but the transparency of the surface was set to 0 % for visualization purposes. These pictures were prepared in PyMOL.
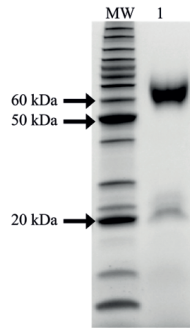
Figure S2. SDS-PAGE Gel of purified *Af*AA11B. Lanes: (MW) BenchMark^TM Protein Ladder (Thermo Fischer Scientific); (1) purified *Af*AA11B after three chromatographic purification steps where the final purification step displayed only one peak in the chromatograms suggesting that the fragments at 20 kDa are the result of degradation of *Af*AA11B during SDS-PAGE analysis.
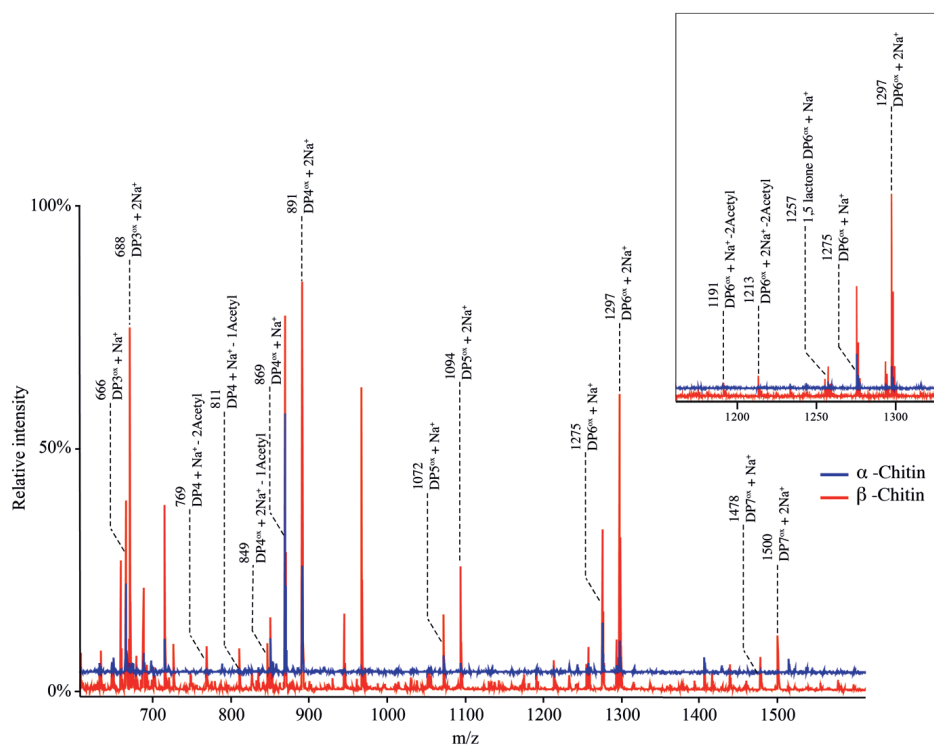
Figure S3. MALDI-ToF MS spectra showing oxidized products ranging from DP3 to DP7 ($\Delta m/z$ 203) originating from α (blue) and β (red) chitin upon reaction with *Af*AA11B in the presence of 1 mM AscA and atmospheric oxygen levels. Labeled peaks represent sodium adducts of C1 oxidized products in the lactone form ($\Delta m/z$ -2) and in the (dominating) aldonic acid form ($\Delta m/z$ +16), as well as the sodium salt of the aldonic acid form ($\Delta m/z$ +38). The insert to the right shows details for the DP6 cluster. The spectra also show small signals for partially de-acetylated native and oxidized products ($\Delta m/z$ -42).
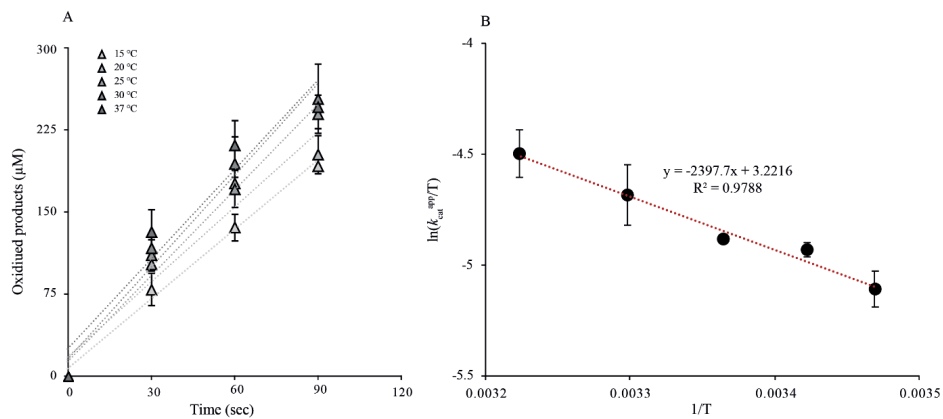
Figure S4. Temperature dependency and Eyring plot for the *Af*AA11B catalyzed oxidation of (GlcNAc)$_4$ in the presence of H$_2$O$_2$. (A) Linear time course experiments with 1 μM LPMO, 300 μM H$_2$O$_2$ and 1 mM AscA in the presence of 2 mM (GlcNAc)$_4$ at different temperatures (15-37 °C). (B) Eyring plot based on the calculated rate constants from (A).

Eyring analysis. Because *Af*AA11B catalyzes a strict peroxygenase reaction with a soluble substrate, it was, for the first time, possible to determine the activation parameters of the reaction by assessing the temperature dependency of the initial rates. The underlying time course experiments were performed with 1 µM LPMO in the presence of 300 µM H_2O_2, 1 mM AscA and 2 mM (GlcNAc)$_4$ at varying temperatures (15-37 °C). We could obtain linear progress curves for all reaction conditions, and the derived catalytic rates confirmed that the rate of catalysis is dependent on the temperature (Figure S4A). An Eyring plot based on the calculated rate constants (Figure S4B) gave a change in activation enthalpy ($\Delta H^{\#}$) of 4.7 ± 1.1 kcal/mol and a change in activation free energy ($\Delta G^{\#}$) of 17.3 ± 0.1 kcal/mol. The change in activation entropy ($\Delta S^{\#}$) was large and negative and the contribution of the entropic term ($-T\Delta S^{\#}$) was calculated to be 12.6 ± 1.2 kcal/mol. The Arrhenius analysis yielded an activation energy (E_a) of 5.5 ± 0.1 kcal/mol with a frequency factor (A) of $2.4 \cdot 10^4$ s^{-1}. Caution must be taken when the parameters are interpreted. Still, the large and negative contribution of the entropic term ($-T\Delta S^{\#}$ = 12.6 kcal/mol) to the activation free energy change suggests a high degree of order in the transition state.

SI References

1.   G. Vaaje-Kolstad, D. R. Houston, A. H. K. Riemen, V. G. H. Eijsink, D. M. F. Van Aalten, Crystal structure and binding properties of the *Serratia marcescens* chitin-binding protein CBP21. *J. Biol. Chem.* **280**, 11313–11319 (2005).

2.   X. Li, W. T. Beeson IV, C. M. Phillips, M. A. Marletta, J. H. D. Cate, Structural basis for substrate targeting and catalysis by fungal polysaccharide monooxygenases. *Structure* **20**, 1051–1061 (2012).

3.   Z. Forsberg, *et al.*, Structural and functional characterization of a conserved pair of bacterial cellulose-oxidizing lytic polysaccharide monooxygenases. *Proc. Natl. Acad. Sci. U. S. A.* **111**, 8446–8451 (2014).

Fast and specific peroxygenase reactions catalyzed by fungal mono-copper enzymes

Lukas Rieder, Anton A. Stepnov, Morten Sørlie, Vincent G.H. Eijsink

Paper III

Fast and specific peroxygenase reactions catalyzed by fungal mono-copper enzymes

Lukas Rieder, Anton A. Stepnov, Morten Sørlie, Vincent G.H. Eijsink

Faculty of Chemistry, Biotechnology, and Food Sciences, Norwegian University of Life Sciences (NMBU), Ås, Norway

Abstract

The copper-dependent lytic polysaccharide monooxygenases (LPMOs) are receiving massive attention because of their role in the degradation of recalcitrant biomass and their intriguing catalytic properties. The fundamentals of LPMO catalysis remain somewhat enigmatic as the LPMO reaction is affected by a multitude of LPMO- and co-substrate-mediated (side) reactions that result in a complex reaction network. We have performed comprehensive kinetic studies with two LPMOs that are active on soluble substrates, NcAA9C and LsAA9A, using various reductants typically employed for LPMO activation. Studies with NcAA9C under "monooxygenase" conditions showed that the impact of the reductant on catalytic activity is correlated with the hydrogen peroxide-generating ability of the LPMO-reductant combination, supporting the idea that the slow apparent monooxygenase reaction in fact is a peroxygenase reaction. Indeed, the apparent monooxygenase reaction could be inhibited by a competing H_2O_2-consuming enzyme. Interestingly, these fungal AA9 type LPMOs were found to have higher oxidase activity than bacterial AA10 type LPMOs. Kinetic analysis of the peroxygenase activity of NcAA9C on a soluble substrate revealed fast and specific peroxygenase activity. The k_{cat} value of 124 ± 27 s^{-1} at 4 °C is 20 times higher than a previously described k_{cat} for peroxygenase activity on an insoluble substrate (at 25 °C) and some four orders of magnitude higher than typical "monooxygenase" rates. Similar studies with LsAA9A revealed differences between the two enzymes but confirmed fast and specific peroxygenase activity. These results show that the catalytic site arrangement of LPMOs provides a unique scaffold for highly efficient copper redox catalysis.

Introduction

Enzymes currently known as lytic polysaccharide monooxygenases (LPMOs) catalyze the oxidative scission of glycosidic bonds and by doing so they boost the activity of classical polysaccharide-degrading hydrolytic enzymes such as chitinases and cellulases [1]–[10]. LPMO catalytic sites contain a single copper ion co-factor [11], [12] that upon reduction reacts with either O_2 or H_2O_2 to generate an oxygen species that is capable of abstracting a hydrogen atom from the C1 or the C4 carbon atom in glycosidic bonds [9], [13]–[16].

Initially, LPMOs were thought to be monooxygenases ([3]; Figure 1A), but recent studies have shown that LPMOs can act as peroxygenases ([15]; Figure 1B) and that this reaction is orders of magnitude faster than the monooxygenase reaction [15]–[20]. Interestingly, LPMOs are not the first oxidoreductases that might depend on a different oxygen source than initially thought as it was reported that the iron-depended epoxidase HppE, originally classified as an oxidase, is in fact a non-heme iron peroxidase [21]. Nonetheless, in case of the LPMOs it has been claimed by some that the peroxygenase reaction is less specific and leads to more enzyme damage compared to the monooxygenase reaction and thus is not likely to be the true LPMO reaction ([22], but this claim is disputed (e.g. [16], [20], [23]). Importantly, under the conditions typically used in LPMO "monooxygenase" reactions, H_2O_2 will be generated *in situ* and there are indications that observed reaction rates in such reactions, typically in the range of a few per minute ([17]), reflect the rate of *in situ* generation of H_2O_2, rather than the rate of a true monooxygenase reaction [24]–[26]. *In situ* generation of H_2O_2 may result from LPMO-independent oxidation of the reductant by O_2, and may also involve the LPMO, since LPMOs have oxidase activity [27]–[29]. These two routes towards H_2O_2 generation are intertwined in a manner that depends on both the reductant and the LPMO. For example, Stepnov *et al*. [25] showed that generation of H_2O_2 in standard reactions with an AA10 type (bacterial) LPMO (i.e., LPMO + 1 mM reductant) was almost independent on the LPMO in reactions with gallic acid, whereas the LPMO increased H_2O_2 production in reactions with ascorbic acid. It is not known whether the same would apply for the AA9 LPMOs that are abundant in biomass-degrading fungi.
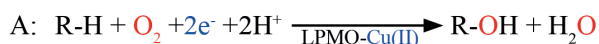
Understanding LPMOs, which requires robust assessment of LPMO kinetics, is complicated due to the many interconnected redox phenomena and catalytic pathways. In the presence of substrate, LPMOs catalyze oxidation of glycosidic bonds using O_2 or H_2O_2 [monooxygenase or peroxygenase reaction; Figure 1; [9], [14], [15], [30]]. In the absence of a carbohydrate substrate, LPMOs catalyze formation of H_2O_2 from molecular oxygen (oxidase reaction) [25], [27]. The inhibitory effect of the substrate on H_2O_2 accumulation may reflect inhibition of the oxidase reaction [26], as originally proposed by Kittl et al [27], but may also reflect consumption of the generated H_2O_2 in a productive LPMO reaction [15]. Next to engaging in oxidase reactions, reduced LPMOs may act as an H_2O_2

67   scavenger in peroxidase like reactions [31]. Both these non-productive (per)oxidase reactions may
68   lead to auto-catalytic enzyme inactivation [15], [20], [23], [32].
69   The substrate of LPMOs is insoluble, which not only complicates analytics, but also generates
70   an additional kinetic complication related to potentially slow substrate association/dissociation. Slow
71   substrate association is of particular importance because a reduced LPMO that is not bound to
72   substrate is prone to side reactions that may consume reactants and lead to enzyme damage, as outlined
73   above [15], [32], [33]. Interestingly, Hangasky *et al.* [22] showed that H_2O_2-consuming horse radish
74   peroxidase (HRP), which has a soluble substrate, inhibited an LPMO acting on an insoluble substrate,
75   while having only a minor inhibitory effect on an LPMO acting on a soluble substrate. This
76   observation with soluble substrate was interpreted to show that the LPMO does not depend on H_2O_2
77   and thus is a true monooxygenase. Although not recognized at the time, another possible explanation
78   for this difference is that the LPMO reaction with soluble substrate is much more efficient, allowing
79   the LPMO to better compete with HRP for the available H_2O_2.
80   In recent years, fungal AA9 type LPMOs active on soluble substrates have been discovered,
81   including *Nc*AA9C from *Neurospora crassa* [34], [35] and *Ls*AA9A from *Lentinus similis* [36]. These
82   enzymes, acting on a diffusible and easy to analyze substrate, provide a unique opportunity to
83   kinetically assess the various LPMO reactions. Here, we present an in-depth kinetic analysis of
84   *Nc*AA9C acting on cellopentaose, showing that this enzyme is a fast and specific peroxygenase,
85   capable of reaching unprecedented high catalytic rates. Similar studies with *Ls*AA9A revealed
86   differences between the two enzymes but confirmed that these AA9 type LPMOs are indeed
87   competent peroxygenases. These results demonstrate the immense catalytic potential of the LPMO
88   scaffold, which is much higher than anticipated when the first ultraslow LPMO reactions were
89   described.
90
91

$$\text{A:} \quad \text{R-H} + O_2 + 2e^- + 2H^+ \xrightarrow[\text{LPMO-Cu(II)}]{} \text{R-OH} + H_2O$$

$$\text{B:} \qquad \text{R-H} + H_2O_2 \xrightarrow[\text{LPMO-Cu(I)}]{} \text{R-OH} + H_2O$$

92
93
94   **Figure 1. Reaction schemes for the monooxygenase (A) and the peroxygenase (B) reaction.** The
95   substrate is indicated by R. Hydroxylation of one of the carbons destabilizes the glycosidic bond,
96   which, once oxidized, undergoes an elimination reaction leading to bond breakage [12]. Note the
97   potential difference in reductant consumption between the two reaction schemes. In the peroxygenase
98   scheme, a once reduced LPMO can carry out multiple reactions [20], [37], [38], meaning that reductant
99   consumption will be low if H_2O_2 is provided externally. If, however, H_2O_2 is generated *in situ* through
100   reduction of O_2, also the peroxygenase reaction will require two electrons per cycle
101   ($O_2 + 2e^- + 2H^+ \rightarrow H_2O_2$).

102

Materials and Methods

Chemicals

All chemicals were, if not stated otherwise, purchased from Sigma-Aldrich, Thermo Fisher Scientific or VWR.

107

Expression and purification and copper saturation.

Recombinant LPMO expression was done as previously described by Rieder *et al.* [39]. In summary: the genes encoding *Ls*AA9A (UniProtKB: A0A0S2GKZ1) and *Nc*AA9C (UniProtKB: Q7SHI8) were codon optimized for *P. pastoris*, using the online tool provided by Thermo Fisher Scientific and cloned into the pBSYP$_{GCW14}$Z plasmid, which facilitates constitutive expression and employs the native LPMO signal peptides for secretion. After *Smi*I linearization, the pBSYP$_{GCW14}$Z-*LPMO* constructs were used for the transformation of killer plasmid free *P. pastoris* BSYBG11 ($\Delta AOX1$, Mut^S) one-shot ready competent cells (bisy GmbH, Hofstätten a.d. Raab, Austria) following the manual provided by the supplier.

For enzyme expression a single yeast colony was used to inoculate 500 ml YPD [1 % (w/v) Bacto™ yeast extract (BD Bioscience, San Jose, CA, USA), 2 % (w/v) peptone from casein (tryptone) (Merck Millipore, Burlington, MA, USA) and 2 % (w/v) glucose]. Incubation was performed over 60 h in a 2 l baffled shake flask at 120 rpm and 28 °C. The LPMO containing supernatant was separated from the cells by centrifugation at 10000 x g for 15 min at 4 °C and filtered using a 0.22 μm Steritop® bottle-top filter (Merck Millipore, Burlington, MA, USA) prior to concentration using a VivaFlow 200 tangential crossflow concentrator (molecular weight cut-off, MWCO, 10 kDa, Sartorius Stedim Biotech Gmbh, Germany) and Amicon Ultra centrifugal filters (MWCO 10 kDa, Merck Millipore, Burlington, MA, USA).

The LPMOs were purified using an Äkta purifier system (GE Healthcare Life Sciences, Uppsala, Sweden) equipped with a HiLoad 16/60 Superdex 75 size exclusion column (GE Healthcare Life Sciences, Uppsala, Sweden) that was equilibrated in 50 mM BisTris-HCl (pH 6.5), 150 mM NaCl. The single step size exclusion purification was performed at a flowrate of 1 ml/min. The protein content of the fractions was assessed by SDS-PAGE and fractions containing pure LPMO were pooled.

To ensure copper saturation of the active site, the enzyme preparation was incubated for 1 h with a threefold molar excess of $CuSO_4$ at 4 °C in 50 mM BisTris-HCl (pH 6.5) with 150 mM NaCl. Unbound copper was removed by 3 repetitions of buffer exchange to 50 mM BisTris-HCl (pH 6.5) using Amicon Ultra centrifugal filters (MWCO 10 kDa, Merck Millipore, Burlington, MA, USA). LPMO concentrations were determined using the Bradford protein assay with bovine serum albumin

137   as standard. The copper saturated and purified proteins were stored in 50 mM BisTris-HCl (pH 6.5)

138   at 4 °C until use.

139   *Af*AA11B, a chitin-active LPMO from *Aspergillus fumigatus* (UniProtKB: Q4WEH3), which

140   will be described in detail elsewhere, was produced, purified and copper-saturated as described above

141   for *Ls*AA9A and *Nc*AA9C [39]. Copper-saturated chitin-active bacterial *Sm*AA10A (CBP21) was

142   prepared as described previously [40].

143

144   **LPMO reactions with soluble substrates.** LPMO reactions typically had a volume of 200 μl and

145   were prepared in a 1.5 ml reaction tube with conical bottom. Standard reactions contained 1 μL

146   LPMO, 1 mM reductant and 1 mM cellopentaose (95% purity; Megazyme, Wicklow, Ireland) in 50

147   mM BisTris-HCl (pH 6.5). Reactions supplemented with H_2O_2 contained typically 0.25 μM enzyme,

148   300 μM H_2O_2, 100 μM reductant and 1 mM of soluble substrate. Deviations from standard conditions

149   were required for some experiments, as indicated in the appropriate figure legends. Stock solutions of

150   50 mM AscA (L-Ascorbic acid, 99%, Simga-Aldrich), 10 mM GA (Gallic acid monohydrate ≥99 %,

151   Sigma-Aldrich), 100 mM cysteine (L-Cysteine ≥98%, Sigma-Aldrich) were prepared in ddH$_2$O,

152   aliquoted and stored at -20°C until use. 10 mM Stock solutions of H_2O_2 (37% Merck) were prepared

153   in pure water (TraceSELECT®, Fluka) and stored at -20°C until use. The H_2O_2 concentration was

154   assessed by measuring the absorbance at 240 nm and using a molar extinction coefficient of 43.6 M^{-}

155   ^{1}cm^{-1}.

156   Since the order of mixing the various components of LPMO reactions matters, we started by

157   mixing H_2O, buffer stock solution and the substrate followed by the LPMO. After incubation for 1

158   min at the desired temperature and rpm, the reaction was initiated by addition of reductant (time point

159   zero). In case the reaction was supplemented with H_2O_2 or HRP (Sigma-Aldrich) these were added

160   after the LPMO but before the pre-incubation step and before addition of reductant. Reactions were

161   incubated either at 37 °C or 4 °C, and at 750 rpm (Thermomixer C, Eppendorf, Hamburg, Germany).

162   For sampling, 25 μl aliquots were withdrawn from the main reaction at regular time points. To quench

163   the reaction and to achieve an appropriate dilution factor for subsequent HPAEC-PAD analysis of

164   products (see below), 175 μl of 200 mM NaOH were added to each sample. For quantification with

165   the Dionex ICS6000 system, the dilution factor was 1:40, due to a higher sensitivity of this system.

166   Reactions with mannopentaose and xylopentaose (95% purity; Megazyme, Wicklow, Ireland), were

167   set up and sampled in the same manner but were diluted 1:4 prior to HPAEC-PAD analysis.

168   The presented data points are the average values of at least three individual replicates and

169   include the standard deviation, which is shown as a vertical line. Negative control reactions were

170   performed by leaving out the reductant.

171

172   **Product detection and quantification.** Reaction products were detected using high-performance

173   anion exchange chromatography with pulsed amperometric detection (HPAEC-PAD). HPAEC was

174 performed on a Dionex ICS5000 or ICS6000 system. The ICS5000 was equipped with a 3×250 mm
175 CarboPac PA200 analytical column and a CarboPac PA200 guard column, and cello-oligomer
176 containing samples were analyzed using a 26 min gradient, as described previously [25]. For analysis
177 with the ICS6000 we used a 1×250 mm CarboPac PA200 analytical column and a guard column of
178 the same type. The flow rate during analysis was 63 μL*min^{-1} and the applied gradient was as follows:
179 1 – 14 min, from 1 to 100 mM potassium methanesulfonate (KMSA), concave; 14 - 17 min, washing
180 step at 100 mM KMSA; 17 – 26 min, re-conditioning at 1 mM KMSA.

181 To assess the LPMO activity on cellopentaose the generation of native cellobiose and
182 cellotriose, which would proportionally increase with the C4-oxidized products, was quantified.
183 Products from reactions with mannopentaose and xylopentaose were analyzed using the Dionex
184 ICS5000 system in the configuration described above. For analysis of mannopentaose containing
185 samples we used the 26 min gradient as for the cellopentaose containing samples. In case the reactions
186 were set up with xylopentaose we used a 39 min gradient as described elsewhere [41]. Chromatograms
187 were recorded and analyzed with Chromeleon 7, and plots were made using Microsoft Excel.

188

189 **H$_2$O$_2$ production assay.** Hydrogen peroxide formation assays were performed as previously
190 described by Kittl *et al*. [27]. The reactions were performed in 96-well microplates with 100 μl 50 mM
191 BisTris/HCl buffer (pH 6.5) containing 1 μM LPMO, 100 μM Amplex Red, 1% (v/v) DMSO and
192 0.025 mg/ml HRP (final concentrations). After 5 min pre-incubation at 30 °C the reactions were started
193 by the addition of 1 mM reductant (final concentration). The formation of resorufin was monitored
194 over 30 min at 540 nm using a Multiskan™ FC Microplate Photometer (Thermo Fisher Scientific,
195 Bremen Germany). Standard solutions for H$_2$O$_2$ quantification were supplemented with reductant and
196 if appropriate with 1 mM Glc$_5$ to capture potential side reactions, as recently explained [19], [25]. The
197 reductant and Glc$_5$ were added prior the addition of HRP.

198
199
200 **Results and Discussion**

201 **The reductant influences the apparent monooxygenase reaction.** It is well known from earlier
202 work that the reductant has a large impact on the efficiency of O$_2$-driven LPMO reactions [24], [25],
203 [42], [43]. In keeping with the monooxygenase paradigm, this dependency has been attributed to
204 variation in the reductant's ability to deliver electrons to the LPMO. As outlined above, considering
205 the peroxygenase activity of LPMOs, it is quite plausible that the observed variation also, or even
206 primarily, reflects reductant-dependent variation in the *in situ* synthesis of H$_2$O$_2$ during the reaction
207 [24], [25]. Here, we addressed the impact of the reductant on *Nc*AA9C by studying degradation of
208 cellopentaose in the presence of ascorbic acid (AscA), cysteine or gallic acid (GA). The reactions were
209 performed using classical aerobic "monooxygenase" conditions with 1 μM enzyme, 1 mM Glc$_5$ and 1
210 mM reductant.

6

211

212
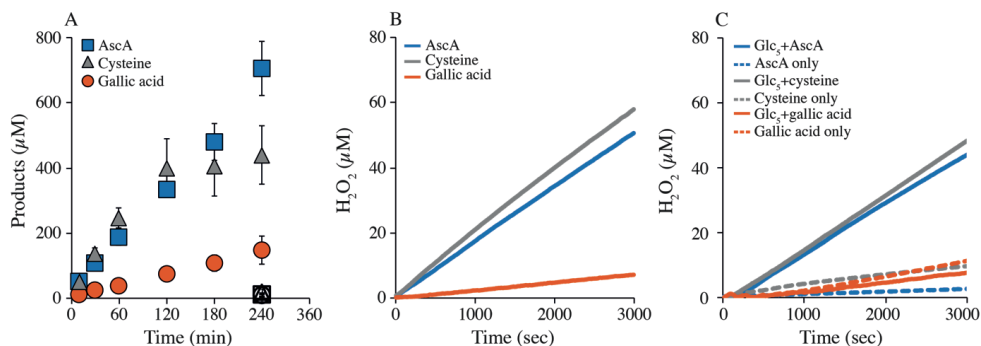
213
214 **Figure 2. Progress curves showing apparent monooxygenase (A) and oxidase (B) activity of**
215 **NcAA9C**. Reactions were performed with 1 μM enzyme and 1mM of either AscA (blue), cysteine
216 (grey) or GA (orange) in the presence (A) or absence (B) of 1 mM Glc_5. The empty symbols in A (at
217 240 min only) show the product levels (~10 μM) found in the control reactions without reductant.
218 Panel (C) shows control reactions, i.e., LPMO independent H_2O_2 accumulation, in reactions with only
219 reductant (dashed lines) or with reductant and 1 mM Glc_5 (solid lines).

220

221

222   Figure 2A shows that stable reaction rates were obtained with AscA and gallic acid, with
223 apparent rate constants (k_{obs}), derived from the linear part of the progress curves, of 0.05 ± 0.01 sec^{-1}
224 and 0.011 ± 0.02 sec^{-1}, respectively (Table 1). The reaction with cysteine showed the highest initial
225 rate ($k_{obs} = 0.06 \pm 0.01$ sec^{-1}), but in this case product formation halted after approximately half of the
226 substrate had been degraded. This is not surprising since, while AscA and gallic acid can donate two
227 electrons per molecule, cysteine can donate only one, meaning that two molecules of cysteine are
228 needed per LPMO reaction and that 1 mM of cysteine can only fuel cleavage of 0.5 mM (i.e., half) of
229 the substrate.

230   To gain insight into the oxidase activity of NcAA9C and a possible connection between this
231 activity and the enzyme's apparent monooxygenase activity, we measured H_2O_2 production in the
232 absence of substrate using the Amplex Red/HRP assay, as described previously [25], [27]. Of note,
233 while this assay is very useful, it suffers from multiple complications (discussed in e.g.[19], [25]) that
234 prevent extrapolation of apparent H_2O_2 production levels in a reaction without substrate (Figure 2B)
235 with expected H_2O_2 production levels in a reaction with substrate (Figure 2A). Firstly, the reductant
236 suppresses the signal of the HRP assay and this will vary between reductants. Although the reductant
237 is included in the standard curve for H_2O_2, this effect cannot be fully compensated for [19], [25].
238 Secondly, H_2O_2 may react with the reductant (meaning that H_2O_2 levels will be underestimated) and
239 this reaction may be promoted by HRP to an extent that differs between the reductants; this situation

7

240 will be entirely different in a reaction with substrate, where the productive LPMO reaction will
241 outcompete slower background reactions with the reductant. Finally, as alluded to above [26], [27],
242 [34], the presence of substrate inhibits the oxidase activity of the LPMO.

243   Figure 2B and the derived reaction rates (Table 1) show that apparent H_2O_2-production rates
244 vary between the reductants, showing trends that align well with apparent monooxygenase reactions
245 rates (Figure 2A; Table 1). The apparent monooxygenase activity is about five times higher with AscA
246 and cysteine than with gallic acid. The variation in the apparent oxidase rates shows a similar trend,
247 but in this case, the rate difference between AscA/cysteine and GA is about 10-fold. For all reductants,
248 the apparent monooxygenase activity is three to five times higher than the apparent oxidase activity,
249 which could indicate that we indeed are observing monooxygenase activity in a reaction that is not
250 limited by generation of H_2O_2. However, this phenomenon could also be due to underestimation of
251 H_2O_2 production for reasons described above, and addressed further below, or be caused by an
252 additional source of H_2O_2 in reactions with the substrate, Glc_5, as discussed below.

253   Intrigued by the difference between the apparent monooxygenase and oxidase activities, we
254 investigated a possible effect of 1 mM Glc_5 on H_2O_2 production in reactions with standard amounts of
255 all three reductants. The obtained results show that, for reactions with AscA and cysteine, incubation
256 of Glc_5 with reductant led to strongly increased H_2O_2 production, relative to reactions with only
257 reductant (Figure 2C). The apparent H_2O_2 production rates in these reactions were not unlike the rates
258 obtained in reactions with reductant and LPMO (Figure 2B) and are thus quite significant (Table 1).
259 This unexpected effect of Glc_5 indicates the presence of significant amounts of transition metals, likely
260 copper, which would strongly enhance H_2O_2 production through oxidation of AscA [25], [44] and
261 cysteine [45], but not of gallic acid [25] since GA is more likely to form complexes with Cu(II) rather
262 than reducing it [46]. This additional source of H_2O_2 helps to close the gap observed between the rates
263 of the apparent monooxygenase and oxidase activities, and thus lends support to the notion that the
264 apparent monooxygenase reaction is in fact a peroxygenase reaction limited by H_2O_2.

265   Of note, the results depicted in Figure 2 show that the combination of *Nc*AA9C and GA is not
266 suitable for assessment of LPMO oxidase activity by the Amplex Red/HRP assay as the apparent rate
267 of H_2O_2-production in reactions with GA alone (Figure 2C, Table 1) is higher that the apparent oxidase
268 activity of in reactions with GA and the LPMO (Figure 2B; Table 1). In this case, the assay is flawed
269 due to the ability of *Nc*AA9C to engage in a H_2O_2-consuming side reaction with GA, as described by
270 Breslmayr *et al*. ([31]). Of note, in a LPMO reaction mixture containing Glc_5, side reactions with GA
271 will be outcompeted by the peroxygenase reaction with Glc_5, which is orders of magnitude faster, as
272 shown below.

273

274

275

276

Table 1. Apparent rate constants (s^{-1}) for reactions catalyzed by *Nc*AA9C, with three different reductants. The values presented are derived from the progress curves shown in Figures 2 and 4 and are either estimates based on the first time point (peroxygenase reaction) or represent the average of three individual replicates (monooxygenase and oxidase reaction).

	Monooxygenase (Fig. 2A; 1 mM reductant, 1 mM Glc$_5$, O$_2$)	Oxidase (Fig. 2B; 1 mM reductant, O$_2$, no substrate)	O$_2$ reduction, reductant only, with substrate (Fig. 2C; 1mM reductant, 1 mM Glc$_5$, O$_2$, no LPMO)	O$_2$ reduction, reductant only (Fig. 2C; 1mM reductant, O$_2$, no LPMO)	Peroxygenase (Fig. 4A; 0.1 mM reductant, 1 mM Glc$_5$, 300 µM H$_2$O$_2$, O$_2$)
AscA	0.05±0.01	0.017±0.001	0.016±0.000	0.0004 ± 0.0001	~70[1]
Gallic acid	0.011±0.002	0.002±0.001	0.004±0.000	0.0040± 0.0009	~25[1]
Cysteine	0.06±0.01	0.019±0.000	0.017±0.000	0.0026 ± 0.0002	~6

[1]The shape of the progress curve in Figure 4A shows that this rate is underestimated.

A recent study on a cellulose-active AA10-type LPMO with AscA and GA as reductants showed that the LPMO had little effect on H$_2$O$_2$ production, which was dominated by the LPMO-independent oxidation of the reductant [25]. Table 1 shows that the situation for *Nc*AA9C is different. In this case, the LPMO may contribute considerably to apparent H$_2$O$_2$ production in reactions with cysteine and AscA (compare "Oxidase" with "O$_2$ reduction, reductant only"). In the case of AscA, the LPMO speeds up the H$_2$O$_2$ production rate by some 40-fold, whereas the increase is some 7-fold for cysteine. Similar comparisons for GA could not be made due to the technical issues discussed above.
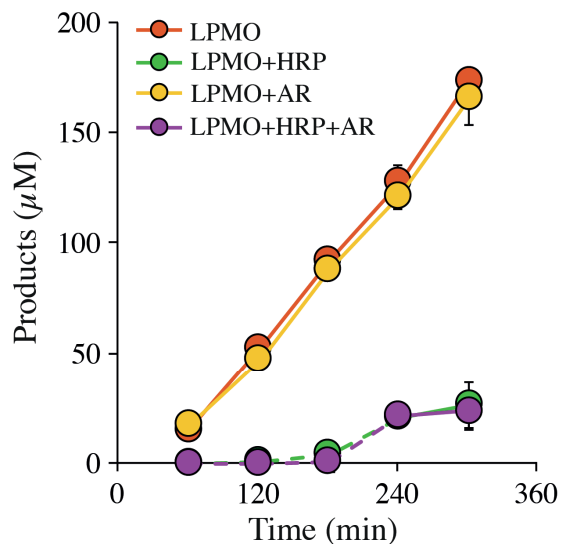
293
Figure 3. HRP inhibition for reactions with *Nc*AA9C and GA. Progress curves showing product
formation by 1 μM LPMO in the presence of 1mM GA and 1 mM Glc_5 with no supplementation
(orange) or supplemented with 100 μM Amplex Red (yellow) or 2 μM HRP (green) or both (purple).
Note that the HRP reaction does not depend on Amplex Red (AR) since GA is a substrate for HRP
(see text). Dashed lines connect points with values that were close to the limit of detection.

If it is the *in-situ* generation of H_2O_2 that is limiting the apparent monooxygenase reaction in
the presence of GA it should be possible to inhibit the LPMO reaction with another H_2O_2-consuming
enzyme. Indeed, both Bissaro *et al*. [15] and Hangasky *et al*. [22] have shown that LPMO reactions
with insoluble substrates under "monooxygenase conditions" are inhibited when adding horseradish
peroxidase (HRP) and its substrate, Amplex Red. While Hangasky *et al*. did not observe similarly
strong inhibition in a reaction with soluble substrate, Figure 3 shows that HRP strongly inhibits the
GA-driven activity of *Nc*AA9C on Glc_5. A similar degree of inhibition was observed in the reaction
containing HRP but lacking Amplex Red, indicating that horseradish peroxidase can oxidize gallic
acid, which is not surprising considering literature data [47]. Of note, it is highly unlikely that the
LPMO inhibition in the presence of HRP is driven by reductant depletion rather than by competition
for H_2O_2, given the high (1 mM) reductant concentration used in the experiment. Note that the
observed side reaction between HRP and GA will also occur in Amplex Red/HRP assay, contributing
to the underestimation of the apparent H_2O_2 production rates derived from Figure 2.

The peroxygenase reaction is dependent on the reductant. To assess the influence of AscA, GA
and cysteine on the peroxygenase activity of *Nc*AA9C, we monitored the consumption of Glc_5 in

10

reactions that contained 300 μM H_2O_2 (Figure 4A). In the presence of 100 μM reductant, we observed apparent rate constants of ~70 s^{-1}, ~25 s^{-1} and ~6 s^{-1} for ascorbic acid, gallic acid and cysteine, respectively, where the first and the second value are underestimated as a major part of the H_2O_2 was consumed at the first time point. These rates are 100 – 2300 times higher than the apparent monooxygenase rates (Table 1). The progress curve for the reaction with AscA shows that the reaction is limited by the availability of H_2O_2 as product formation levels of at about 300 μM of product, reflecting a 1:1 ratio with the added H_2O_2. It is worth noting that these reactions were monitored by measuring the generation of cellobiose and cellotriose, which means that uncertainties related to the instability of C4-oxidized products [41] were avoided. It is also worth noting that reactions with a starting concentration of 300 μM H_2O_2 would lead to rapid LPMO inactivation reactions with insoluble substrate [15] but that in the present case, with a rapidly diffusing soluble substrate, stoichiometric catalytic conversion of the H_2O_2 was achieved.
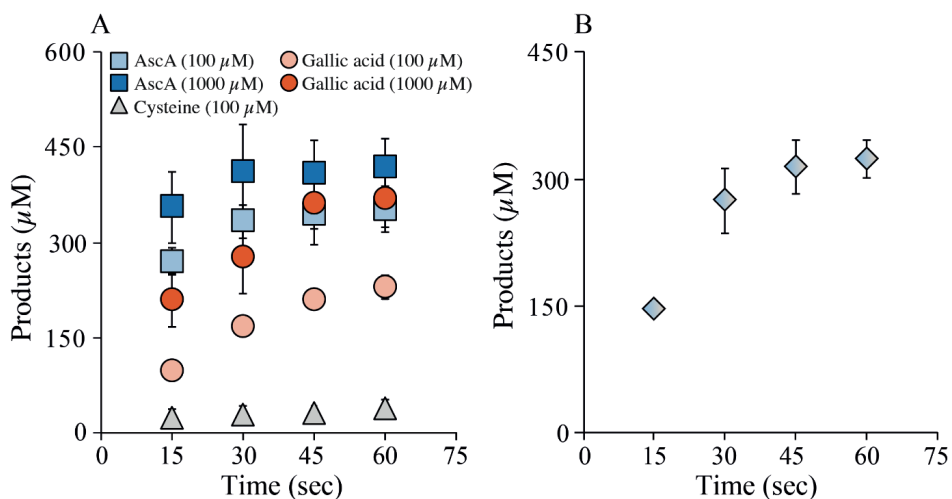
Figure 4. Peroxygenase reactions with *Nc*AA9C. (A) Time course experiments showing the impact of AscA (blue), cysteine (grey) and GA (orange) on the peroxygenase reaction catalyzed by *Nc*AA9C. Reaction mixtures containing 0.25 μM enzyme, 300 μM H_2O_2, 100 or 1000 μM reductant and 1 mM Glc$_5$ were incubated at 37 °C and reactions were started by adding the reductant. No products were detected in control reactions without added reductant. (B) Product formation in a reaction with 0.25 μM *Nc*AA9C, 300 μM H_2O_2, 1 mM Glc$_5$, 0.1 mM ascorbic acid and 0.1 mM cysteine. Note that this reaction was incubated at 4 °C, hence the slower rate compared to panel A.

341   To investigate if the availability of reductant is rate limiting, the experiments depicted in

342   Figure 4A were redone with 1 mM (i.e., 10-fold more) reductant concentrations. By doing so, the

343   already high and most certainly underestimated rate for the reaction with AscA increased slightly,

344   whereas the reaction with gallic acid became approximately twice as fast. While this clearly shows

345   that the reductant to some extent limits the very high rates of these peroxygenase reactions (note the

346   difference in time scale with the monooxygenase reactions of Figure 2), increasing the amount of

347   reductant had no effect on the (lower) rate of the reaction with cysteine (results not shown). The lower

348   activity with cysteine was not due to H_2O_2 scavenging by the reductant, as the addition of 0.1 mM

349   cysteine to a reaction with 0.1 mM AscA did not affect product formation (Figure 4B), which shows

350   that all added H_2O_2 was used by the LPMO. This result is in line with literature data showing that,

351   while cysteine can react with H_2O_2, the rate of this reaction is orders of magnitude lower [48] than the

352   rate of the peroxygenase reaction of *Nc*AA9C. Possibly, reduction of copper by cysteine leads to the

353   formation of a relatively stable cuprous thiolate complex [49] that limits LPMO reactivity under "fast"

354   peroxygenase conditions, whereas this inhibitory effect could remain unnoticed under the much

355   slower monooxygenase conditions. Of note, even with cysteine, the k_{obs} of ~6 s^{-1} is still much higher

356   than typical k_{obs} values for monooxygenase reactions.

357   These results show that the peroxygenase reaction of *Nc*AA9C is much faster than the

358   apparent monooxygenase reaction (Table 1), which implies that minor variations in the levels of *in*

359   *situ* H_2O_2 generation will have dramatic effects on the low rates of the latter reaction. Within the time

360   scale of the peroxygenase reaction, the main contribution of the reductant is to keep the LPMO reduced

361   (i.e., catalytically competent) and our data reveal differences between the reductants in this respect.

362   While experiments with polymeric substrates have shown that once reduced LPMOs may catalyze 15-

363   20 peroxygenase reactions before being re-oxidized [20], [37], [38], the re-oxidation frequency, and,

364   thus, the reductant dependency may be higher in the case of a soluble substrate, which will bind less

365   strongly and, upon binding, create less confinement of the copper site, thus increasing the chances for

366   side reactions that involve copper reoxidation and the loss of electrons.

367

368   **Kinetics of the LPMO catalyzed peroxygenase reaction.** To gain more insight into the

369   peroxygenase reaction we performed Michaelis-Menten kinetics (Figure 5A). The underlying linear

370   progress curves covered Glc$_5$ concentrations ranging from 75 μM to 2500 μM and reactions were run

371   at 4 °C to obtain manageable product formation rates. This set-up resulted in a hyperbolic curve,

372   yielding a K_m (for Glc$_5$) of 2.1 ± 0.3 mM, a k_{cat} of 124 ± 27 s^{-1} and a k_{cat}/K_m of 3.5*10^4 M^{-1}s^{-1} (Figure

373   5A). This k_{cat} value, determined at 4 °C, is 2.5 x 10^3 fold higher than the k_{obs} value for the apparent

374   monooxygenase reaction with AscA described above (37 °C), 1.1 x 10^3 fold higher than a k_{cat} value

375   reported for *Ls*AA9A acting on an analogue of Glc$_4$ in a monooxygenase set-up with AscA (37 °C ;

376   [36]) and 19-fold higher that the k_{cat} reported for a peroxygenase action on chitin nanowhiskers by a

377   bacterial AA10-type LPMO at 25 °C [18]. The K_m measured for *Nc*AA9C of ~2 mM is comparable to

378   the K_d of 0.81 ± 0.08 mM that Borisova *et al*. [35] measured for the same enzyme binding to Glc$_6$

379   under non-turnover conditions.

380

381

382
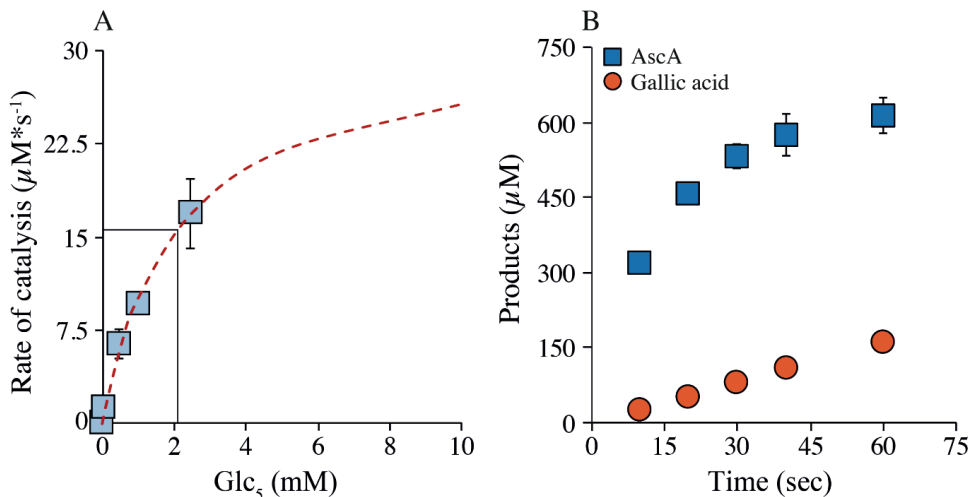
383
384   **Figure 5. Kinetics of the *Nc*AA9C catalyzed peroxygenase reaction with Glc$_5$.** (A) Michealis-

385   Menten kinetics showing the dependency of the catalytic activity on the Glc$_5$ concentration. The rates

386   were derived from linear progress curves and the dashed line shows the fit to the Michaelis-Menten

387   equation. Reactions were set up with 0.25 μM enzyme and 600 μM H$_2$O$_2$ at 4 °C and were started by

388   adding 0.1 mM AscA (note that the K_m for H$_2$O$_2$ is expected to be below 10 μM; [18]). (B) Progress

389   curves for the peroxygenase reaction at 4 °C. The data points show product formation in a reaction

390   with 0.25 μM *Nc*AA9C, 600 μM H$_2$O$_2$, 1 mM Glc$_5$ and either 1 mM AscA (blue) or GA (orange) that

391   was incubated at 4 °C.

392

393

394   To further substantiate the strikingly high catalytic rate of *Nc*AA9C, we then conducted

395   additional initial rate measurements to obtain k_{obs} values that would be more reliable that those

396   obtained from the non-linear progress curves shown in Figure 4A. To do so, we decreased the reaction

397   temperature to 4 °C and increased the H$_2$O$_2$ concentration to 600 μM to ensure that the oxygen

398   donating substrate would not become limiting within seconds. The resulting progress curve for the

399   reaction with AscA (Figure 5B) showed the formation of 600 μM products within 30 seconds showing

400   that the reaction was limited by the availability of H$_2$O$_2$. Based on the first 20 seconds of the

401   experiment (R^2 = 0.95), we calculated a k_{obs} of 90.8 ± 3.6 s^{-1}. As expected, based on Figure 4A, the

402   reaction with GA was slower. This reaction showed a linear increase in product level and gave a k_{obs}

13

of 10.7 ± 0.3 s^{-1} (Figure 5B). Of note, these rates were obtained using sub-saturating substrate conditions as the used Glc$_5$ concentration was just about 50 % of the measured K_m. Still the obtained k_{obs} of ~ 90 s^{-1} and ~11 s^{-1} for NcAA9C in combination with AscA and GA, respectively, represent the two highest rates ever measured for LPMO-catalyzed oxidation of a carbohydrate substrate.

AA9 LPMOs acting on soluble substrates have different properties. One of the other AA9 LPMOs known to act on soluble substrates is LsAA9A [36]. A previous kinetic characterization of this enzyme using a Förster-resonance-energy-transfer (FRET) substrate analogue of Glc$_4$ as substrate and monooxygenase conditions (5 mM AscA, no added H$_2$O$_2$) yielded a k_{cat} = 0.11 ± 0.01 s^{-1}, i.e., a typical value for LPMOs acting in "monooxygenase mode", and in the same range as apparent oxidase and monooxygenase rates reported here for reactions with AscA (Table 1). The obtained K_m value of 43±9 µM is remarkably low, compared to e.g., the K_m for Glc$_5$ cleavage by NcAA9C reported above and suggests high substrate affinity, which could perhaps be due in part to the presence of aromatic groups that appear at the reducing and non-reducing end of the FRET substrate analogue.

Our studies confirmed high, albeit not necessarily specific, substrate affinity as we observed substrate inhibition at Glc$_5$ concentrations in the 0.1 - 1 mM range (results not shown). Due to this substrate inhibition, quantitative comparison of the catalytic properties of the two LPMOs is not straightforward. Assays identical to those described above for NcAA9C showed apparent monooxygenase and oxidase rates in the same order of magnitude and confirmed the considerable impact of the reductant of LPMO activity (Figure 6; Table 2). The most notable difference is that H$_2$O$_2$ production by LsAA9A in the presence of AscA is less efficient compared do NcAA9C (Figure 2B, 6B). Accordingly, the AscA-driven apparent monooxygenase reaction is slower, making cysteine the clearly most efficient reductant for this LPMO in a "monooxygenase" set-up (Figure 6A).

The peroxygenase reactions were slower than for NcAA9C, possibly due to substrate inhibition (Figure 6C). Still, the apparent rates recorded for reactions with two concentrations of AscA (Table 2) are 35 – 141 times higher than the previously determined k_{cat} for an apparent monooxygenase reaction [36] and 280 – 1100 times higher than the apparent monooxygenase reaction rates determined here. For this LPMO, peroxygenase reactions with both cysteine and gallic acid were relatively slow and not or hardly dependent on the reductant concentration. Still, these rates were some 10 and 100 times higher than the determined apparent monooxygenase rates (Table 2).
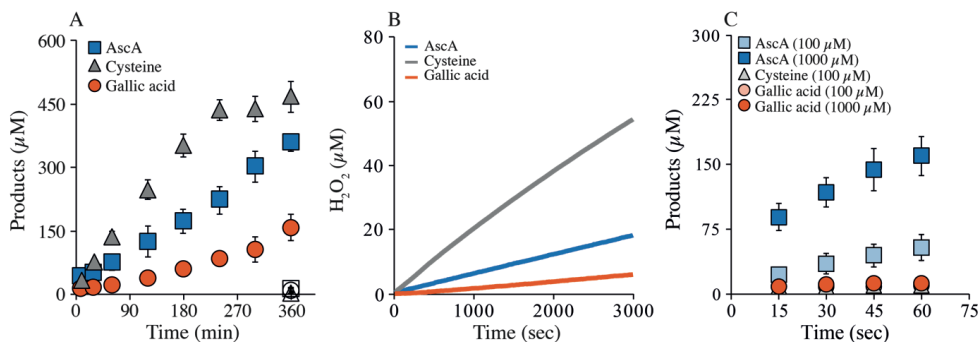
14

Figure 6. Monooxygenase, peroxygenase and oxidase activity for *Ls*AA9A. The monooxygenase
(A) and oxidase (B) reactions were performed with 1 μM LPMO and either 1 mM AscA (blue),
cysteine (grey) or gallic acid (orange) in the presence (A) and absence (B) of 1 mM Glc$_5$. For the
peroxygenase reactions shown in panel (C) we lowered the enzyme concentration to 0.25 μM and
added 300 μM H$_2$O$_2$ with the same reductants as used for the monooxygenase reaction at
concentrations of either 100 or 1000 μM at 37 °C. In panel C, the points for the reaction with 100 μM
GA and cysteine, respectively are hidden by the points for the reaction with 1000 μM GA; the reaction
with 1000 μM cysteine yielded the same curve as the reaction with 100 μM and is not shown, for
clarity.

**Table 2. Apparent rate constants (s^{-1}) for the oxidation of 1 mM Glc$_5$ by *Ls*AA9A under various
conditions.** The values presented are estimates derived from the progress curves shown in Figure 6.
The oxidase values are also expressed as percentage of the oxidase value observed for *Nc*AA9C (Table
1). Other quantitative comparisons between the two LPMOs are not straightforward due to the
occurrence of substrate inhibition in the reactions with *Ls*AA9A.

|	Monooxygenase (Fig. 6A; 1 mM reductant, 1 mM Glc$_5$, O$_2$)	Oxidase (Fig. 6B; 1 mM reductant, O$_2$, no substrate)	O$_2$ reduction, reductant only (Fig. 2C; 1mM reductant, O$_2$, no LPMO)	Peroxygenase (Fig. 6C; 0.1 mM reductant, 1 mM Glc$_5$, 300 μM H$_2$O$_2$, O$_2$)	Peroxygenase (Fig. 6C; 1 mM reductant, 1 mM Glc$_5$, 300 μM H$_2$O$_2$, O$_2$)
AscA	0.014 ± 0.002	0.006±0.000 (35 %)	0.0004±0.0001	5.8 ± 2.3	23.4 ± 4.2
Gallic acid	0.006 ± 0.001	0.002±0.000 (100 %)	0.0040±0.0009	0.1 ± 0.0	0.4 ± 0.1
Cysteine	0.029 ± 0.001	0.018±0.000 (95 %)	0.0026±0.0002	0.3 ± 0.1	0.2 ± 0.1

It is interesting to note that the efficient peroxygenase reaction catalyzed by *Ls*AA9A in the
presence of AscA was much more dependent on the reductant concentration (Figure 6C; Table 2)

458   compared to NcAA9C (Figure 2). This reflects that, compared to NcAA9C, LsAA9A is more prone to

459   oxidation and a subsequent need for re-reduction. Substrate-binding and the resulting confinement of

460   the reduced catalytic copper form a major determinant of the degree of non-productive LPMO

461   oxidation. The data could thus indicate that LsAA9A binds the substrate less firmly or less precisely,

462   where the first option is in conflict with the previously reported low K_m value. A more oxidation-prone

463   copper site in the enzyme-substrate complex would also translate into decreased enzyme stability at

464   higher H_2O_2 concentrations, as non-productive reactions between the reduced enzyme and H_2O_2 may

465   lead to oxidative damage [15]. Indeed, Figure 7 shows that LsAA9A is more sensitive to H_2O_2-induced

466   damage than NcAA9C. While product formation by NcAA9C first started decreasing at 1000 μM, the

467   highest tested H_2O_2 concentration, LsAA9A showed signs of enzyme inactivation already at 250 μM

468   (Figure 7).

469

470
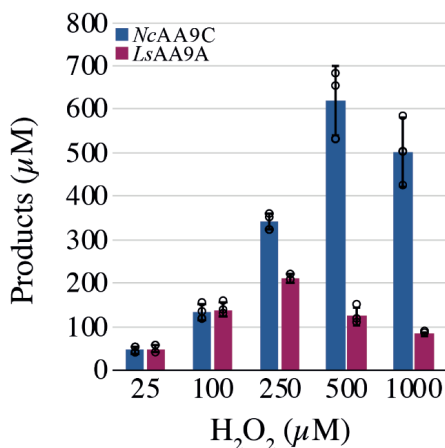
471

472   **Figure 7. Sensitivity of NcAA9C and LsAA9A for oxidative damage.** The graph shows product

473   levels obtained after a 2-minute reaction containing 1 mM AscA and various amounts of H_2O_2.

474   Reaction mixtures containing 1 μM LsAA9A (purple) or 1 μM NcAA9C (blue), 1 mM Glc$_5$ and

475   varying H_2O_2 concentrations (25 - 1000μM) were preincubated for 1 min, after which the reaction was

476   started by adding the reductant. In reactions not showing signs of enzyme inactivation product levels

477   were slightly higher than the amount of added H_2O_2 due to the combination of AscA-mediated H_2O_2

478   generation and a small systematic error in the concentration of the H_2O_2 stock solution.

479

480

481   Taken together, the comparison of the results obtained for NcAA9C and LsAA9A show two

482   important things. Firstly, the data reveal functional differences between these two C4-oxidizing

483   cellulose-active LPMOs, which are reductant-dependent. Since soluble cello-oligomers, can easily be

16

484 degraded by hydrolytic enzymes, it is not likely that Nature has evolved LPMOs for the purpose of
485 cleaving these compounds (as also suggested by the high K_m value for NcAA9C). Therefore, we
486 hypothesize that the functional differences between NcAA9C and LsAA9A should be considered as a
487 proxy for hitherto undescribed differences in substrate preferences that relate to the structural and
488 compositional complexity of true biomass. Secondly, while our studies show quite different
489 peroxygenase reaction rates and reductant dependencies for NcAA9C and LsAA9A and while they
490 suggest that Glc_5 is a far from optimal substrate for LsAA9A, all observed peroxygenase rates are
491 much higher than any reported apparent rate for apparent monooxygenase reactions.

492

493 **The LPMO-catalyzed peroxygenase reaction is specific.** Previously, it has been claimed that the
494 addition of H_2O_2 to LPMO reactions results a loss in specificity [22] and some argue that this shows
495 that H_2O_2 is not a bonafide co-substrate for LPMOs and that, thus, LPMOs are not bonafide
496 peroxygenases. In the present study, we used high H_2O_2 amounts, that were stoichiometrically used to
497 convert cellopentaose to cellobiose and cellotriose. This shows that there is little, if any, random
498 oxidation of the substrate and that the reaction is highly specific (Figure 8).
499   To further assess specificity, we set up aerobic reactions with 1 μM LsAA9A or 1 μM
500 NcAA9C with either 1mM xylopentaose (Xyl_5) or 1 mM mannopentaose (Man_5) as substrate (Figure
501 S1; Figure S2). The conditions used were: (i) 1 mM AscA ("monooxygenase" conditions), (ii) 20 μM
502 H_2O_2 and 20 μM AscA, or (iii) 300 μM H_2O_2 and 100 μM AscA. Note that the latter reaction conditions
503 would lead to very fast (within < 1 min) conversion of Glc_5 by NcAA9C (Figure 4A). Additionally,
504 we tested well-characterized chitin-active SmAA10A [3] and a recently described chitin-active AA11,
505 called AfAA11B [39] for their ability to oxidize 1 mM Glc_5 using the same reaction conditions (Figure
506 S3).
507   None of these reactions yielded detectable turnover of the substrate, except the positive control
508 reactions with NcAA9C or LsAA9A and Glc_5 (Figure S3). We were not able to detect any degradation
509 products by MALDI-TOF MS, whereas the HPAEC-PAD chromatograms only showed a few minimal
510 signals that could indicate a low level of oxidative cleavage of xylopentaose, which, for LsAA9A,
511 would be in accordance with a previously observed weak xylan-degrading ability [50].
512 Crystallographic studies have shown that xylopentaose binds atypically to LsAA9A, leaving a not
513 properly confined copper site prone to engaging in potentially enzyme-inactivating side reactions [10],
514 [50]. One would thus expect rapid enzyme inactivation in reactions with large amounts of H_2O_2, which
515 could explain why, if at all present, only trace amounts of LPMO products were observed,
516   The main take home message of these experiments is that the addition of H_2O_2 at low or high
517 concentration, in combination with different concentrations of AscA, does not result in a loss of
518 substrate specificity. The chromatograms and mass spectra for the peroxygenase reactions did not
519 show any conspicuous features compared to the negative controls or the chromatograms for the
520 apparent monooxygenase reactions.

17

521
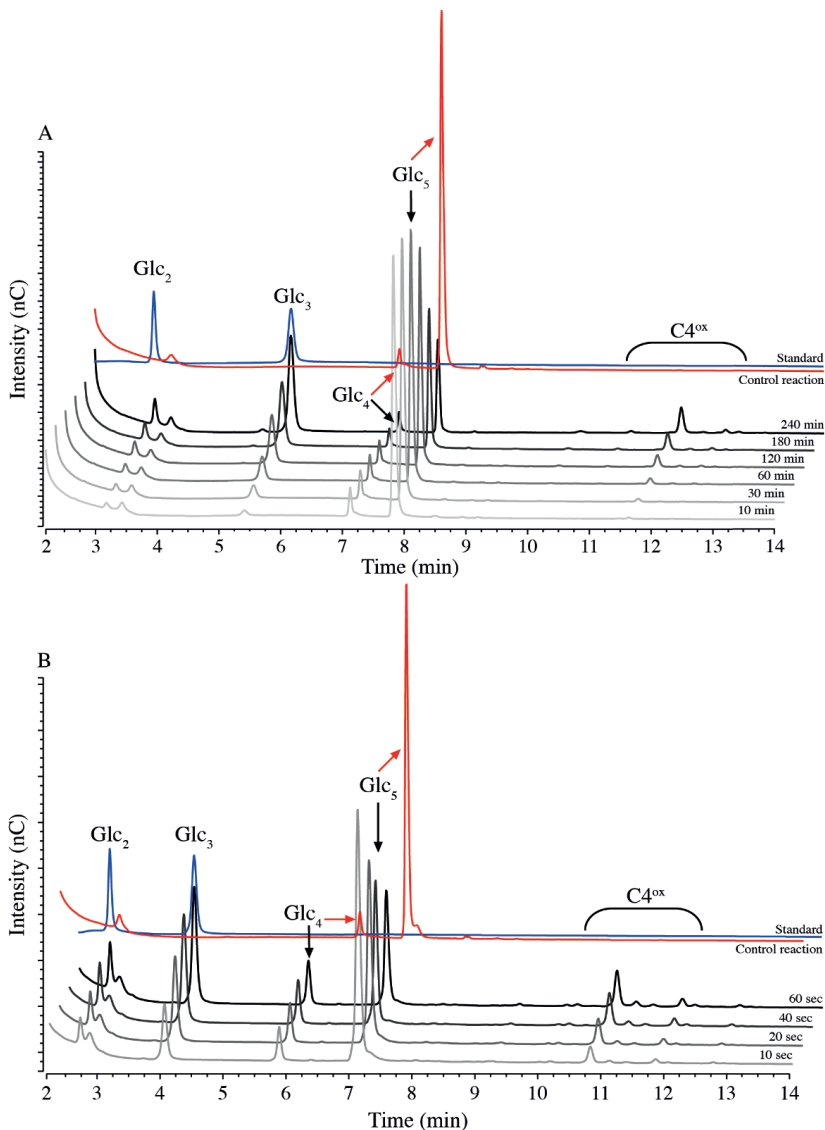
522
523 **Figure 8. HPAEC-PAD chromatograms showing product formation in reactions with *Nc*AA9C**
524 **and Glc$_5$, using a monooxygenase (A) or a peroxygenase (B) set-up.** Chromatograms for the
525 monooxygenase reaction (1 μM LPMO, 1 mM AscA and 1 mM Glc$_5$ at 37 °C) and peroxygenase
526 reaction (0.25 μM LPMO, 600 μM H$_2$O$_2$, 1mM AscA, 1 mM Glc$_5$ at 4°C) are shown as lines in
527 gradations of grey and black. The chromatograms correspond to the time course experiments shown
528 in Figure 2A and Figure 5B, respectively. The red lines show the chromatograms of the appropriate
529 control reaction without reductant, after incubation for 240 min (A) or 60 s (B). The blue
530 chromatograms show the Glc$_2$+Glc$_3$ standard.

18

531

Concluding remarks

The experiments described above show two important aspects of LPMO enzymology. Firstly, they illustrate that it is complicated to properly assess LPMO catalysis experimentally, due to the plethora of interconnected (side) reactions. Many of these complications emerged in our experiments and by studying multiple reductants, each with own peculiarities, we were able to overcome most of these complications and generate insight into LPMO catalysis. Secondly, we show that LPMOs, when acting on rapidly diffusing soluble substrates and provided with H_2O_2, indeed are very efficient peroxygenases. We observed stoichiometric conversion of high starting amounts of H_2O_2 that would lead to rapid LPMO inactivation in reactions with insoluble substrate. Importantly, it has been claimed that the fact that LPMOs, like many other redox active enzymes, are prone to damage by H_2O_2 suggests that these enzymes are not true peroxygenases. Our data for reactions with soluble substrates show that the peroxygenase reaction is stable and specific.

We observed a clear correlation between the H_2O_2 producing potential of an LPMO-reductant combination and the observed apparent monooxygenase activity, which supports the idea that the apparent monooxygenase activity may in fact be the result of an H_2O_2-limited peroxygenase reaction, as originally suggested by Bissaro *et al.* [15]. This is supported by the strong inhibitory effect of HRP on the LPMO reaction. Still, it is almost impossible to exclude the monooxygenase reaction and it is well known that reduced LPMOs react with O_2 [13], [27]. It is also known that this reaction may be influenced by substrate binding ([30], [36]), suggesting that monooxygenase reactions may occur. Still, the rates of the two reactions vary by orders of magnitude for both soluble and insoluble substrates ([16]–[19]; this study).

Notably, our data indicate that the oxidase activity of the AA9 type LPMOs studied here is higher that the oxidase activity of a previously studied AA10 type LPMO [25]. This could imply that, compared to AA10 LPMOs, the AA9 LPMOs are more active under monooxygenase conditions than AA10 LPMOs since they generate more H_2O_2. However, extrapolation of oxidase activities measured in the absence of substrate to oxidase activities under turnover conditions is not straightforward because of the impact of substrate-binding on oxidase activity [26]. Further studies are warranted to study whether the observed difference in oxidase activity is general and to identify its structural determinants. It is also worth noting that in systems where the LPMO peroxygenase reaction is driven by the oxidase activity of the LPMO itself, the nature of the reductant will have a decisive impact on LPMO efficiency.

Our study revealed differences between *Nc*AA9C and *Ls*AA9A, which suggests that these enzymes have different substrate specificities and biological roles. It is important to realize that laboratory experiments with substrates such as Glc_5 or pure cellulose only give limited insight into to true role of an LPMO during fungal biomass conversion.

567   The most important and novel finding of the present study is that the unique LPMO scaffold

568   enables highly efficient copper-catalyzed peroxygenase reactions with a soluble substrate. This high

569   efficiency may in part be due to the copper site being exposed and rather rigid ([51]), with an open

570   coordination position for co-substrate binding. Thus, as originally pointed out by Kjærgaard *et al*.

571   [13]), catalysis requires little reorganization energy, which may contribute to efficiency. It is

572   encouraging that high specificity and high catalytic rates were achieved with a low affinity substrate

573   (the K_m for Glc$_5$ is in the low mM range). It may be possible to engineer similar or better affinities for

574   other, perhaps non-carbohydrate, substrates, which eventually could endow these powerful enzymes

575   with the ability to catalyze efficient peroxygenation of such substrates. Furthermore, the unique

576   peroxygenase chemistry of these mono-copper enzymes may open new avenues for future design of

577   enzyme-inspired synthetic copper catalysts.

578
579

20

Associated content
Supporting information

See file attached

Author information

Corresponding author

Vincent G.H. Eijsink

E-Mail: vincent.eijsink@nmbu.no

Phone: +47 67232463

Postal address: Faculty of Chemistry, Biotechnology and Food Science; NMBU - Norwegian University of Life Sciences, P.O. Box 5003, 1432 Ås, Norway

ORCID ID

Lukas Rieder: 0000-0002-3632-2007

Anton A. Stepnov: 0000-0002-6754-5852

Morten Sørlie: 0000-0001-7259-6710

Vincent G.H. Eijsink: 0000-0002-9220-8743

Author contributions

LR designed the experiments, performed research, and wrote the first draft of the manuscript. AAS designed experiments, performed research, and contributed to writing the manuscript. MS and VGHE provided funding, initiated the research, carried out supervision, helped to design experiments, interpreted results, and contributed to writing the manuscript.

Conflict of interest disclosure

The authors declare no competing interest.

Acknowledgment

References

[1] G. Vaaje-Kolstad, S. J. Horn, D. M. F. Van Aalten, B. Synstad, and V. G. H. Eijsink, "The non-catalytic chitin-binding protein CBP21 from *Serratia marcescens* is essential for chitin degradation," *J. Biol. Chem.*, vol. 280, pp. 28492–28497, 2005.

[2] P. V. Harris *et al.*, "Stimulation of lignocellulosic biomass hydrolysis by proteins of glycoside hydrolase family 61: Structure and function of a large, enigmatic family," *Biochemistry*, vol. 49, pp. 3305–3316, 2010.

[3] G. Vaaje-Kolstad *et al.*, "An oxidative enzyme boosting the enzymatic conversion of recalcitrant polysaccharides," *Science*, vol. 330, pp. 219–223, 2010.

[4] Z. Forsberg *et al.*, "Cleavage of cellulose by a cbm33 protein," *Protein Sci.*, vol. 20, pp. 1479–1483, 2011.

[5] S. J. Horn, G. Vaaje-Kolstad, B. Westereng, and V. G. H. Eijsink, "Novel enzymes for the degradation of cellulose," *Biotechnol. Biofuels*, vol. 5, 45, 2012.

[6] G. R. Hemsworth, E. M. Johnston, G. J. Davies, and P. H. Walton, "Lytic polysaccharide monooxygenases in biomass conversion," *Trends Biotechnol.*, vol. 33, pp. 747–761, 2015.

[7] W. T. Beeson, V. V. Vu, E. A. Span, C. M. Phillips, and M. A. Marletta, "Cellulose degradation by polysaccharide monooxygenases," *Annu. Rev. Biochem.*, vol. 84, pp. 923–946, 2015.

[8] K. S. Johansen, "Discovery and industrial applications of lytic polysaccharide mono-oxygenases," *Biochem. Soc. Trans.*, vol. 44, pp. 143–149, 2016.

[9] P. Chylenski *et al.*, "Lytic polysaccharide monooxygenases in enzymatic processing of lignocellulosic biomass," *ACS Catal.*, vol. 9, pp. 4970–4991, 2019.

[10] Z. Forsberg *et al.*, "Polysaccharide degradation by lytic polysaccharide monooxygenases," *Curr. Opin. Struct. Biol.*, vol. 54, pp. 54–64, 2019.

[11] R. J. Quinlan *et al.*, "Insights into the oxidative degradation of cellulose by a copper metalloenzyme that exploits biomass components," *Proc. Natl. Acad. Sci. U. S. A.*, vol. 108, pp. 15079–15084, 2011.

[12] C. M. Phillips, W. T. Beeson, J. H. Cate, and M. A. Marletta, "Cellobiose dehydrogenase and a copper-dependent polysaccharide monooxygenase potentiate cellulose degradation by *Neurospora crassa*," *ACS Chem. Biol.*, vol. 6, pp. 1399–1406, 2011.

[13] C. H. Kjaergaard *et al.*, "Spectroscopic and computational insight into the activation of O_2 by the mononuclear Cu center in polysaccharide monooxygenases," *Proc. Natl. Acad. Sci. U. S. A.*, vol. 111, pp. 8797–8802, 2014.

[14] P. H. Walton and G. J. Davies, "On the catalytic mechanisms of lytic polysaccharide monooxygenases," *Curr. Opin. Chem. Biol.*, vol. 31, pp. 195–207, 2016.

[15] B. Bissaro *et al.*, "Oxidative cleavage of polysaccharides by monocopper enzymes depends on H_2O_2," *Nat. Chem. Biol.*, vol. 13, pp. 1123–1128, 2017.

[16]   S. M. Jones, W. J. Transue, K. K. Meier, B. Kelemen, and E. I. Solomon, "Kinetic analysis of amino acid radicals formed in H_2O_2-driven Cu^I LPMO reoxidation implicates dominant homolytic reactivity," *Proc. Natl. Acad. Sci. U. S. A.*, vol. 117, pp. 11916–11922, 2020.

[17]   B. Bissaro, A. Várnai, Å. K. Røhr, and V. G. H. Eijsink, "Oxidoreductases and reactive oxygen species in conversion of lignocellulosic biomass," *Microbiol. Mol. Biol. Rev.*, vol. 82, e00029-18, 2018.

[18]   S. Kuusk *et al.*, "Kinetics of H_2O_2-driven degradation of chitin by a bacterial lytic polysaccharide monooxygenase," *J. Biol. Chem.*, vol. 293, pp. 523–531, 2018.

[19]   R. Kont, B. Bissaro, V. G. H. Eijsink, and P. Väljamäe, "Kinetic insights into the peroxygenase activity of cellulose-active lytic polysaccharide monooxygenases (LPMOs)," *Nat. Commun.*, vol. 11, 5786, 2020.

[20]   T. M. Hedison *et al.*, "Insights into the H_2O_2-driven catalytic mechanism of fungal lytic polysaccharide monooxygenases.," *FEBS J.*, 2021.

[21]   C. Wang *et al.*, "Evidence that the fosfomycin-producing epoxidase, HppE, is a non–heme-iron peroxidase," *Science*, vol. 342, pp. 991–995, 2013.

[22]   J. A. Hangasky, A. T. Iavarone, and M. A. Marletta, "Reactivity of O_2 versus H_2O_2 with polysaccharide monooxygenases," *Proc. Natl. Acad. Sci. U. S. A.*, vol. 115, pp. 4915–4920, 2018.

[23]   D. M. Petrović *et al.*, "Comparison of three seemingly similar lytic polysaccharide monooxygenases from *Neurospora crassa* suggests different roles in plant biomass degradation," *J. Biol. Chem.*, vol. 294, pp. 15068–15081, 2019.

[24]   O. Hegnar, D. Petrovic, B. Bissaro, A. Varnai, and V. G. H. Eijsink, "pH-Dependent relationship between catalytic activity and hydrogen peroxide production shown via characterization of a lytic polysaccharide monooxygenase from *Gloeophyllum trabeum*," *Appl. Environ. Microbiol.*, vol. 85, e02612-18, 2019.

[25]   A. A. Stepnov *et al.*, "Unraveling the roles of the reductant and free copper ions in LPMO kinetics," *Biotechnol. Biofuels*, vol. 14, 28, 2021.

[26]   F. Filandr, P. Man, P. Halada, H. Chang, R. Ludwig, and D. Kracher, "The H_2O_2-dependent activity of a fungal lytic polysaccharide monooxygenase investigated with a turbidimetric assay," *Biotechnol. Biofuels*, vol. 13, 37, 2020.

[27]   R. Kittl, D. Kracher, D. Burgstaller, D. Haltrich, and R. Ludwig, "Production of four *Neurospora crassa* lytic polysaccharide monooxygenases in *Pichia pastoris* monitored by a fluorimetric assay," *Biotechnol. Biofuels*, vol. 5, 79, 2012.

[28]   O. Caldararu, E. Oksanen, U. Ryde, and E. D. Hedegård, "Mechanism of hydrogen peroxide formation by lytic polysaccharide monooxygenase," *Chem. Sci.*, vol. 10, pp. 576–586, 2019.

[29]   B. Wang, P. H. Walton, and C. Rovira, "Molecular mechanisms of oxygen activation and hydrogen peroxide formation in lytic polysaccharide monooxygenases," *ACS Catal.*, vol. 9,

690 pp. 4958–4969, 2019.

691 [30] G. Courtade *et al.*, "Mechanistic basis of substrate-O_2 coupling within a chitin-active lytic
692 polysaccharide monooxygenase: An integrated NMR/EPR study," *Proc. Natl. Acad. Sci. U. S.*
693 *A.*, vol. 117, pp. 19178–19189, 2020.

694 [31] E. Breslmayr *et al.*, "A fast and sensitive activity assay for lytic polysaccharide
695 monooxygenase," *Biotechnol. Biofuels*, vol. 11, 79, 2018.

696 [32] J. S. M. Loose, M. Arntzen, B. Bissaro, R. Ludwig, V. G. H. Eijsink, and G. Vaaje-Kolstad,
697 "Multipoint precision binding of substrate protects lytic polysaccharide monooxygenases from
698 self-destructive off-pathway processes," *Biochemistry*, vol. 57, pp. 4114–4124, 2018.

699 [33] G. Courtade, Z. Forsberg, E. B. Heggset, V. G. H. Eijsink, and F. L. Aachmann, "The
700 carbohydrate-binding module and linker of a modular lytic polysaccharide monooxygenase
701 promote localized cellulose oxidation," *J. Biol. Chem.*, vol. 293, pp. 13006–13015, 2018.

702 [34] T. Isaksen *et al.*, "A C4-oxidizing lytic polysaccharide monooxygenase cleaving both cellulose
703 and cello-oligosaccharides," *J. Biol. Chem.*, vol. 289, pp. 2632–2642, 2014.

704 [35] A. S. Borisova *et al.*, "Structural and functional characterization of a lytic polysaccharide
705 monooxygenase with broad substrate specificity," *J. Biol. Chem.*, vol. 290, pp. 22955–22969,
706 2015.

707 [36] K. E. H. Frandsen *et al.*, "The molecular basis of polysaccharide cleavage by lytic
708 polysaccharide monooxygenases," *Nat. Chem. Biol.*, vol. 12, pp. 298–303, 2016.

709 [37] G. Müller, P. Chylenski, B. Bissaro, V. G. H. Eijsink, and S. J. Horn, "The impact of hydrogen
710 peroxide supply on LPMO activity and overall saccharification efficiency of a commercial
711 cellulase cocktail," *Biotechnol. Biofuels*, vol. 11, 209, 2018.

712 [38] S. Kuusk *et al.*, "Kinetic insights into the role of the reductant in H_2O_2-driven degradation of
713 chitin by a bacterial lytic polysaccharide monooxygenase," *J. Biol. Chem.*, vol. 294, pp. 1516–
714 1528, 2019.

715 [39] L. Rieder, K. Ebner, A. Glieder, and M. Sørlie, "Novel molecular biological tools for the
716 efficient expression of fungal lytic polysaccharide monooxygenases in *Pichia pastoris*,"
717 *Biotechnol. Biofuels*, vol. 14, 122, 2021.

718 [40] G. Vaaje-Kolstad, D. R. Houston, A. H. K. Riemen, V. G. H. Eijsink, and D. M. F. Van Aalten,
719 "Crystal structure and binding properties of the *Serratia marcescens* chitin-binding protein
720 CBP21," *J. Biol. Chem.*, vol. 280, pp. 11313–11319, 2005.

721 [41] B. Westereng, M. T. Arntzen, F. L. Aachmann, A. Várnai, V. G. H. Eijsink, and J. W. Agger,
722 "Simultaneous analysis of C1 and C4 oxidized oligosaccharides, the products of lytic
723 polysaccharide monooxygenases acting on cellulose," *J. Chromatogr. A*, vol. 1445, pp. 46–54,
724 2016.

725 [42] D. Kracher *et al.*, "Extracellular electron transfer systems fuel cellulose oxidative
726 degradation," *Science*, vol. 352, pp. 1098–1101, 2016.

[43]   M. Frommhagen, A. H. Westphal, W. J. H. van Berkel, and M. A. Kabel, "Distinct substrate specificities and electron-donating systems of fungal lytic polysaccharide monooxygenases," *Front. Microbiol.*, vol. 9, 1080, 2018.

[44]   G. R. Buettner and B. A. Jurkiewicz, "Catalytic metals, ascorbate and free radicals: Combinations to avoid," *Radiat. Res.*, vol. 145, pp. 532–541, 1996.

[45]   A. V. Kachur, C. J. Koch, and J. E. Biaglow, "Mechanism of copper-catalyzed autoxidation of cysteine," *Free Radic. Res.*, vol. 31, pp. 23–34, 1999.

[46]   J. F. Severino, B. A. Goodman, T. G. Reichenauer, and K. F. Pirker, "Is there a redox reaction between Cu(II) and gallic acid?," *Free Radic. Res.*, vol. 45, pp. 123–132, 2011.

[47]   X. Zhang, H. Wu, L. Zhang, and Q. Sun, "Horseradish peroxidase-mediated synthesis of an antioxidant gallic acid-g-chitosan derivative and its preservation application in cherry tomatoes," *RSC Adv.*, vol. 8, pp. 20363–20371, 2018.

[48]   D. Luo, S. W. Smith, and B. D. Anderson, "Kinetics and mechanism of the reaction of cysteine and hydrogen peroxide in aqueous solution," *J. Pharm. Sci.*, vol. 94, pp. 304–316, 2005.

[49]   A. Rigo, A. Corazza, M. Luisa Di Paolo, M. Rossetto, R. Ugolini, and M. Scarpa, "Interaction of copper with cysteine: Stability of cuprous complexes and catalytic role of cupric ions in anaerobic thiol oxidation," *J. Inorg. Biochem.*, vol. 98, pp. 1495–1501, 2004.

[50]   T. J. Simmons *et al.*, "Structural and electronic determinants of lytic polysaccharide monooxygenase reactivity on polysaccharide substrates," *Nat. Commun.*, vol. 8, 1064, 2017.

[51]   F. L. Aachmann, M. Sorlie, G. Skjak-Braek, V. G. H. Eijsink, and G. Vaaje-Kolstad, "NMR structure of a lytic polysaccharide monooxygenase provides insight into copper binding, protein dynamics, and substrate interactions," *Proc. Natl. Acad. Sci.*, vol. 109, pp. 18779–18784, 2012.
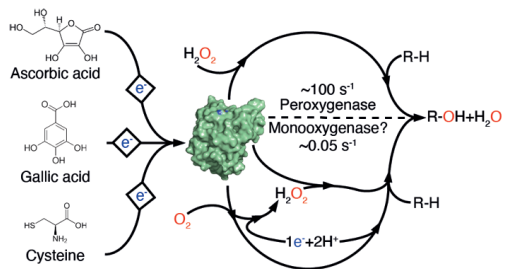
752

753   **For table of contents only**

Fast and specific peroxygenase reactions catalyzed by fungal mono-copper enzymes

Lukas Rieder, Anton A. Stepnov, Morten Sørlie, Vincent G.H. Eijsink

Faculty of Chemistry, Biotechnology, and Food Sciences, Norwegian University of Life Sciences (NMBU), Ås, Norway

Supporting information

Table of contents

Figure S1. HPLC product profiles for reactions with 1 μM *NcAA9C* (bluish colours) or *LsAA9A* (purple colours) and 1 mM xylopentaose performed under standard aerobic conditions with the additions indicated in the chromatograms, and incubated overnight, at 37 °C. The dashed lines are chromatograms for corresponding reactions without AscA. Unlabeled arrows indicate minor amounts of unidentified products that may derive form oxidative cleavage of xylopentaose.
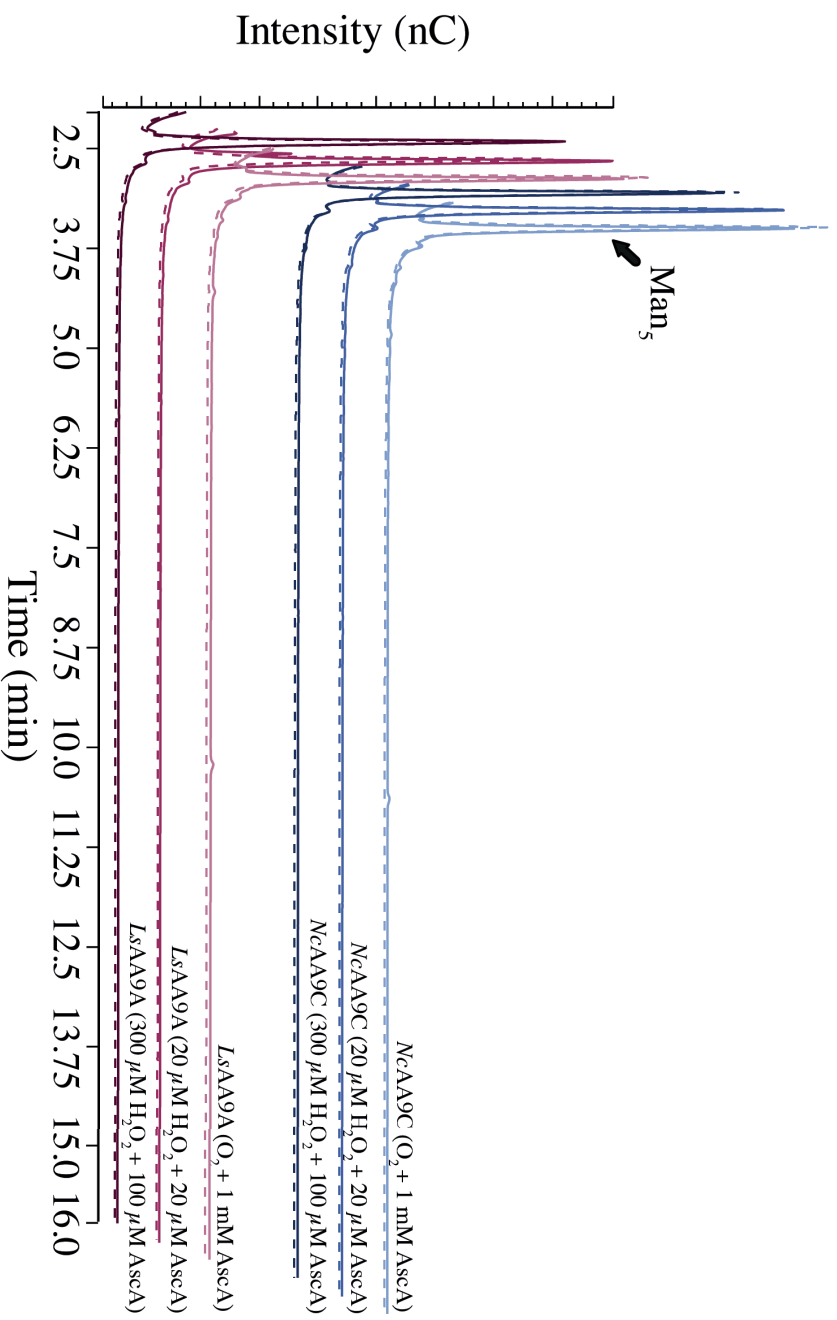
Figure S2. HPLC product profiles for reactions with 1 μM *Nc*AA9C (bluish colours) or *Ls*AA9A (purple colours) and 1 mM mannopentaose performed under standard aerobic conditions with the additions indicated in the chromatograms, and incubated overnight, at 37 °C. The dashed lines are chromatograms for corresponding reactions without AscA.
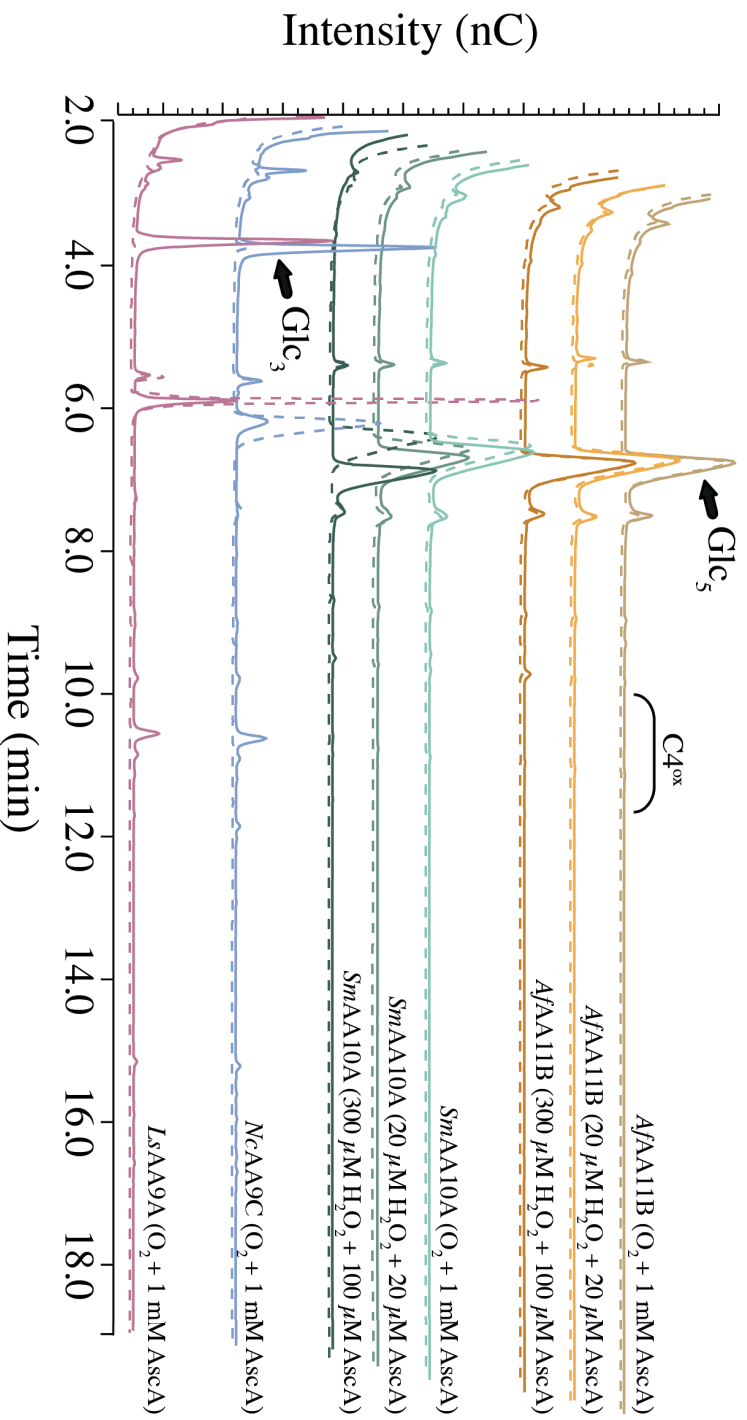
Figure S3. HPLC product profiles for reactions with 1 μM Af/AA11B (yellow colours) or SmAA10A (green colours) and 1 mM cellopentaose performed under standard aerobic conditions with the additions indicated in the chromatograms, and incubated overnight, at 37 °C. For comparison, positive controls showing products generated upon aerobic overnight reactions with NcAA9C (blue) and LsAA9A (purple) are included. The position of peaks corresponding to C4-oxidized products is indicated by "C4^{ox}". The dashed lines are chromatograms for corresponding reactions without AscA.

Norwegian University
of Life Sciences